

博士論文

**Study on heat shock protein 90 complex formation with
SCAP/SREBP and regulation of SREBP function**
(熱ショックタンパク質 90 による SCAP/SREBP 複合体形
成と SREBP 活性調節に関する研究)

東京大学大学院 農学生命科学研究科
応用生命化学専攻 食品生化学研究室
平成 26 年度入学 官 彦州
指導教員 佐藤 隆一郎

Outline

List of Abbreviation	1
Chapter 1: <i>Introduction</i>	3
1-1. Sterol regulatory element-binding protein (SREBP)	4
1-2. SREBP cleavage-activating protein (SCAP)	6
1-3. Heat shock protein 90	7
1-4. Hsp90 and SREBP in metabolic diseases and cancers	8
1-5. Aim of study	8
Chapter 2: <i>Hsp90 physically interacts with the C-termini of SCAP and SREBP</i>	9
2-1. Preface	10
2-2. Materials and Methods	10
2-3. Results	13
2-4. Discussion	21
Chapter 3: <i>Hsp90 modulates lipid homeostasis by regulating the stability of SCAP and SREBP</i>	22
3-1. Preface	23
3-2. Materials and Methods	23
3-3. Results	27
3-4. Discussion	51
Chapter 4: <i>SREBP-binding sites in SCAP WD40 domain</i>	53
4-1. Preface	54
4-2. Materials and Methods	54
4-3. Results	56
4-4. Discussion	66
Chapter 5: <i>Comprehensive Discussion</i>	68
References	75
Abstract	82
Acknowledgement	86
Appendix	88

List of Abbreviations (I)

17-AAG: 17-N-allylamino-17-demethoxygeldanamycin
17-DMAG: 17-dimethylaminoethylamino-17-demethoxygeldanamycin
25-HC: 25-hydroxycholesterol
ACC: acetyl-CoA carboxylase
Akt: protein kinase B
AMPK: activated protein kinase
ATP: adenosine triphosphate
CHO: Chinese hamster ovarian
COPII: coat protein complex II
CREB: cAMP response element-binding protein
CRTC2: cAMP response element-binding protein (CREB) regulated transcription coactivator
DDB1: DNA damage-binding protein 1
DMEM: Dulbecco's modified Eagle's medium
EDTA: Ethylenediaminetetraacetic acid
ER: endoplasmic reticulum
ESI-Q-TOF MS: electrospray ionization quadrupole time-of-flight mass spectrometry
FASN: fatty acid synthase
FBS: fetal bovine serum
Fbw7: F-box/WD40 protein 7
GA: geldanamycin
GSK-3: glycogen synthase kinase 3
HBSS: Hanks' balanced salt solution
HEK293: human embryonic kidney 293
HMGCS: 3-hydroxy-3-methyl-glutaryl-coenzyme A synthase
HMGCR: 3-hydroxy-3-methyl-glutaryl-coenzyme A reductase
HRP: horse reddish peroxidase
HSF-1: heat shock factor 1
Hsp: Heat shock protein
Hsp90: Heat shock protein 90
Insig: insulin-induced gene protein
ip: intraperitoneal
IRF3: interferon regulatory factor 3
MAPK: mitogen-activated protein kinase
microRNA (miR)
mTOR: mammalian target of rapamycin
mTORC1: mammalian target of rapamycin complex 1
NAFLD: non-alcoholic fatty liver disease
NCC: thiazide-sensitive cotransporter

List of Abbreviations(II)

PAGE: polyacrylamide gel electrophoresis
PAQR3: Progestin and adipoQ receptor 3
PBS: phosphate buffer saline
PI3K: phosphatidylinositol-4,5-bisphosphate 3-kinase
RIPA: radio immunoprecipitation assay buffer
RNF5: ring finger protein 5
RNF20: ring finger protein 20
PPAR γ : peroxisome proliferator-activated receptor gamma
S1P: site-1 protease
S2P: site-2 protease
S6K: p70 S6 kinase
SCAP: sterol regulatory element-binding protein (SREBP) cleavage-activating protein
SDS: sodium dodecyl sulfate
SCD: stearoyl-coA desaturase SREBP: sterol regulatory element-binding protein
SCF: Skp, Cullin, F-box-containing complex
siRNA: small interfering RNA
SQS: squalene synthase
SRE: sterol regulatory element
SREBP: sterol regulatory element-binding protein
STING: stimulator of interferon genes
TSC2: tuberous sclerosis complex 2
TU: transducing unit

Non-standard abbreviations:
fl-SCAP: full length SCAP
N-SCAP: N-terminal SCAP
C-SCAP: C-terminal SCAP
fl- SREBP: full length SREBP
N- SREBP: N-terminal SREBP
C- SREBP: C-terminal SREBP

CHAPTER 1

INTRODUCTION

1-1. Sterol regulatory element-binding protein (SREBP)

Sterol regulatory element-binding proteins (SREBPs) are a family of basic helix-loop-helix leucine zipper transcription factors that regulate the induction of the key lipogenic enzymes such as fatty acid synthase (FASN), acetyl-CoA carboxylase (ACC), stearoyl-coA desaturase (SCD), 3-hydroxy-3-methyl-glutaryl-coenzyme A synthase and reductase (HMGCS and HMGCR), and squalene synthase (SQS) (1). There are three isoforms of SREBP in mammal, SREBP1a, SREBP-1c, and SREBP2. SREBP1a and SREBP1c are produced from the same gene *SREBF1* by using different promoters and alternative splicing. The transcription active domain in SREBP-1c is therefore 24-amino acid shorter than that of SREBP1a, causing a reduced transcription activity (2). While SREBP1a activates genes involving both fatty acid and cholesterol biosynthesis, SREBP1c regulates genes involving fatty acid biosynthesis. The expression of SREBP1 isoforms reflects their functional differences. While, SREBP1a is ubiquitously expressed in most tissues including kidney, brain, fat, and muscle, SREBP1c is primarily expressed in liver. On the other hand, SREBP2 is encoded by the *SREBF2* gene and regulates gene expression of the enzymes involving in cholesterol biosynthesis. Since cholesterol is a key component of cell membrane and is indispensable for cell survival, SREBP2 is ubiquitously expressed in all tissues (3).

SREBPs are synthesized on the membrane of endoplasmic reticulum (ER). The structural domain of SREBP is consisted of an N-terminal acidic transactivation domain containing a basic helix-loop-helix leucine zipper DNA-binding domain, a transmembrane domain that contain 2 helices linked by a small loop that projects to the ER lumen, and a C-terminal cytosolic regulatory domain that interacts with SREBP cleavage-activating protein (SCAP), the SREBP chaperone (4). The amino acid sequences of SREBP1a and SREBP2 share 47% of identical amino acids (5). The transcription active N-terminal domain of SREBP, often termed as the 'matured' SREBP, binds to a 5'-ATCACCCAC-3' nucleotide sequence termed sterol regulatory element (SRE), thus giving the name of the protein as SRE-binding protein. For example, SREBP2 binds to the SRE sequences in the promoters of *HMGCS*, *HMGCR*, and *SQS* and activates gene expression. SREBP also binds to a SRE-like sequence 5'-CANNTG-3' termed the E-box. For example, SREBP1c binds to the E-box sequences in the promoters of *FASN*, *ACCI*, and *SCD1* and activates gene expression. Interestingly, SRE and E-box sequences are also presented in the promoter regions of *SREBP1c* and *SREBP2*; therefore, SREBP can induce its own gene expression.

SREBPs are synthesized on the ER membrane as inactive precursors. Immediately upon synthesis, SREBP bind to SCAP and form a stable SREBP/SCAP complex. In the absence of SCAP, SREBP is rapidly degraded, highlighting the requirement of SCAP to maintain a stable protein level of SREBP precursor (6). In addition, SCAP is also required for the ER-to-Golgi transport of the SREBP/SCAP complex. In the Golgi apparatus, SREBP is sequentially cleaved by site-1 protease (S1P) and site-2 protease (S2P). S1P cleaves SREBP2 at or near arginine 519 located in the luminal loop, generating an intermediate SREBP2 that is bound to the Golgi membrane. This cleavage is accelerated under sterol depleted condition, but is reduced when sterol level rises. The second cleavage by S2P occurs within the first transmembrane helix and requires the D₄₇₈RSR sequence immediately adjacent to the helix.

The second cleavage is not regulated by sterol, but occurs only after the first cleavage (7). After the sequential proteolytic cleavages, the N-terminal transcription factor domain of SREBP is released from the membrane and translocate to the nucleus, where it transactivate genes involving lipogenesis.

The proteolytic activation of SREBP, often referred to as ‘SREBP processing’, is tightly regulated by the intracellular cholesterol and oxysterol levels. When the intracellular cholesterol level rises, SCAP is bound to the insulin-induced gene protein (Insig), which anchors the SREBP/SCAP complex to the ER membrane, prohibiting ER-to-Golgi transport of the complex, thereby inhibiting SREBP processing and the release of matured SREBP to translocate to the nucleus (8). Mechanistically, cholesterol binds to the membrane-bound portion of SCAP, and 25-hydroxycholesterol (25-HC) binds to the membrane-bound domain of Insig, and the bindings change the conformation of both SCAP and Insig into which favors SCAP/Insig interaction and inhibits SCAP to bind to transport vesicle proteins (9–12)

SREBP processing is also regulated by growth factor-receptor binding through the PI3K/Akt/mTOR pathway. Mechanistically, growth factors or hormones, such as epidermal growth factor or insulin, bind to their corresponding receptors and activates the phosphorylation of PI3K, which in turn activates the phosphorylation of Akt. Phosphorylated Akt then activates formation of mTOR complex 1 (mTORC1), inducing SREBP processing via a p70 S6 kinase (S6K)-dependent pathway (13–16). In contrast to the positive regulation of SREBP processing by Akt pathway, activated protein kinase (AMPK) suppresses SREBP via 2 possible ways. First, by phosphorylating tuberous sclerosis complex 2 (TSC2) and Raptor, AMPK inhibits mTORC1 and inhibits SREBP processing (17). Second, AMPK interacts with SREBP precursor and phosphorylates serine 372 of both the precursor and matured SREBP. Phosphorylation at serine 372 might potentially inhibit ER-to-Golgi transport of SREBP (18).

Recent findings also reveal other factors that modulate SREBP processing. It was demonstrated that the CREB regulated transcription coactivator, CRTC2, inhibited ER-to-Golgi transport of SREBP by disrupting the formation of the COPII vesicle complex of SCAP/SREBP. Interestingly, the report also showed that during feeding, mTOR phosphorylated CRTC2, attenuating its inhibitory effect on SREBP processing (19). This result provides another example of mTOR positively regulates SREBP processing. In addition to factors that regulate COPII transport complex formation, Xu and colleagues discovered a new SCAP/SREBP-interacting protein that anchors the SCAP/SREBP complex to the Golgi apparatus. The progestin and adipoQ receptor 3 (PAQR3) is a Golgi-localized membrane protein that binds to the SCAP/SREBP complex. PAQR3 promoted SCAP/SREBP complex formation and facilitated SREBP processing. The bindings of SCAP to PAQR3 and Insig are mutually exclusive and are modulated by cholesterol. Mechanistically, PAQR3 binds to SCAP and SREBP with distinct motifs and acted as a Golgi-counterpart of Insig, in which PAQR3 tethers SCAP/SREBP to the Golgi to ensure proteolytic activation, while Insig anchors SCAP/SREBP to the ER membrane, inhibiting SREBP processing (20).

1-2. SREBP cleavage-activating protein (SCAP)

SREBP cleavage-activating proteins (SCAPs) are membrane-bound cholesterol-sensing proteins that chaperone SREBP from the ER to the Golgi apparatus. The amino acid sequences of mammalian SCAP is highly conserved sharing approximately 90% of identical sequences (Supplementary Fig. S1). While human SCAP is consisted of 1279 amino acids, the most studied Chinese hamster SCAP is consisted of 1276 amino acids. The domain structure of SCAP is consisted of a ~750-aa N-terminal transmembrane domain and a ~550-aa C-terminal cytosolic domain. The N-terminal domain contains 8 transmembrane helices connected by 3 large loops (L1, L6, and L7) and 4 smaller loops (L2–L5), in which L1, L3, L5, and L7 project into the ER lumen, whereas L2, L4, and L6 project to the cytosol (21).

The membrane-bound portion of hamster SCAP (aa1–753) has been studied in molecular detail (22–24). The luminal L1 (aa46–284) consisted the cholesterol-binding domain (22). The transmembrane helices 2–6 consisted the Insig-binding domain. The cytosolic L6 contains the MELADL sequence motif that binds to Sec24/Sec23, subunits of Sar1-COPII proteins (22). The luminal L7 (aa535–710) interacts with L1. The L1-L7 interaction is regulated by cholesterol and mediates the conformation of L6, thereby controlling the binding between SCAP and COPII vesicle proteins (22). Mechanistically, cholesterol binding dissociates L1 from L7, causing a conformational change in L6 that block access of the MELADL motif from Sec24. The dissociation of L1 and L7 also open the space for Insig binding to transmembrane helices 2–6, thereby increases Insig binding to SCAP (23). It was revealed that tyrosine 234 in L1 and tyrosine 640 in L7 are critical to L1-L7 interaction (23). In addition, 3 N-glycosylation sites arginine 263 that locates in L1 and arginine 590 and 641 that locate in L7 (24). N-glycosylation of SCAP increases the protein stability by protecting SCAP from proteasomal degradation and is required for SREBP processing in response to sterol depletion or growth factor induced signalings (25).

Notwithstanding the detail knowledge about the functional domains in N-terminal of SCAP, the only known function of C-terminal SCAP is its ability to bind to SREBP (26). Based on sequence homology analysis, there are at least 4 and maybe 7 WD40-repeats that may presumably form a WD40 domain in the C-terminus of human SCAP. Indeed, as demonstrated by the crystal structure of Scp1-Sre1 complex, the homologs of human SCAP-SREBP1 complex in fission yeast, the C-terminal of Scp1 is comprised of a WD40 domain (27, 28). The WD40 domain is characterized by its unique β -propeller structure that creates 3 large surfaces, the top, bottom, and circumference, for multiple protein-protein interactions. Hence, a WD40 domain-containing protein, often referred to as a WD40 protein, can serve as a protein hub that mediates protein-protein interaction between a wide array of proteins and helps the formation of large protein complexes (29). Hence, it is likely that in addition to SREBP, SCAP may also interact with other proteins using its WD40 domain and regulate or be regulated by such interactions.

Supporting the idea that SCAP may also bind to other proteins, a recent finding reveals that SCAP acted as an ER adaptor that interacted with the stimulator of interferon genes (STING) and recruited interferon regulatory factor 3 (IRF3). By interacting with STING and IRF3, SCAP aided the formation

of the STING/IRF3 signalosome in antiviral response triggered by foreign DNA (30). Mechanistically, STING interacted with the N-terminal transmembrane domain of SCAP, whereas IRF3 bound to the C-terminal cytosolic domain of SCAP. Interaction between SCAP and STING facilitated the translocation of the complex from ER to Golgi and then to the perinuclear microsome, where IRF3 was recruited to the STING signalosome to trigger antiviral responses. This report demonstrated the ability of SCAP to interact with proteins beyond SREBP and regulate pathways beyond lipid metabolism.

1-3. Heat shock protein 90

Heat shock proteins (Hsp) are a family of protein chaperones that ensure the correct folding of newly synthesized proteins. These proteins are often upregulated upon heat and are therefore given the name as 'heat shock proteins.' However, they can function beyond responding to heat stress but also to other form of stress, including cold, oxidative, and ER stress (31). Heat shock protein 90 (Hsp90) is one of the most conserved and universally expressed chaperones that stabilizes and mediates the maturation of a wide array of proteins, often referred to as Hsp90 'clients.' Hsp90 is conserved in bacteria, plants, and animals, and expresses in most tissues and cellular compartments including mitochondria, chloroplasts, membranes, and cytosol (32). Hsp90 interacts with more than 20 co-chaperones and forms complexes with more than 200 protein clients that are involved in most of the key cellular processes, including cell proliferation, signal transduction, protein trafficking, and immune responses. Moreover, Hsp90 is also one of the most abundant proteins in the cytoplasm, accounting 1–2% of total protein levels (33).

Although Hsp90 is already highly abundant in the cytoplasm, it is further transcriptionally induced in response to stress. In most species, eukaryotic genomes include genes of both constitutively expressed and inducible Hsp90. For instance, human genome includes genes of constitutively expressed Hsp90- β and inducible Hsp90- α . Induction of Hsp90 gene expression is controlled by heat shock factor 1 (HSF-1), which also induces hundreds of other stress response genes (34, 35). Mechanistically, under normal condition, HSF-1 is itself also a client of Hsp90; however, after maturation it is locked with Hsp90 and Hsp70, a co-chaperone of Hsp90, thus keeping it in an inactive state. When induced by stress, HSF-1 is released from the Hsp90-Hsp70 chaperoning complex to exert transcription activity. Therefore, Hsp90 plays an important role in regulating stress responses such as heat shock response since HSF-1 induces the transcription of Hsp90 gene and the genes of other heat shock proteins, including Hsp70 (36).

The structure of Hsp90 is consisted of an N-terminal ATP-binding domain, a middle domain, and a C-terminal dimerization domain containing a Met-Glu-Glu-Val-Asp (MEEVD) motif that is critical to the spontaneous dimerization of Hsp90. The 3 domains are linked by linkers rich in charged amino acid residues (37–39). Although the chaperoning mechanism by which Hsp90 mediate the maturation of its client is complex and not yet fully understood, it is demonstrated that ATP-binding to the N-terminus of Hsp90 is critical to the chaperoning cycle of Hsp90. Mechanistically, Hsp90 dimer forms a clamp-like

shape and transforms between an open and a closed conformation. ATP-binding locks Hsp90 dimer in a closed state whereas hydrolysis of ATP had the opposite effect. Hsp90 inhibitors that bind to the ATP-binding site inhibit the activity of Hsp90. Such inhibitors include natural products like Radicol, and chemicals like geldanamycin (GA) and its analogs 17-N-allylamino-17-demethoxygeldanamycin (17-AAG) and 17-dimethylaminoethylamino-17-demethoxygeldanamycin (17-DMAG).

1-4. Hsp90 and SREBP in metabolic diseases and cancers

The multi-functional ability of Hsp90 to regulate most of the important cellular processes made it an attractive target for anti-cancer therapy, providing an opportunity for a single-target multi-hit strategy. In fact, Hsp90 is highly expressed in most human cancers, presumably resulting in the dysregulation of key signaling pathways including the MAPK, PI3K/Akt, mTOR, AMPK, and p53 pathways (40). Thus, Hsp90-based anti-cancer strategies and specific Hsp90 inhibitors have been developed in past decades (41). In addition to playing pivotal roles in cancer, recent studies also imply the implication of Hsp90 in metabolic diseases like non-alcoholic fatty liver disease (NAFLD) and alcoholic cirrhosis (42, 43).

On the other hand, it has been demonstrated that both the expression and processing of SREBPs are enhanced in diabetic and obese mice (14, 44, 45). Moreover, the activation of SREBP and the resultant accumulation of excessive lipids is one of the major causes of insulin resistance (46). Thus, strategies targeting SREBP have been developed in the past decades to fight metabolic diseases such as obesity and type 2 diabetes. Interestingly, since lipids not only comprise a significant portion of stored energy but are also key constituent of cellular membrane and the backbone of steroid hormone, they are also critical to the survival, function and proliferation of cells. Thus, it is expected that dysregulated SREBP activation and lipid biogenesis are observed in most cancers (47). Correspondingly, recent studies have demonstrated the involvement of the SCAP/SREBP pathway in tumorigenesis (25, 48, 49).

1-5. Aim of study

Despite the detail knowledge of the membrane-bound portion of SCAP, little is known about the C-terminal domain of SCAP. In this study, we aimed to uncover the molecular detail of the SCAP/SREBP interaction. In addition, with the attempt to discover new SCAP-binding proteins that participate in the regulation of SREBP pathways, we identified Hsp90 as a new SCAP/SREBP regulator. We performed a series of experiments to investigate the interaction between Hsp90 and SCAP/SREBP complex and to elucidate the regulatory mechanism of Hsp90 on SREBP and lipid biogenesis. We showed that Hsp90 regulated lipid homeostasis through directly controlling the protein level of SCAP and SREBP.

CHAPTER 2

**Hsp90 physically interacts with
the C-termini of SCAP and SREBP**

2-1. Preface

The C-terminal of SCAP is consisted of a WD40 domain, which is capable of interacting with a wide arrays of proteins. In this study, we aimed to identify the proteins that bind to SCAP C-terminus of by a mass spectrum-based proteomic approach. In brief, we overexpressed human SCAP C-terminus tagged with 3 tandem FLAG epitopes (FLAG-SCAP) in human embryonic kidney 293 cells. SCAP-binding proteins were co-precipitated with FLAG-SCAP by anti-FLAG immunoprecipitation and subjected to electrospray ionization quadrupole time-of-flight mass spectrum (ESI-Q-TOF MS) analysis. We found Hsp90 as a potential SCAP-binding protein and perform subsequent experiments to study interactions involved in the Hsp90/SCAP/SREBP protein complex.

2-2. Materials and Methods

Reagents

Protease inhibitor cocktail and calpain inhibitor were purchased from Nacalai Tesque (Kyoto, Japan). PMSF and 3× FLAG peptides were purchased from Sigma-Aldrich (Saint Louis, MO). HyClone FBS and Protein G Sepharose 4 Fast Flow were purchased from GE Healthcare Life Sciences (Chicago, IL). DMEM was purchased from Wako (Osaka, Japan). Other commonly used chemicals were purchased either from Wako or Nacalai Tesque.

Antibodies

Anti-FLAG M2 affinity gel, mouse IgG-agarose, EZview™ red anti-c-Myc affinity gel, EZview™ red protein G affinity gel, monoclonal mouse anti-FLAG (M2), polyclonal rabbit anti-c-Myc, and monoclonal mouse anti-β-actin (AC-15) antibodies were purchased from Sigma-Aldrich. Monoclonal mouse anti-SREBP1 (2A4), anti-SREBP2 (1C6), anti-Hsp90 (F-8), and anti-Hsp70 (3A3), polyclonal goat anti-SCAP (C-20) antibodies, normal mouse IgG control antibodies were purchased from Santa Cruz Biotechnology (Santa Cruz, CA). Peroxidase-conjugated affinity-purified donkey anti-mouse IgG, peroxidase-conjugated affinity-purified donkey anti-rabbit IgG, and peroxidase-conjugated affinity-purified donkey anti-goat IgG were purchased from Jackson ImmunoResearch (West Grove, PA).

Plasmid constructs

The coding sequence of full length (aa2–1279) and C-terminus (aa732–1279) of human SCAP was cloned into p3×FLAG-CMV-7.1 vector (Sigma-Aldrich) using NotI and XbaI restriction enzyme sites to construct FLAG-fl-SCAP and FLAG-C-SCAP, respectively. The N-terminus (aa2–731) of human SCAP was cloned into p3×FLAG-CMV-7.1 vector (Sigma-Aldrich) using HindIII and NotI restriction enzyme sites to construct FLAG-N-SCAP plasmid. The coding sequence of full length (aa2–1177), N-terminus (aa2–487), and C-terminus of human SREBP1a (aa593–1177) were cloned into p3×FLAG-CMV-7.1 vector by NotI and XbaI restriction sites to construct FLAG-fl-, N-, and C-SREBP1 plasmids,

respectively. The coding sequence of full length (aa2–1141), N-terminus (aa2–481), and C-terminus of human SREBP1a (aa555–1141) were cloned into p3×FLAG- CMV-7.1 vector using NotI and XbaI restriction sites to construct FLAG-fl, N-, and C-SREBP2 plasmids, respectively. The coding sequence of human Hsp90-β (aa1–724) and a synthesized oligonucleotide encoding two tandem c-Myc epitopes were cloned into pcDNA3.1/Hygro (+) vector (Thermo Fischer Scientific, Waltham, MA) by NheI/NotI and NotI/XbaI sites, respectively to construct Myc-Hsp90 plasmid. The primer sequences for cloning PCR fragments for plasmid construction are listed in Supplementary Table S1.

Cell cultures

HEK293 cells were maintained in complete DMEM supplemented with 10% (v/v) FBS, 100 units per ml penicillin, and 100 µg per ml streptomycin. One day before transfection, the cells were seeded in 100-mm dishes or 6-well plates at a density of 1×10^6 per dish or 2.5×10^5 per well, respectively. At a confluency of 50%–70%, the cells were transfected with indicated plasmids by the calcium phosphate method. In brief, plasmids were mixed with 125 mM calcium chloride in 1×HBSS buffer by bubbling for 20–30 times. The plasmids/calcium mix was incubated at room temperature for 20 min and then was applied to the cells. A total of 5 µg or 2 µg of plasmids were applied to the cells cultured in 100-mm dishes or 6-well plates, respectively. One day after transfection, the culture medium was replaced by fresh medium. The cells were harvested for anti-FLAG or anti-c-Myc immunoprecipitation 36–48 h after transfection. We also used HepG2 cells to study the binding between endogenous Hsp90 to SCAP and SREBP. The cells were maintained in complete DMEM medium and seeded in 100-mm dishes at a density of 3×10^6 cells per dish and harvested 48 h after seeding for anti-Hsp90 immunoprecipitation. All cell cultures were maintained in a humidified incubator at 37°C under an atmosphere of 5% CO₂.

Immunoprecipitation

The lysis buffer for immunoprecipitation is consisted of 25 mM Tris-HCl (pH 7.4), 150 mM NaCl, 1 mM EDTA, 5% glycerol, and 0.5% Nonidet P-40. Immediately before applying to the cells, protease inhibitor cocktail, PMSF, and Calpain inhibitors were added to the lysis buffer to a final concentration of 1% (v/v), 1 mM, and 0.5 mM, respectively. For anti-FLAG or anti-c-Myc immunoprecipitation, HEK293 cells transfected with indicated plasmids were washed with 2.5 ml per dish or 0.5 ml per well of ice-cold PBS and then harvested in 2.5 ml or 0.5 ml of ice-cold PBS by a cell scraper. The following procedures were carried out either on ice or at 4°C using ice-cold buffers. The cells were centrifuged at $1,500 \times g$ for 5 min and the cell pellet was resuspended in 2.5 ml or 0.5 ml of lysis buffer by vortexing for 10 sec. The cells were homogenized by passing through a 25-gauge needle 20 times followed by centrifugation at $13,000 \times g$ for 10 min to remove debris and insoluble. The supernatant cell lysates were collected, in which 50 µl was saved as the sample for input control, and the rest of the cell lysates were precleared by incubating with either mouse IgG agarose or EZview™ red protein G affinity gel (100 µl or 20 µl per sample) for at least 1 h with gentle rotation to remove non-specific binding proteins. Anti-FLAG or anti-c-Myc immunoprecipitation was performed using the cell lysates precleared by mouse IgG agarose or EZview™ red protein G affinity gel, respectively. Immunoprecipitation was carried out using anti-FLAG M2 affinity gel or EZview™ red anti-c-Myc affinity gel following the manufacturer's

protocol. For mass spectrum analysis, the anti-FLAG immunoprecipitated samples were eluted by 3× FLAG peptides. For the other immunoprecipitation experiments, the immunoprecipitated gels were washed with 25 volumes of PBS for three times and then resuspended in 1× Laemmli dye. The 50 µl input cell lysates were mixed with 10 µl of 6× Laemmli dye. The suspended gels and the input lysates were incubated in a 95°C heat block for 5 min, cooled down on ice for 10 min, and then centrifuged at 13,000×g for 10 min. The supernatant was collected for immunoblotting. A similar method was used for anti-Hsp90 immunoprecipitation. In brief, HepG2 cell lysates were precleared by incubation with 60 µl protein G Sepharose for at least 2 h with gentle rotation, and then the precleared cell lysates were incubated with either anti-Hsp90 antibody or normal mouse control antibody for at least 2 h with gentle rotation. Finally, 60 µl of protein G Sepharose was applied to the lysates/antibody mix, and the reaction was incubated for at least 2 h with gentle rotation. The 6× Laemmli dye is consisted of 1 M Tris-HCl pH 6.8, 30% glycerol, 10% SDS, and 0.03% bromophenol blue.

Silver staining and protein mass spectrometry analysis

Anti-FLAG immunoprecipitated samples from HEK293 cells transfected with either control vectors or FLAG-C-SCAP expression plasmids were subjected to SDS-PAGE and analyzed by silver staining by SilverQuest™ Silver Staining Kit (Thermo Fisher Scientific) following the manufacturer's protocol. The immunoprecipitated samples from control or FLAG-C-SCAP transfected cells were digested with sequence-grade trypsin. The resulting peptides were analyzed by electrospray ionization-quadrupole-time of flight mass spectrometry. The peptide sequences acquired from mass spectrum were analyzed using the Swiss-Prot protein sequence database under genus restriction of *Homo sapiens* using the in-house licensed Mascot searching program (version 2.1.03).

Immunoblotting

The input and immunoprecipitated samples were separated by SDS PAGE and then transferred to an Immobilon-P membrane (GE Healthcare Life Sciences). The membrane was blocked by 5% skim milk for 1 h at room temperature and was then immunoblotted with indicated primary antibodies following manufacture's manuals. The primary antibodies were incubated with peroxidase-conjugated secondary antibodies, and detected by using Amersham ECL Western Blotting Detection Reagent (GE Healthcare Life Sciences) or Immobilon Western Chemiluminescent HRP Substrate (Merck Millipore). In between the application of primary antibody, secondary antibody, and detection reagents, the membrane was washed with PBS supplemented with 0.1% TWEEN 20 for three times. Data acquisition and analysis were performed using an ImageQuant LAS 4000 system (GE Healthcare and Life Sciences).

2-3. Results

To search for potential regulator of SCAP/SREBP that binds to SCAP C-terminus, we transfected HEK293 cells with FLAG-tagged C-terminal SCAP (FLAG-C-SCAP) expression plasmids or control vectors and performed immunoprecipitation using anti-FLAG affinity resin. Silver staining analysis of the precipitated samples revealed a number of specific proteins that was bound to FLAG-C-SCAP (**Fig. 1A**). The precipitated protein samples were trypsinized, and the resulting peptides were analyzed with an electrospray ionization quadrupole time-of-flight mass spectrum. Mass spectrum analysis revealed 28,262 sequences matching 293 proteins from the FLAG-C-SCAP sample, and 25,373 sequences that matched 128 proteins from the control sample. Proteins that were identified only in the FLAG-C-SCAP sample were viewed as potential SCAP-binding partners. The potential SCAP-binding proteins that had high sequence coverage among other candidate proteins are shown in **Table 1**, which include a number of heat shock proteins Hsp90- β , Hsp90- α , and Hsp70. A list of proteins that were specifically identified in the FLAG-C-SCAP sample is shown in Supplementary Tables S2. We were particularly interested in Hsp90 because of emerging evidence of Hsp90 involvement in lipid metabolism (50–52).

Immunoblot analysis of the anti-FLAG immunoprecipitated samples showed that endogenous Hsp90 were bound to FLAG-C-SCAP and that SREBP precursors were also presented in the precipitates (**Fig. 1B**). We next employed overexpressed protein system to further study the protein-protein interactions in Hsp90/SCAP and Hsp90/SREBP. Myc-tagged Hsp90 was co-overexpressed with FLAG-tagged full length (fl) SCAP, SREBP1, or SREBP2 in HEK293 cells for anti-Myc IP. As a result, FLAG-fl-SCAP as well as FLAG-fl-SREBP1 and FLAG-fl-SREBP2 were co-precipitated with Myc-Hsp90 (**Fig. 2**). These results exhibit the ability of Hsp90 to interact with both SCAP and SREBP, suggesting the formation of a Hsp90/SCAP/SREBP complex. To verify the formation of Hsp90/SCAP/SREBP by endogenous proteins, anti-Hsp90 immunoprecipitation was performed using HepG2 cell lysates. The experiment showed that both SCAP and SREBP precursors were co-precipitated with Hsp90 (**Fig. 3**). The co-chaperone Hsp70 was also co-precipitated with Hsp90 (**Fig. 3**).

We showed that Hsp90 binds to the membrane-bound full-length and the C-terminus of SCAP (**Fig. 1–3**). To exclude the possibility that Hsp90 might also bind to the N-terminal transmembrane domain of SCAP, we examined the binding between overexpressed FLAG-tagged N-terminal SCAP (N-SCAP) to Myc-Hsp90. We demonstrated that only the C-terminal and full-length SCAP but not the N-terminal domain of SCAP were capable of interacting with Myc-Hsp90 (**Fig. 4**). Since the C-terminal domain of SCAP bound to Hsp90 and interacted with the C-terminal domain of SREBPs, it seemed plausible that Hsp90 associates with the C-terminal domain of SREBPs. To rule out the possibility of the interaction between Hsp90 and the N-terminal transcription factor domain of SREBPs, we tested the binding between FLAG-tagged N-terminus of SREBPs (N-SREBP) to Myc-Hsp90. Anti-Myc immunoprecipitation revealed that only the C-terminus of SREBPs but not the N-terminus were co-precipitated with Myc-Hsp90 (**Fig. 5 and 6**), indicating that Hsp90 interacted with SREBPs via the C-terminal domains.

Table 1. Mass spectrometric identification of SCAP and its binding Hsps

Protein	Accession No.	# of identified peptides	#of matching sequences	Sequence coverage
SCAP	NM_012235	49	14	32%
Hsp90- β	NM_001271969	32	17	31%
Hsp90- α	NM_001017963	21	14	21%
Hsp70	NM_002155	16	8	15%

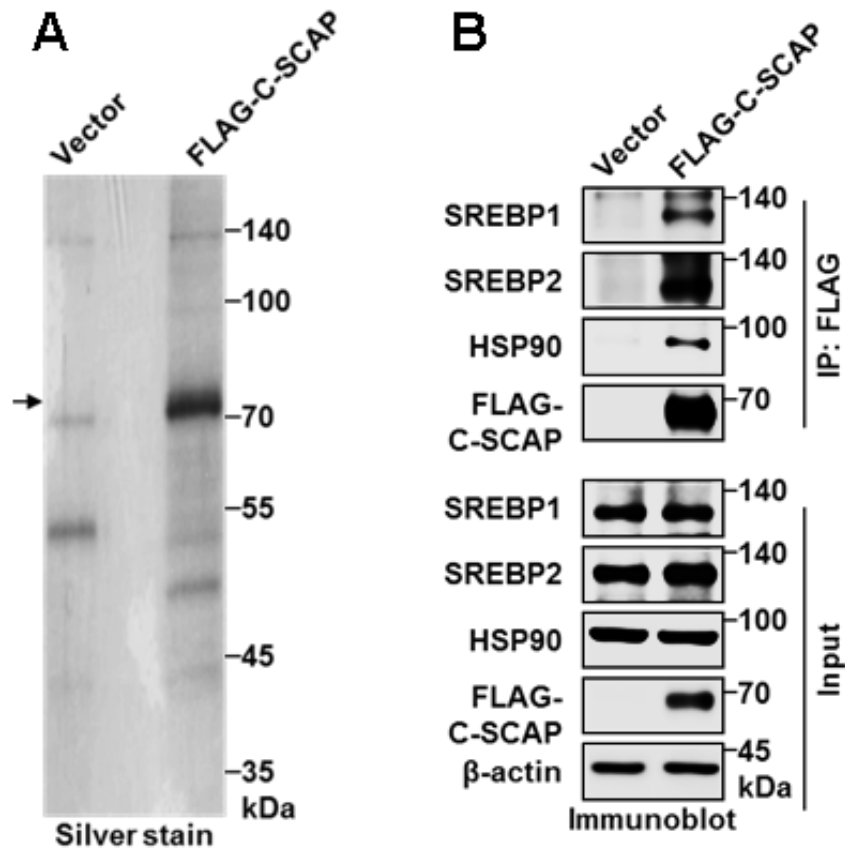


Fig. 1. Silver staining and immunoblot analysis of the anti-FLAG immunoprecipitates obtained from vectors or FLAG-C-terminal SCAP plasmids transfected HEK293 cells

Anti-FLAG immunoprecipitation was conducted using HEK293 cells transfected with control vectors or FLAG-C-terminal SCAP (FLAG-C-SCAP) plasmids. The precipitated samples were analyzed by (A) silver staining and (B) immunoblotting using anti-SREBP1 (2A4), anti-SREBP2 (1C6), anti-Hsp90 (F-8), anti-FLAG (M2), and anti- β -actin (AC15) antibodies. The input samples were immunoblotted as controls. The arrow indicates the major band corresponding to FLAG-C-SCAP.

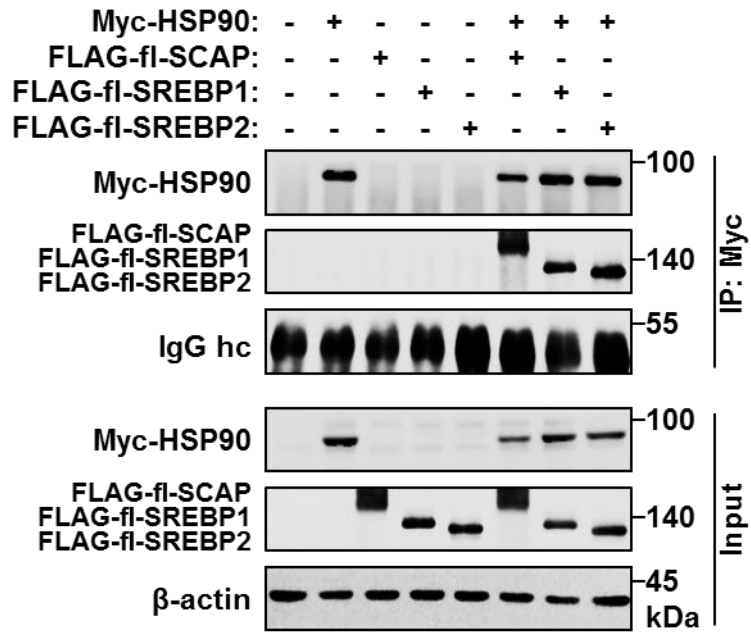


Fig. 2. Myc-Hsp90 interacts with FLAG-tagged full-length (fl) SCAP and SREBPs

Anti-Myc immunoprecipitation was conducted using HEK293 cells transfected with control vectors or indicated combination of plasmids. The immunoprecipitated samples and the input cell lysates were analyzed by immunoblots using anti-c-Myc, anti-FLAG (M2), and anti- β -actin antibodies. Heavy chain of IgG (IgG hc) and β -actin serves as loading controls for precipitated and input samples, respectively.

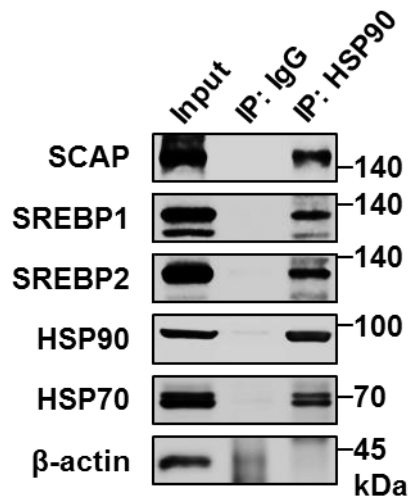


Fig. 3. Endogenous Hsp90 interacts with SCAP and SREBPs in HepG2 cells

Immunoprecipitation was conducted using anti-Hsp90 (F-8) or normal mouse antibodies on HepG2 cells. Precipitated samples and input lysates were analyzed by immunoblots using anti-SREBP1 (2A4), anti-SREBP2 (1C6), anti-Hsp90 (F-8), anti-Hsp70 (3A3), and anti- β -actin (AC15) antibodies.

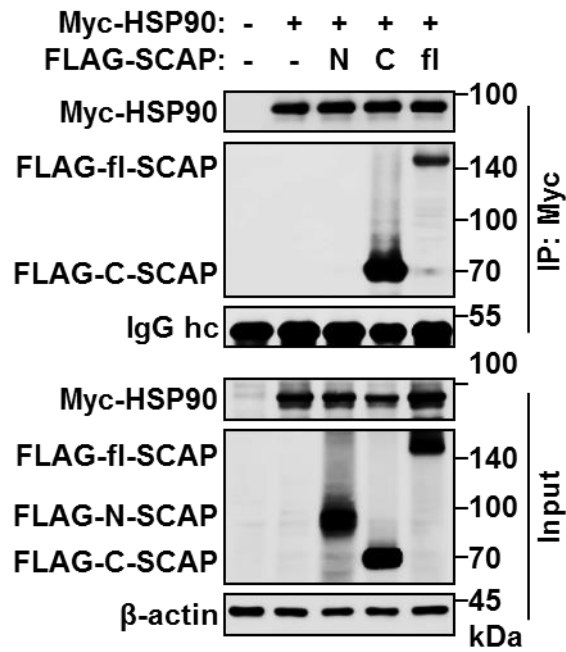


Fig. 4. Hsp90 interacts with the C-terminal but not the N-terminal of SCAP

Anti-Myc immunoprecipitation was conducted using HEK293 cells transfected with control vectors or Myc-Hsp90 plasmids in combination with vectors, FLAG-tagged full-length (fl), N-terminal (N), or C-terminal (C) SCAP plasmids. The immunoprecipitated samples and the input lysates were analyzed by immunoblots using anti-c-Myc, anti-FLAG (M2), and anti- β -actin antibodies. The heavy chain of IgG (IgG hc) and β -actin serves as the input control for immunoprecipitated and input samples, respectively.

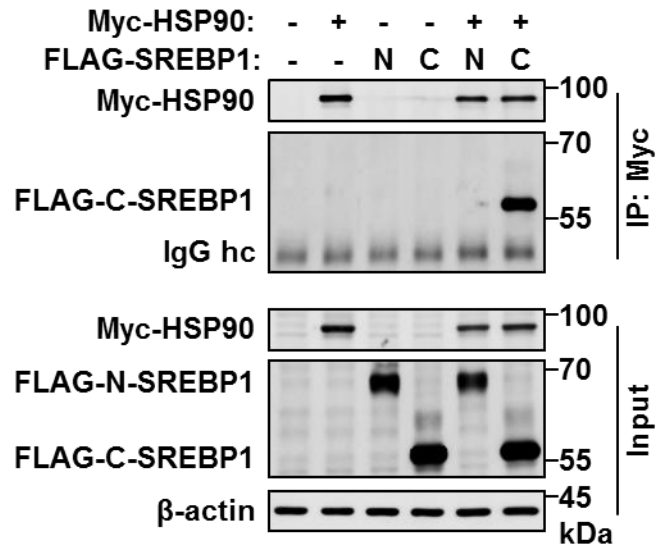


Fig. 5. Hsp90 interacts with the C-terminal but not the N-terminal of SREBP1

Anti-Myc immunoprecipitation was conducted using HEK293 cells transfected with control vectors or Myc-Hsp90 plasmids in combination with vectors, FLAG-tagged N-terminal (N), or C-terminal (C) SREBP1 plasmids. The precipitated samples and the input cell lysates were analyzed by immunoblots using anti-c-Myc, anti-FLAG (M2), and anti- β -actin antibodies. The heavy chain of IgG (IgG hc) and β -actin serves as the input control for immunoprecipitated and input samples, respectively.

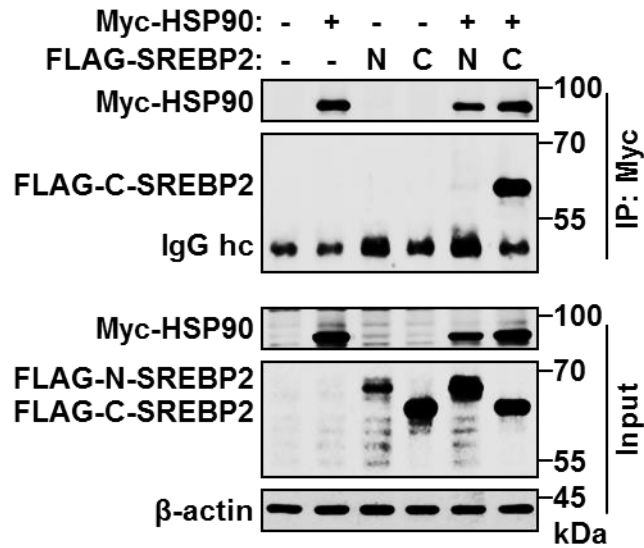


Fig. 6. Hsp90 interacts with the C-terminal but not the N-terminal of SREBP2

Anti-Myc immunoprecipitation was conducted using HEK293 cells transfected with control vectors or Myc-Hsp90 plasmids in combination with vectors, FLAG-tagged N-terminal (N), or C-terminal (C) SREBP2 plasmids. The precipitated samples and the input cell lysates were analyzed by immunoblots using anti-c-Myc, anti-FLAG (M2), and anti- β -actin antibodies. The heavy chain of IgG (IgG hc) and β -actin serves as the input control for immunoprecipitated and input samples, respectively.

2-4. Discussion

Taking advantage of its β -propeller structure, WD40 domain is perhaps one of the most promiscuous domains that can form protein-protein interactions with multiple partners. As shown by the structure of the fission yeast SCAP homolog Scp1, the C-terminus of SCAP is consisted of a WD40 domain (26, 27), suggesting the potential of SCAP to interact with other protein partners in addition to SREBP.

Here we demonstrate by a mass spectrum-based protein screening experiment that SCAP C-terminus can indeed interact with potentially a wide array of proteins. We were particularly interested in Hsp90 owing to its implications in cancer and lipid metabolism. We show that Hsp90 binds to the cytosolic C-termini of SCAP/SREBPs using overexpressed or endogenous protein systems. Taipale and colleagues has previously uncovered a potential Hsp90 client-binding fold in WD40 domains (53). The SCAP-Hsp90 interaction demonstrated here can serve as a biochemical evidence. We noticed that Hsp90 is a cytoplasmic chaperone that stabilizes or facilitates maturation of mostly cytoplasmic proteins. However, it is also reported that Hsp90 interacts with or is a subunit of membrane-bound protein complexes. The Hsp90 chaperone system was reported to control the ER-associated degradation and maturation of the thiazide-sensitive cotransporter (NCC), which is the primary mediator of salt reabsorption in animals. Inhibition of Hsp90 activity accelerated NCC degradation through a proteasomal pathway, whereas Hsp70/Hsp90 organizer proteins stabilized NCC proteins (54).

In summary, we discovered Hsp90 as a new SCAP C-terminus-binding partner, and as supported by our immunoprecipitation experiments and by previous researches, we confirm that cytoplasmic Hsp90 can interact with the cytosolic C-terminal domains of membrane-bound proteins, such as SREBPs and SCAP. Since Hsp90 functions as one of the most important protein chaperones that regulates most of the key cellular processes and has been reported to participate in adipocyte differentiation and lipid biosynthesis (50–52), we went on to investigate its functions on SCAP and SREBPs.

CHAPTER 3

**Hsp90 modulates lipid homeostasis by
regulating the stability of SCAP and SREBP**

3-1. Preface

In **Chapter 2**, we demonstrate the discovery of Hsp90 as a SCAP C-terminal-binding protein. Hsp90 is involved in most of the important cellular processes, including cell proliferation, cell cycle, and cell metabolism (55, 56). Since Hsp90 regulates most of the vital signaling pathways in cells, it is therefore not surprising that Hsp90 is highly expressed in human cancers (57–59). Notably, increased expression of SREBP is also a common feature in cancer cells and is usually accompanied by a dysregulated lipid biosynthesis (47). SREBP provides cancer cells with fatty acids and cholesterol, which are essential for survival and progression of cancer. However, the link between Hsp90 and SREBP is poorly understood. In this study, we conducted a series of *in vitro* and *in vivo* experiments using mostly HepG2 cells and C57/BL6 mice to demonstrate the relation between Hsp90, SCAP/SREBP, and lipid homeostasis.

3-2. Materials and Methods

Reagents

17-N-allylamino-17-demethoxygeldanamycin (17-AAG) was purchased from LKT Laboratories (St. Paul, MN). 17-Dimethylaminoethylamino-17-demethoxygeldanamycin (17-DMAG) was purchased from FERMENTEK (Jerusalem, Israel). Cholesterol, protease inhibitor cocktail, and Calpain inhibitor, were purchased from Nacalai Tesque (Kyoto, Japan). 25-hydroxycholesterol, cycloheximide, MG132, DMEM, and DMEM/Ham's F-12 were purchased from Wako (Osaka, Japan). HyClone FBS were purchased from GE Healthcare Life Sciences (Chicago, IL). Lipofectamine® RNAiMAX Transfection Reagent, Lipofectamine® LTX with Plus™ Reagent, and High Capacity cDNA Reverse Transcription Kits were purchased from Thermo Fisher Scientific (Waltham, MA). L-mevalonic acid sodium salt, control siRNA-A and Hsp 90 α/β siRNA (h) were purchased from Santa Cruz Biotechnology (Santa Cruz, CA). ISOGEN was purchased from Nippon Gene (Tokyo, Japan). Other common chemicals were purchased either from Wako or Nacalai Tesque.

Antibodies

Monoclonal mouse anti-Golgi 58K protein/formiminotransferase cyclodeaminase (58K-9), anti-FLAG (M2), and anti- β -actin (AC-15) antibodies were purchased from Sigma-Aldrich. Monoclonal mouse anti-SREBP1 (2A4), anti-SREBP2 (1C6), anti-Hsp90 (F-8), anti-Hsp70 (3A3) antibodies, polyclonal goat anti-SCAP (C-20) antibody, polyclonal rabbit anti-SREBP1 (C-20) antibody, and normal mouse IgG antibody were purchased from Santa Cruz Biotechnology (Santa Cruz, CA). Monoclonal rabbit anti-calnexin (C5C9) antibody was purchased from Cell Signaling Technology (Danvers, MA). Rabbit polyclonal anti-SREBP2 (RS004) antibody was produced in-house as described in a previous publication (60). Peroxidase-conjugated affinity-purified donkey anti-mouse IgG, donkey anti-rabbit

IgG, and donkey anti-goat IgG were purchased from Jackson ImmunoResearch (West Grove, PA).

Cell cultures

HepG2 cells were maintained in complete DMEM supplemented with 10% (v/v) FBS, 100 units per ml penicillin, and 100 µg per ml streptomycin. In some experiments, HepG2 cells were cultured under sterol depleted condition in DMEM supplemented with 100 units/ml penicillin, 100 µg/ml streptomycin, 50 µM sodium mevalonate, 12.5 µM fluvastatin, and 5% (v/v) lipoprotein deficient serum and treated with or without 1 µg/ml 25-HC or 10 µg/ml cholesterol to manipulate SREBP processing. CHO-7 cells were maintained in complete DMEM/Ham's F12 medium supplemented with 5% (v/v) FBS, 100 units per ml penicillin, and 100 µg per ml streptomycin. SRD-13A cells were maintained in DMEM/Ham's F12 medium supplemented with 5% (v/v) FBS, 100 units per ml penicillin, 100 µg per ml streptomycin, 5 µg/ml cholesterol, 1 mM sodium mevalonate, and 20 µM sodium oleate. All cell cultures were maintained in a humidified incubator at 37°C under an atmosphere of 5% CO₂.

17-AAG inhibition and small interfering RNA knockdown of Hsp90

HepG2, CHO-7, or SRD-13A cells were seeded in 6-well plates at a density of 5×10^5 per well. One day after seeding, the cells were treated with 0–3 µM of 17-AAG for 24–48 h. In some experiments, HepG2 cells were pretreated with 50 µM of cycloheximide, 10 µM of MG132, 50 µM of chloroquine, or 10 mM of ammonium chloride 30 min before 17-AAG treatment. In some experiments, SRD-13A cells were transfected with control vectors or FLAG-fl-SCAP plasmids (described in **Section 2-2, page 10–11**) using Lipofectamine® LTX with Plus™ Reagent following manufacture's protocol after the cells reached 50–70% confluency. One day after lipofection, the transfected cells were treated with 0–3 µM of 17-AAG for 24h. After appropriate treatments, the cells were harvested for immunoblot analysis, total RNA extraction, or intracellular triglycerides and total cholesterol measurements. For small interfering RNA (siRNA) knockdown experiments, HepG2 cells were reverse-transfected with Hsp 90α/β siRNA or control siRNA-A using Lipofectamine® RNAiMAX Transfection Reagent following manufacturer's protocol. The cells were harvested for immunoblotting experiments and intracellular triglycerides and total cholesterol measurements 3 days after lipofection.

Lentivirus preparation and transduction

The coding sequence of human Hsp90-β (aa1–724) was cloned into a lentiviral vector CSII-EF-MCS-IRES2-Venus (RIKEN, Japan) using NotI and BglII/BamHI restriction enzyme sites to construct Hsp90 lentivector. For virus packaging, HEK293T cells were cultured in 100-mm dishes at 2×10^6 overnight until reaching 70% confluence. The cells were transfected with Hsp90 or empty lentivector along with packaging plasmids pCAG-HIVgp (RIKEN) encoding VSV-G protein and HIV-1 Gag and Pol, and pCMV-VSV-G-RSV-Rev (RIKEN) encoding VSV-G protein and RSV Rev by the calcium phosphate method. To increase viral protein expression, 10 µM forskolin was applied to the cells 12 h after transfection. The virus-containing culture supernatant was collected 48 h after transfection and filtered through 0.45-µm sterile discs (Advantec, Japan). Viral titer was determined by transducing 2×10^6 HEK293T cells with 10-fold dilutions of virus supernatant. The percentage of Venus positive

cells was calculated 48 h after transduction to determine the transducing unit (TU) per ml of the virus. For Hsp90 overexpression, HepG2 cells were seeded in 6-well plates at 5×10^5 and transduced with Hsp90 or control lentivirus at a multiplicity of infection of 5 TU per cell in the presence of 4 $\mu\text{g/ml}$ polybrene 24 h after seeding. The virus-containing medium was replaced by fresh medium 24 h after transduction. Transduction efficiency was over 80% as estimated by the percentage of Venus positive cells 48 h after transduction. The cells were harvested for further analysis 72 h after transduction.

Immunoblotting

The following procedures were conducted on ice or at 4°C using ice-cold buffers. Properly treated HepG2, CHO-7, or SRD-13A cells were washed with 0.5 ml ice-cold PBS and then harvested with 0.5 ml ice-cold PBS. The cells were spin downed by centrifugation at $1,500 \times g$ for 5 min and resuspended in 150–300 μl of complete RIPA lysis buffer supplemented with 1% protease inhibitor cocktail, 1 mM PMSF, and 0.5 mM Calpain inhibitor. The RIPA buffer is consisted of 50 mM Tris-HCl pH 8.0, 150 mM NaCl, 0.5% deoxycholate, 0.1% SDS, and 1% Triton X-100. The cells were lysed for 30 min and then the insoluble and debris were removed by centrifugation at $13,000 \times g$ for 10 min. Total protein concentration in the cleared lysates were measured by BCA method using kits purchased from Thermo Fisher Scientific following company's protocol. The total protein concentration of each sample was adjusted to equality using RIPA buffer. The samples were mixed with 1/6 volume of 6 \times Laemmli dye, incubated in a heat block set at 95°C for 5 min, and then analyzed by immunoblotting or stored at -20°C. The method for immunoblotting is described in **Section 2-2 (page 12)**.

Real-time quantitative PCR

Total RNA in HepG2 cells or 100–150 mg of mouse liver was extracted using ISOGEN following manufacturer's protocol. RNA was reverse-transcribed to complementary DNA using High Capacity cDNA Reverse Transcription Kits following the manufacturer's protocol. Real-time quantitative PCR reaction mix were prepared using FastStart Universal SYBR Green Master (Roche, Indianapolis, IN) following manufacturer's protocol. The final cDNA concentration in each reaction is 0.5–1 μg . Data acquisition and analysis were conducted on an Applied Biosystems StepOnePlus™ Real-Time PCR System (Thermo Fisher Scientific). Relative mRNA level in HepG2 cells and mouse liver tissues were normalized to *18S* and *36B4*, respectively. Primer sequences are listed in Supplementary Table S3.

Triglyceride and cholesterol measurements

The following procedures were conducted on ice using ice-cold buffers. Properly treated HepG2 cells were washed twice with 0.5 ml PBS. Intracellular lipids were extracted by incubating the cells in 0.6 ml of hexane/chloroform (3:2 v/v) for 20 min. The lipid-containing solution was collected, vacuum dried, and resuspended in 60 μl of 2-propanol. Triglycerides and total cholesterol level was measured using kits purchased from Wako. The remaining cells were harvested to determine total protein content, which is used to normalize the lipid levels. To determine liver triglycerides and total cholesterol level, 100–150 mg of liver samples were weighed, homogenized in ice-cold chloroform/methanol (2:1, v/v), and incubated for 30 min at room temperature followed by adding 50 mM NaCl to separate organic

phase. The organic phase was washed twice with 0.36 M of CaCl₂/methanol (1:1, v/v) and then diluted with appropriate volume of chloroform to a final volume of 5 ml per sample. Triglycerides and total cholesterol level was measured using kits purchased from Wako.

Cell fractionation

To separate the ER and Golgi membranes, properly treated HepG2 cells were seeded in 100-mm dishes at a density of 3×10^6 per dish and cultured for 2 days. The following procedures were conducted on ice or at 4°C using ice-cold buffers. The cells were washed with 3 ml of PBS and then harvested with 3 ml PBS. The cells were spin downed by centrifugation at 1,500×g for 5 min and resuspended in 1 ml of fractionation buffer consisted of 50 mM Tris-HCl (pH 7.5) and 150 mM NaCl supplemented with 15% (w/v) sucrose. The cells were disrupted by passing through a 25-gauge needle 20 times. The homogenates was centrifuged at 3,000×g for 10 min for collecting supernatant. A discontinuous sucrose density gradient was prepared in a 2.2 ml polypropylene tube (Beckman Coulter, item# 347357) by layering fractionation buffer supplemented with the following densities of sucrose from bottom to top: 0.45 ml 45% sucrose, 0.75 ml 30% sucrose, 0.45 ml cell supernatant in 15% sucrose, and 0.3 ml 7.5% sucrose. The gradient solution was centrifuged in a Optima™ MAX-TL installed with a TLS-55 swing-bucket rotor (Beckman Coulter) with a program set as follows: 36,000 rpm for 2 h, 30,000 rpm for 1 h, 24,000 rpm for 1 h, 18,000 rpm for 1 h, 12,000 rpm for 1 h, and then slow down without application of a break. The resulting solution was collected from top to bottom into 10 fractions and analyzed by immunoblots. Presence of calnexin and Golgi 58K protein was viewed as markers for the ER and the Golgi apparatus, respectively. The ER and Golgi fractions were collected for further analysis.

Immunoprecipitation

Properly treated HepG2 cells were harvested for anti-Hsp90 immunoprecipitation as described in **section 2-2 (page 11–12)**. CHO-7 and SRD-13A cells were seeded in 100-mm dishes at a density of 3×10^6 per dish, cultured for 2 days and then harvested for anti-Hsp90 immunoprecipitation as described in **section 2-2 (page 11–12)**. The ER and Golgi fractions obtained from cell fractionation were diluted with lysis buffer to reduce sucrose concentration to 5%. The lysis buffer is consisted of 25 mM Tris-HCl pH 7.4, 150 mM NaCl, 1 mM EDTA, 5% glycerol, 0.5% Nonidet P-40, and supplemented with 1% protease inhibitor cocktail, 1 mM PMSF, and 0.5 mM Calpain inhibitor. The diluted ER and Golgi fractions were subjected to anti-Hsp90 immunoprecipitation as described in **section 2-2 (page 11–12)**.

In vivo evaluation of Hsp90 inhibition by 17-DMAG

All animal experiments were approved by the Institutional Animal Care and Use Committee of the University of Tokyo. A total of 10 male 8-week-old C57/BL6Ncrl mice were purchased from Charles River Laboratories (Wilmington, MA) and housed in the animal facility under controlled temperature and humidity with a 12-h light/dark cycle. The mice were acclimatized for 7 days and then randomly divided into 2 groups ($n = 5$). The mice were intraperitoneally (ip) injected with 5 mg/kg body weight of 17-DMAG or equal volume of PBS as a control for three times at 12-h intervals. The mice were euthanized 4 h after the last ip injection and the livers were excised for analysis.

Statistical analysis

Data are presented as mean \pm SD. Significant difference was determined by computing the *p*-values between groups using two-tailed equal-variance Student's *t* tests. The null hypothesis was rejected at *p* < 0.05. Statistical analysis was performed using Microsoft Excel software.

3-3. Results

3-3-1. Hsp90 regulates lipids biosynthesis by controlling SCAP and SREBP protein levels

To investigate the potential role of Hsp90 in SCAP/SREBP regulation, HepG2 cells were treated with Hsp90 inhibitor 17-N-allylamino-17-demethoxygeldanamycin (17-AAG), and the protein level of SCAP and SREBPs were determined. Dose-dependent decreases of SCAP protein and the precursor, N-terminal, and C-terminal SREBP1 and SREBP2 proteins were observed in the cells treated with 0–2 μ M of 17-AAG, whereas Hsp70 was dose-dependently increased by Hsp90 inhibition (**Fig. 7A**). The increase in Hsp70 protein served as a positive control of Hsp90 inhibition (61, 62). Corresponded to the decrease of matured N-terminal SREBP, the expression of SREBP-target genes was downregulated, and the intracellular triglycerides and total cholesterol levels were reduced by 17-AAG (**Fig. 7B and 7C**). Treating another hepatoma cell line Huh-7 and a Chinese hamster ovarian cell line CHO-7 with 17-AAG also resulted in dose-dependent reductions in SCAP and SREBP proteins (Supplementary Fig. S2), indicating that the effect was not limited to HepG2 or hepatoma cells.

To confirm the regulatory effect of Hsp90 on SCAP/SREBP, Hsp90 was knocked down by siRNA transfection. Hsp90 knockdown dramatically reduced the protein levels of SCAP and both the matured and precursor forms of SREBP1 and SREBP2 (**Fig. 8A**) and significantly decreased the intracellular triglycerides and total cholesterol levels (**Fig. 8B**). It has been observed in alcohol-induced livers that the protein and mRNA levels of Hsp90 were increased in parallel to the elevated triglyceride level (43). However, the causal relation between the increase of Hsp90 and triglycerides was not demonstrated. To investigate whether increase expression of Hsp90 protein directly affect SREBP and lipid homeostasis, we infected HepG2 cells with Hsp90-expressing lentivirus. As compared to the cells infected with control virus, the protein levels of Hsp90, SCAP, and both the precursor and matured SREBP1 and SREBP2, and the triglycerides and total cholesterol levels were higher in the cells infected with Hsp90-expressing lentivirus (**Fig. 9A and 9B**) These results indicated that Hsp90 played a critical role in regulating SCAP and SREBP proteins and lipid homeostasis.

3-3-2. 17-AAG induces proteasome degradation of SCAP/SREBP by inhibiting Hsp90-binding

To further study the effect of Hsp90 on SCAP/SREBP, we performed a time-course experiment revealing the different kinetics of SCAP and SREBP proteins in response to Hsp90 inhibition. A significant reduction in SCAP protein level was observed after 6 h of 17-AAG treatment, whereas SREBP protein level was decreased only after 10 h of 17-AAG treatment (**Fig. 10**). To test whether Hsp90 affects protein stability of SCAP and SREBP, we performed a cycloheximide chase assay to track the degradation rate of SCAP and SREBP. This assay revealed that treating HepG2 cells with 17-AAG accelerated SCAP and SREBP precursor degradation by 4-fold and 2-fold, respectively. The protein half-life of SCAP reduced from 32 h to 8 h, precursor SREBP1 decreased from 14 h to 6 h, and precursor SREBP2 decreased from 19 h to 9 h, respectively upon 17-AAG treatment (**Fig. 11**).

SCAP can be degraded through both the lysosome-dependent (63) and the proteasome dependent (25) pathways. We thus investigated whether 17-AAG-induced SCAP and SREBP degradation was through either pathway. HepG2 cells were treated with 17-AAG with or without the co-treatment of proteasome inhibitor MG132. While 17-AAG substantially reduced SCAP and SREBP precursor proteins, MG132 co-treatment abolished the effect, suggesting that Hsp90 protects SCAP and SREBP precursors from proteasome-dependent degradation (**Fig. 12A**). HepG2 cells were also cultured with 17-AAG with or without the co-treatment of lysosomal inhibitors chloroquine or ammonium chloride. However, these lysosomal inhibitors had negligible effect on 17-AAG-induced SCAP and SREBP degradation (**Fig. 12B**), ruling out the involvement of the lysosomal pathway.

17-AAG binds to the N-terminal ATP-binding pocket of Hsp90, which can cause the inhibition of the binding between Hsp90 and its clients (33). To investigate if 17-AAG hindered the interaction between Hsp90 and SCAP/SREBP, HepG2 cells were treated with 17-AAG in the presence of MG132 to protect SCAP and SREBP from degradation, and the binding between Hsp90 and SCAP/SREBP was studied by anti-Hsp90 immunoprecipitation. As demonstrated in **Fig. 12A**, in the presence of MG132, SCAP and SREBP proteins were protected from 17-AAG-mediated degradation (**Fig. 13, bottom**); however, the amount of SCAP and SREBP precursor proteins that was co-precipitated with Hsp90 was decreased substantially (**Fig. 13, top**), implying that 17-AAG hindered the Hsp90-SCAP/SREBP interaction. The increase in Hsp70 serves as a control of Hsp90 inhibition (**Fig. 12–13**).

3-3-3. SCAP is required for Hsp90-mediated SREBP regulation

The protein level of SCAP affects the stability of SREBP precursors and SREBP processing (6). Thus, we examined the possibility that Hsp90 regulates SREBP via SCAP. We took advantage of SRD-13A cells, a SCAP-deficient cell line derived from CHO-7 (6). Compared with CHO-7 cells, SRD-13A cells expressed negligible SCAP, relatively low level of SREBP1 precursor, and comparable levels of Hsp90 and β -actin (Supplementary Fig. S3).

When treated with 17-AAG, SREBP1 precursor was dose-dependently degraded in CHO-7 cells but not in SRD-13A cells (**Fig. 14 and 15, lanes 1–6**), implying that 17-AAG-induced SREBP degradation was SCAP-dependent. To demonstrate the direct involvement of SCAP, we transfected FLAG-fl-SCAP expression plasmids into SRD-13A cells and then treated the cells with 17-AAG. In cells transfected with control vectors, the protein level of SREBP1 precursor was nearly undetectable and remained at a steady level even in the presence of 17-AAG (**Fig. 15, lanes 4–6**). On the other hand, in the SRD-13A cells transfected with FLAG-fl-SCAP, SREBP1 precursor protein was restored to a comparable level to its CHO-7 counterpart, and was dose-dependently reduced by 17-AAG (**Fig. 15, lanes 7–9**). In addition, FLAG-fl-SCAP was also dose-dependently reduced by 17-AAG. Taken together, these results indicate that Hsp90 stabilizes SREBP1 precursor protein through an SCAP-dependent mechanism.

Since Hsp90 regulated SREBP through SCAP, we next investigated if it also interacted with SREBP via SCAP. To this end, anti-Hsp90 immunoprecipitation was performed using CHO-7 and SRD-13A cells. Unexpectedly, we detected SREBP1 precursor in the anti-Hsp90 precipitates from both CHO-7 and SRD-13A cell lysates (**Fig. 16**). This finding infers that Hsp90 interacts with SREBP independently to SCAP; however, this interaction alone is insufficient to fulfill its regulatory function on SREBP.

3-3-4. Hsp90 regulates SCAP/SREBP independently to intracellular sterols levels

The conformation of SCAP is modulated by its binding to cholesterol and to Insig, a sterol sensing protein that anchors SCAP to the ER membrane. The binding of cholesterol and 25-hydroxycholesterol (25-HC)-bound Insig to the transmembrane domain of SCAP alters the conformation of ER luminal loop 1 and loop 7 of SCAP, tightening the binding between SCAP and Insig. The conformation change also blocks the access of Sec24/23/Sar1 COPII proteins to the MELADL motif of cytosolic loop 6 of SCAP, which leads to the inhibition of ER-to-Golgi transport of the SCAP/SREBP complex (23, 24).

To further study the regulatory function of Hsp90 on SCAP and SREBP, we investigated whether changes in the intracellular sterol level modulate the binding between Hsp90 and SCAP/SREBP or the effect of 17-AAG. HepG2 cells were cultured in sterol depleted medium in the absence or presence of 25-HC or cholesterol, and the binding between Hsp90 and SCAP/SREBP was examined by anti-Hsp90 immunoprecipitation. A substantial increase in SREBP1 precursor and a modest increase in SREBP2 precursor proteins were observed when 25-HC was applied to the cells, whereas cholesterol moderately increased both SREBP precursor proteins (**Fig. 17, top**). The increase in SREBP precursors was caused by the inhibition of SREBP processing, judging from the corresponding decrease of processed SREBPs. Nonetheless, the amount of SCAP and SREBP precursor proteins that were co-precipitated with Hsp90 remained constant upon either 25-HC or cholesterol treatment (**Fig. 17, bottom**).

To study the regulation of Hsp90 on SCAP/SREBP during active or halted SREBP processing, we examined the effect of 17-AAG under sterol depleted condition in the absence or presence of 25-HC.

SREBP processing was highly activated in HepG2 cells cultured under sterol depleted condition and was drastically inhibited by application of 25-HC as observed by the phenomenal rise of precursor to processed SREBP ratio (**Fig. 18**). Nevertheless, 17-AAG consistently reduced both SCAP and SREBP proteins under both active and halted SREBP processing (**Fig. 18**). These results suggest that Hsp90 regulates SCAP and SREBP independently to the state of intracellular sterol level or SREBP processing.

We next examined the intracellular localization of the Hsp90/SCAP/SREBP complex. Since Hsp90 is known to be a cytoplasmic protein, we first examined the existence of Hsp90 on the membrane of ER and Golgi apparatus. HepG2 cells were cultured in complete or sterol depleted medium for 24 h and then harvested. The total cell lysates were separated by sucrose-density gradient ultracentrifugation into 10 fractions. The total cell lysates (input, fraction #0) and the density fractions were analyzed by immunoblot. The ER fractions (#8–10) and the Golgi fractions (#3–4) were determined by predominant existence of calnexin and Golgi 58K protein, respectively (**Fig. 19**). SCAP was predominantly found in the ER fractions under complete medium condition, whereas it was predominantly found in the Golgi fractions under sterol depleted condition. Under both conditions, Hsp90 was predominantly found in the light fractions (#2–5), while it was still detectable in the heavy fractions (**Fig. 19**). These findings demonstrate the co-existence of Hsp90 and SCAP on the ER and Golgi membrane.

To examine the binding between Hsp90 and SCAP, the input, ER, and Golgi fractions shown in **Fig. 19** were analyzed by anti-Hsp90 IP. As a result, Hsp90 was readily recovered by IP in the input (#0) and the Golgi (#3–4) fractions (**Fig. 20, lanes 3 and 9**). Although the Hsp90 protein level is relatively low in the ER (#8–10) fractions, it was enriched by IP (**Fig. 20, lanes 4 and 6**). Under both complete medium and sterol depleted conditions, we were able to detect SCAP in the anti-Hsp90 precipitates of the input (#0), ER (#8–10), and the Golgi (#3–4) fractions (**Fig. 20, lanes 3, 6, and 9**). This data infers that SCAP might be constantly bound to Hsp90 during its localization and its transport around ER and Golgi. Moreover, using antibodies against the C-terminal of SREBP, we were able to detect the cleaved C-terminal SREBP in the anti-Hsp90 IP precipitates (**Fig. 21**). This finding shows that Hsp90 stays associated with SCAP and SREBP after the cleavage of N-terminal SREBP. This finding also supports that Hsp90 regulates the stability of SCAP and SREBP proteins rather than their response to sterols.

The proposed role of Hsp90 to maintain lipid homeostasis is illustrated as in **Fig. 22**. Hsp90 binds to SCAP/SREBP precursor on the ER membrane, stabilizing the protein complex throughout the ER-to-Golgi transport and continues to associate and stabilize SCAP and the cleaved C-terminal of SREBP after SREBP processing in the Golgi apparatus. The dramatic decreases of SCAP and SREBP proteins and intracellular lipid levels underline the importance of Hsp90 in preserving a steady level of SREBP and SCAP protein, thereby allowing SREBP to perform its duty as the master transcription regulator of lipid biosynthesis. Nonetheless, the mechanism by which the cleaved C-terminal SREBP dissociates from SCAP and Hsp90, and how it affects SCAP recycling to the ER require further research.

3-3-5. Hsp90 regulates SCAP and SREBP and lipid homeostasis in mouse liver

Seeing the effect of Hsp90 inhibition in human hepatoma cells, we investigated whether Hsp90 had similar functions in mouse primary hepatocytes and livers. Primary mouse hepatocytes were prepared from C57/BL6NCrl mice and treated with 0–1 μ M of 17-DMAG, a chemical analog of 17-AAG that is preferentially used in *in vivo* experiments owing to its better water solubility (42, 43). Treating mouse primary hepatocytes with 17-DMAG resulted in a decrease in SCAP, SREBP1, and SREBP2 proteins and an increase in Hsp70 protein in a dose-dependent manner (**Fig. 23A**). Furthermore, 17-DMAG downregulated the mRNA levels of SREBP-target genes in mouse primary hepatocytes (**Fig. 23B**).

To examine the *in vivo* effect of Hsp90 inhibition, C57BL/6NCrl mice were ip injected with 5 mg/kg body weight of 17-DMAG or equivalent volume of PBS as a control for three times at 12-h intervals. Livers were excised from euthanized mice 4 h after the last injection. Corresponded to our *in vitro* data, 17-DMAG substantially reduced the protein level of SCAP, SREBP1, and SREBP2 proteins. A marked increase of Hsp70 protein indicated that 17-DMAG was delivered and inhibited Hsp90 activity in the mouse livers (**Fig. 24**). We also quantified the mRNA levels of SREBP-target genes in the liver tissues. Expression of SREBP1-target genes *Fasn*, *Acc1*, and *Scd1* was downregulated by 40%–60%, and expression of SREBP2-target genes *Hmgcr* and *Sqs* was reduced by 30%. Expressions of *Srebp1c* and *Srebp2* were also downregulated by 30%, whereas *Srebp1a*, which is not an SREBP-target, was not affected by 17-AAG (**Fig 25A**). Finally the triglycerides and total cholesterol levels in mouse livers were measured. In agreement with the decreased SREBP proteins and the downregulated SREBP-target genes, both triglycerides and total cholesterol levels in the mouse livers were reduced by 17-DMAG treatment (**Fig 25B**). Altogether, we conclude that Hsp90 is essential in stabilizing SCAP and SREBP proteins and facilitating SREBP function as a transcription regulator of lipid biosynthesis *in vivo*.

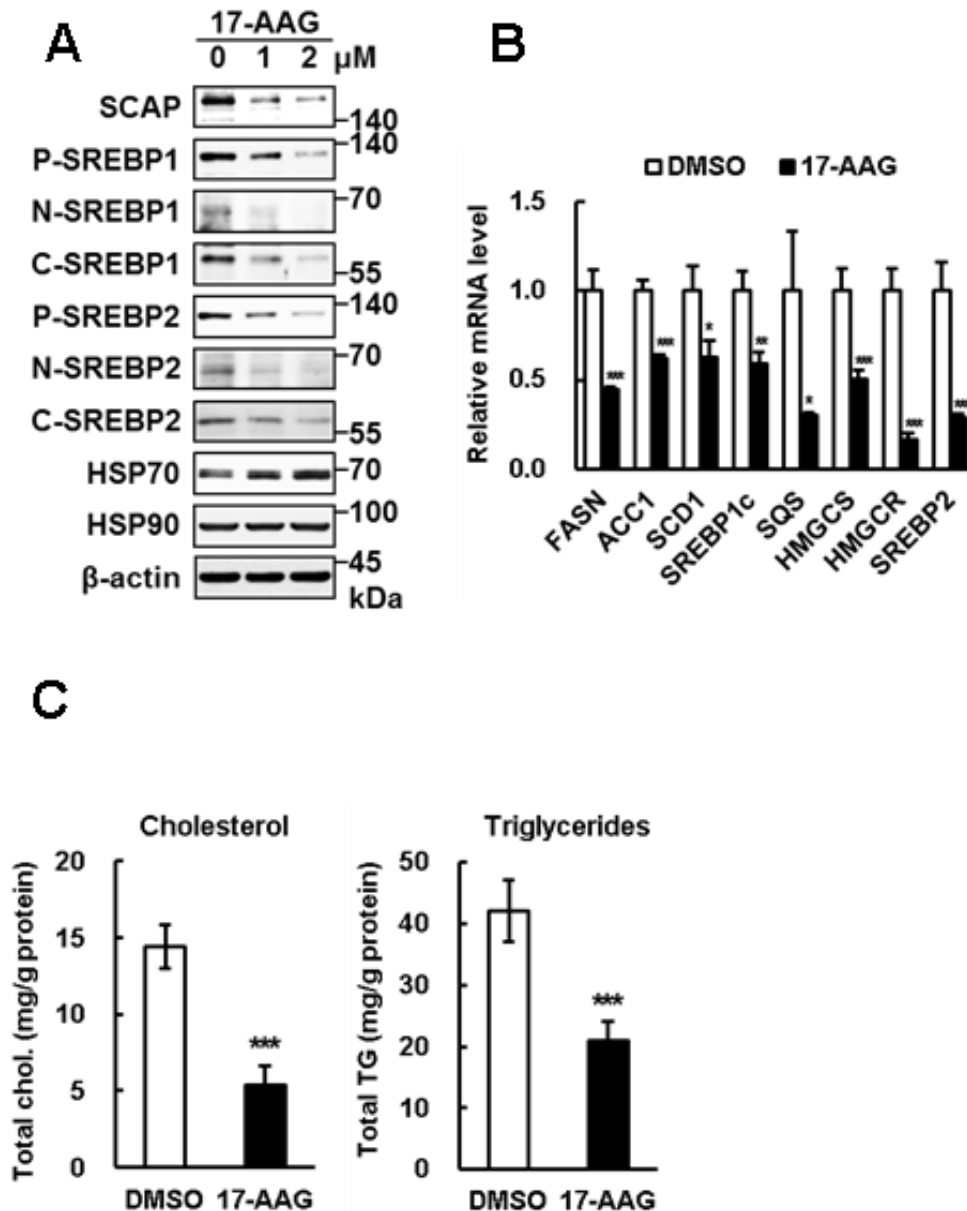


Fig. 7. 17-AAG decreases SCAP/SREBP proteins and inhibits SREBP

(A) Immunoblot analysis of HepG2 cells treated with 0–2 μ M of 17-AAG for 24 h. P, N, and C indicate the precursor, matured N-terminal, and cleaved C-terminal SREBP, respectively. The precursor and N-terminal SREBP1 were detected by anti-SREBP1 (2A4) antibody. C-terminal of SREBP1 was detected by anti-SREBP1 (C-20) antibody. Precursor and C-terminal SREBP2 were detected by anti-SREBP2 (1C6) antibody. N-terminal SREBP2 was detected by anti-SREBP2 (RS004) antibody. (B) Real-time qPCR analysis of SREBP-target gene expressions in HepG2 cells treated with DMSO or 3 μ M of 17-AAG for 36 h. (C) Triglyceride and total cholesterol levels in HepG2 cells treated with DMSO or 2 μ M of 17-AAG for 48 h. Data are represented as mean \pm SD ($n = 3$). Asterisks indicate data is significantly different from DMSO (*, $p < 0.05$; **, $p < 0.01$; ***, $p < 0.005$).

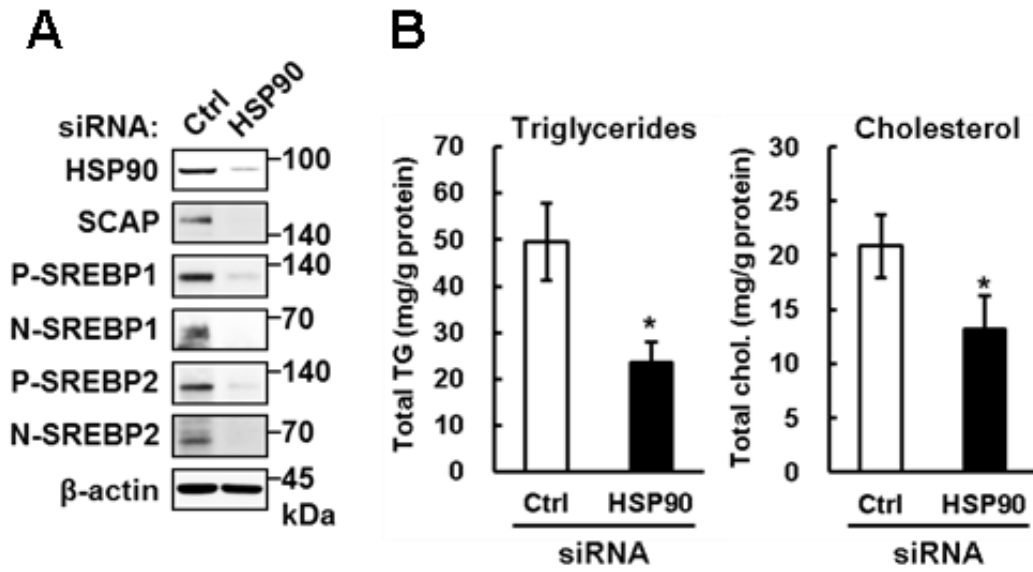


Fig. 8. Hsp90 knockdown decreases SCAP/SREBP proteins and decreases lipid levels

(A) Immunoblot analysis and (B) triglycerides and total cholesterol levels in HepG2 cells transfected with control scramble siRNA or Hsp90 specific siRNA. Data are represented as mean \pm SD ($n = 3$). Asterisks indicate data is significantly different from control (*, $p < 0.05$).

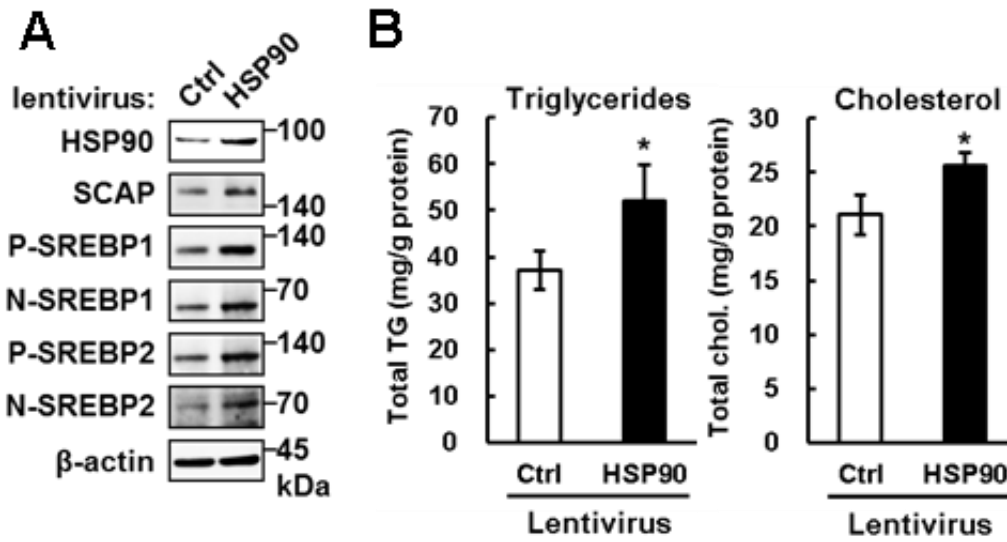


Fig. 9. Hsp90 overexpression increases SCAP/SREBP proteins and lipid levels

(A) Immunoblot analysis and (B) triglycerides and total cholesterol levels in HepG2 cells infected with control lentivirus or Hsp90 expression lentivirus. Data are represented as mean \pm SD ($n = 3$). Asterisks indicate data is significantly different from control (*, $p < 0.05$).

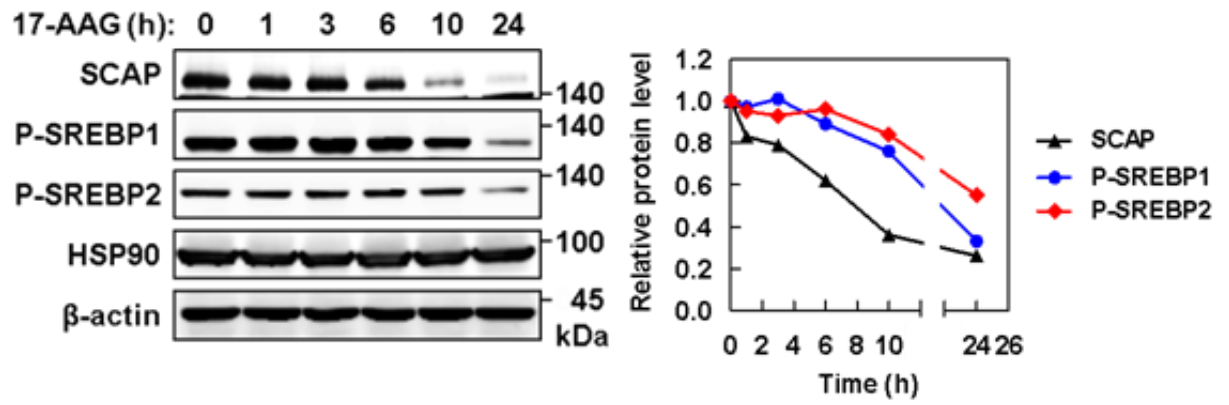


Fig. 10. Time-course of 17-AAG on SCAP and SREBP precursor proteins

Immunoblot analysis of HepG2 cells treated with indicated hours of 3 μ M 17-AAG and analyzed by immunoblots analysis using anti-SCAP (C-20), anti-SREBP1 (2A4), anti-SREBP2 (1C6), anti-Hsp90 (F-8), and anti- β -actin (AC-15) antibodies. Relative protein level was normalized to β -actin.

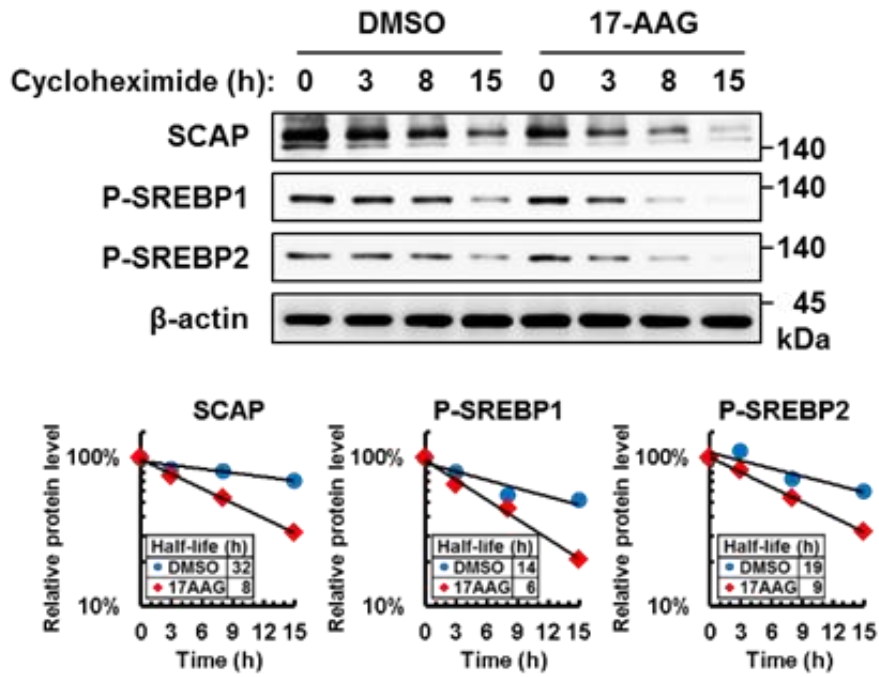


Fig. 11. 17-AAG accelerates SCAP and SREBP precursor degradation

Immunoblots of HepG2 cells treated with indicated hours of 3 μ M 17-AAG in the presence of 50 μ M of cycloheximide. Immunoblots was conducted using anti-SCAP (C-20), anti-SREBP1 (2A4), anti-SREBP2 (1C6), and anti- β -actin (AC-15) antibodies. Relative protein level was normalized to β -actin. The protein half-lives were calculated by linear regression method with the x and y axes set to time and the logarithmic value of relative protein level, respectively.

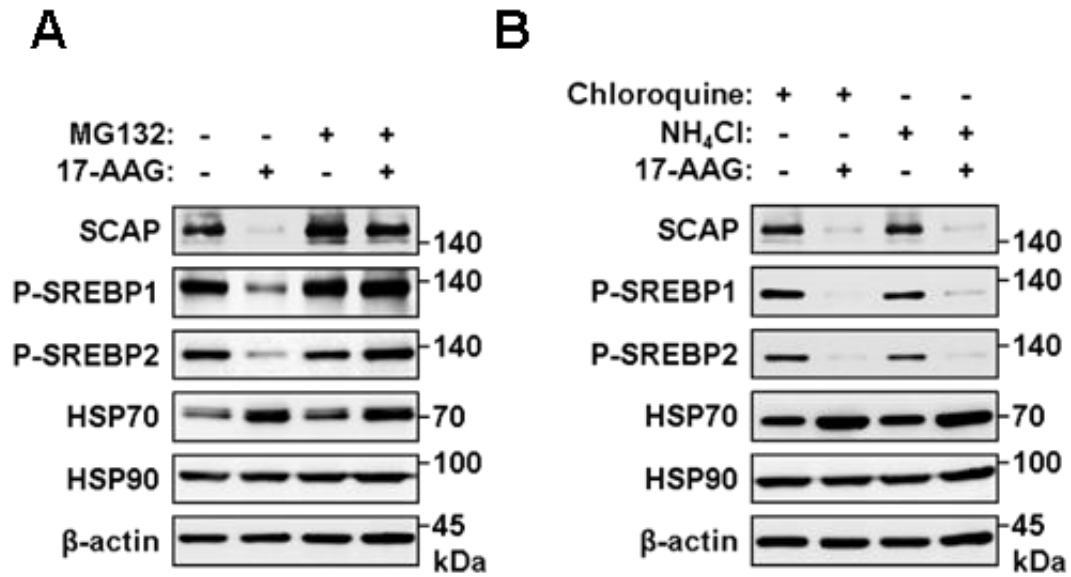


Fig. 12 17-AAG induced proteasome-dependent SCAP/SREBP degradation

(A) Immunoblot analysis of HepG2 cells cultured in the absence or presence of 10 μ M MG132 and treated with DMSO or 3 μ M of 17-AAG for 16 h. (B) Immunoblot analysis of HepG2 cells cultured in the presence of 50 μ M chloroquine or 10 mM ammonium chloride and treated with DMSO or 3 μ M of 17-AAG for 24 h. Immunoblots was conducted using anti-SCAP (C-20), anti-SREBP1 (2A4), anti-SREBP2 (1C6), anti-Hsp70 (3A3), anti-Hsp90 (F-8) and anti- β -actin (AC-15) antibodies.

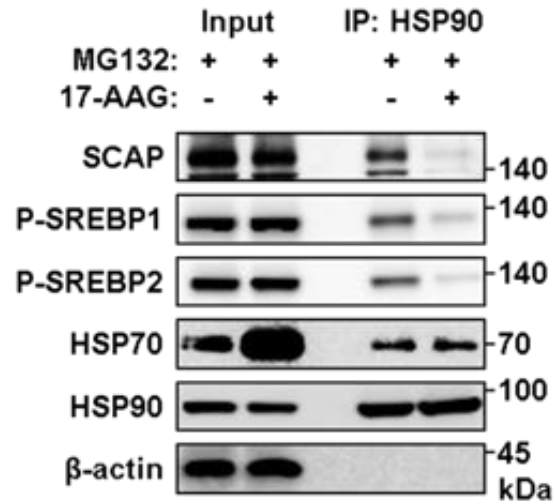


Fig. 13. 17-AAG inhibits Hsp90-SCAP/SREBP interaction

Immunoblot analysis of the input cell lysates and anti-Hsp90 immunoprecipitated samples of HepG2 cells pretreated 10 μ M MG132 and treated with DMSO or 3 μ M 17-AAG for 16 h. Immunoblots was conducted using anti-SCAP (C-20), anti-SREBP1 (2A4), anti-SREBP2 (1C6), anti-Hsp70 (3A3), anti-Hsp90 (F-8) and anti- β -actin (AC-15) antibodies.

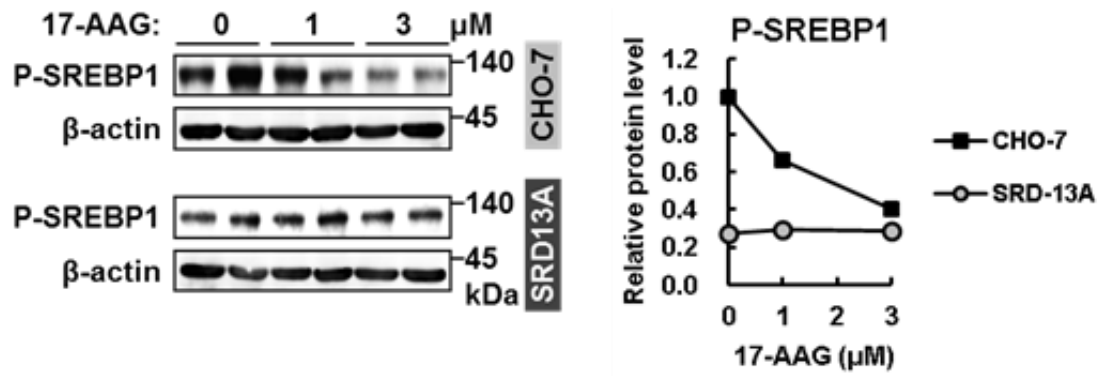


Fig. 14. 17-AAG fails to decrease SREBP precursor in *SCAP*-deficient SRD-13A cells

Immunoblot analysis of CHO-7 and *SCAP*-deficient SRD-13A cells treated with 0–3 μ M of 17-AAG for 24 h. Immunoblots was conducted using anti-SREBP1 (2A4) and anti- β -actin (AC-15) antibodies. Relative protein level was normalized to β -actin.

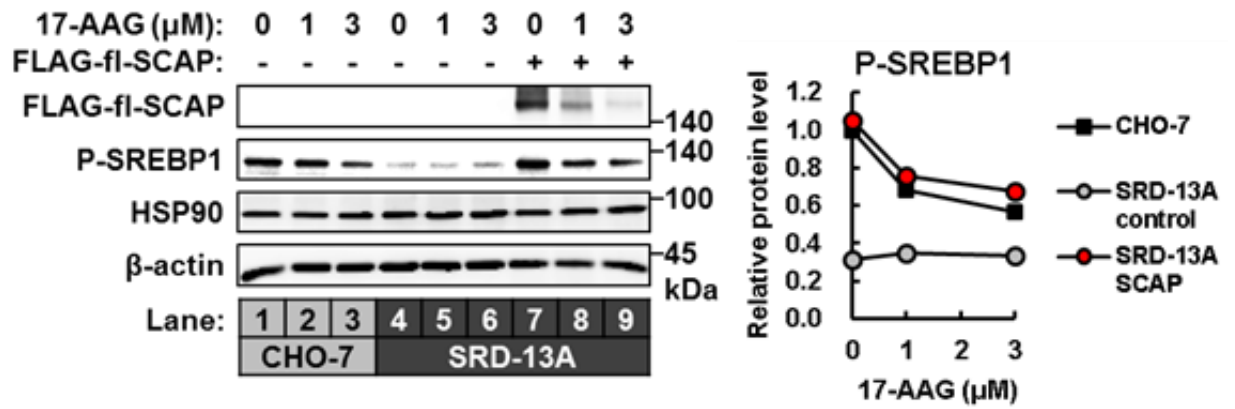


Fig. 15. Overexpressed SCAP restores the effect of 17-AAG on SREBP in SRD-13A cells

Immunoblot analysis of CHO-7 cells, empty vector-transfected *SCAP*-deficient SRD-13A cells, and FLAG-fl-SCAP-transfected *SCAP*-deficient SRD-13A cells treated with 0–3 μM of 17-AAG for 24 h. Immunoblots was conducted using anti-FLAG (M2), anti-SREBP1 (2A4), anti-Hsp90 (F-8) and anti- β -actin (AC-15) antibodies. Relative protein level was normalized to β -actin.

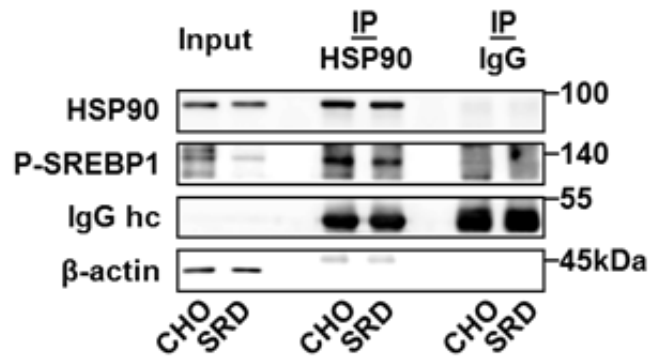


Fig. 16. Hsp90 interacts with SREBP in CHO-7 and SRD-13A cells

Immunoblot analysis of input cell lysates and anti-control IgG or anti-Hsp90 immunoprecipitated samples obtained from CHO-7 and *SCAP*-deficient SRD-13A cells. Immunoblots was conducted using anti-SREBP1 (2A4), anti-Hsp90 (F-8) and anti-β-actin (AC-15) antibodies. Relative protein level was normalized to β-actin. CHO: CHO-7; SRD: SRD-13A.

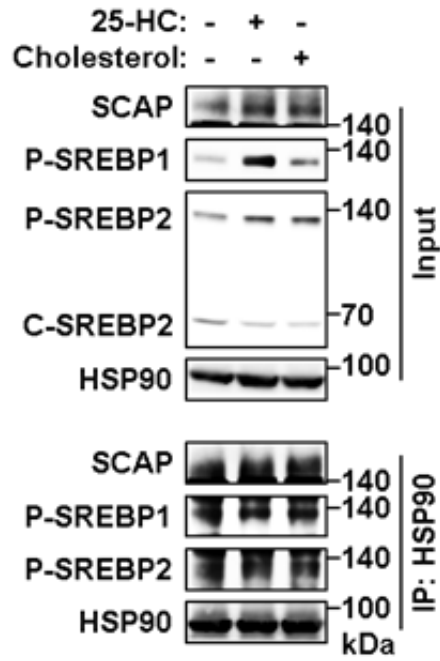


Fig. 17. Hsp90-SCAP/SREBP interaction is independent to sterol condition

Immunoblot analysis of the input and anti-Hsp90 immunoprecipitated samples of HepG2 cells cultured in the absence or presence of 1 $\mu\text{g/ml}$ 25-HC or 10 $\mu\text{g/ml}$ of cholesterol. Immunoblots was conducted using anti-SCAP (C-20), anti-SREBP1 (2A4), anti-SREBP2 (1C6), anti-Hsp90 (F-8) antibodies.

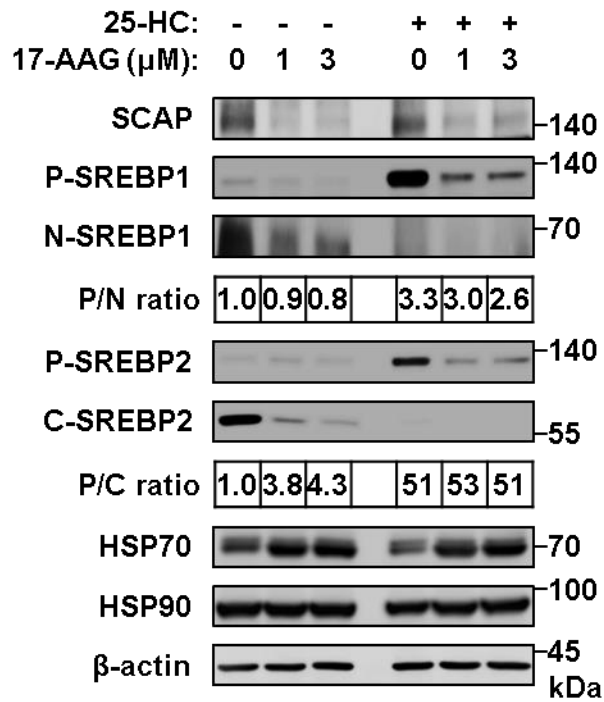


Fig. 18. Hsp90 regulates SCAP/SREBP independently to the state of SREBP processing

Immunoblot analysis of HepG2 cells cultured in sterol depleted medium for 16 h and then treated with 0–3 μ M of 17-AAG for 24 h with or without the co-treatment of 1 μ g/ml 25-HC. Immunoblots was conducted using anti-SCAP (C-20), anti-SREBP1 (2A4), anti-SREBP2 (1C6), anti-Hsp70 (3A3), anti-Hsp90 (F-8) and anti- β -actin (AC-15) antibodies.

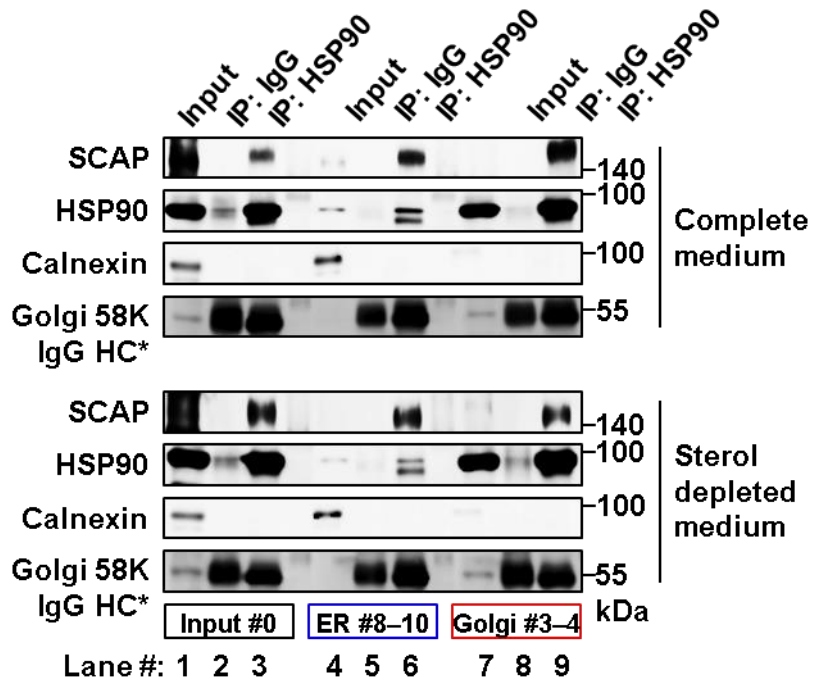


Fig. 20. Hsp90 interacts with SCAP in the ER and Golgi apparatus

Immunoblot analysis of the input and the precipitated samples of the input lysates, ER, and the Golgi fractions. Immunoblot was conducted using anti-SCAP (C-20), anti-Hsp90 (F-8), anti-calnexin, and anti-Golgi 58k protein (58k-9) antibodies.

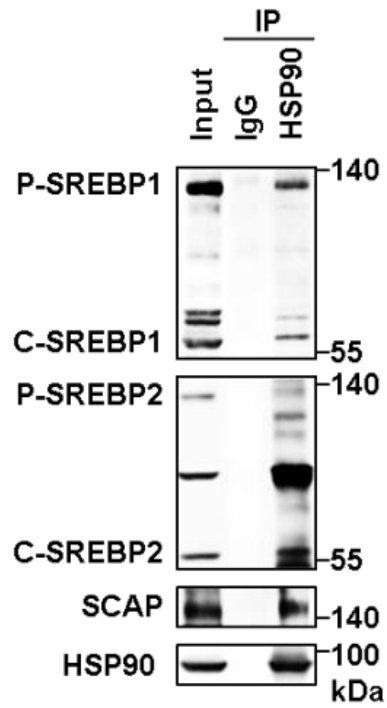


Fig. 21. Hsp90 interacts with the cleaved C-terminal SREBP

Immunoblot analysis of HepG2 input and the precipitated samples. Immunoblots was conducted using anti-SCAP (C-20), anti-Hsp90 (F-8), anti-SREBP1 (C-20), and anti-SREBP2 (1C6) antibodies.

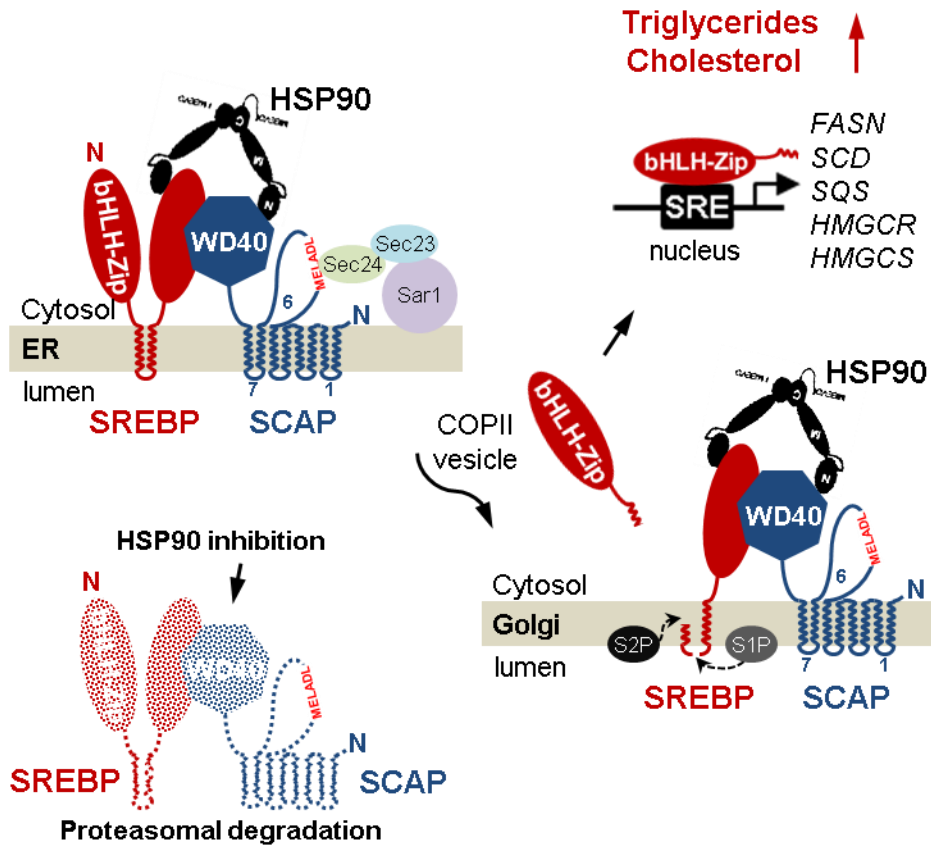


Fig. 22. Schematic illustration of Hsp90 regulation on SCAP/SREBP

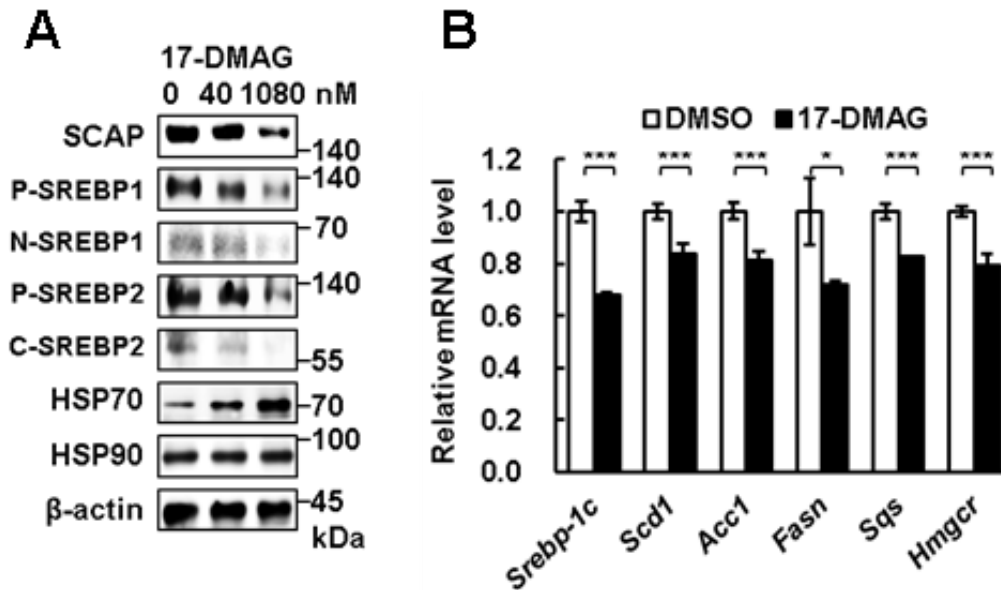


Fig. 23. Effect of 17-DMAF on SCAP/SREBP in mouse primary hepatocytes

(A) Immunoblot analysis of primary mouse hepatocytes treated with 0–1.08 μ M 17-DMAG for 24 h. anti-SCAP (C-20), anti-SREBP1 (2A4), anti-SREBP2 (1C6), anti-Hsp70 (3A3), anti-Hsp90 (F-8) and anti- β -actin (AC-15) antibodies. (B) SREBP-target mRNA expression in mouse primary hepatocytes treated with 40 nM 17-DMAG for 36 h. Data are represented as mean \pm SD ($n = 3$). Asterisks indicate values significantly different from DMSO control (*, $p < 0.05$; **, $p < 0.01$; ***, $p < 0.005$).

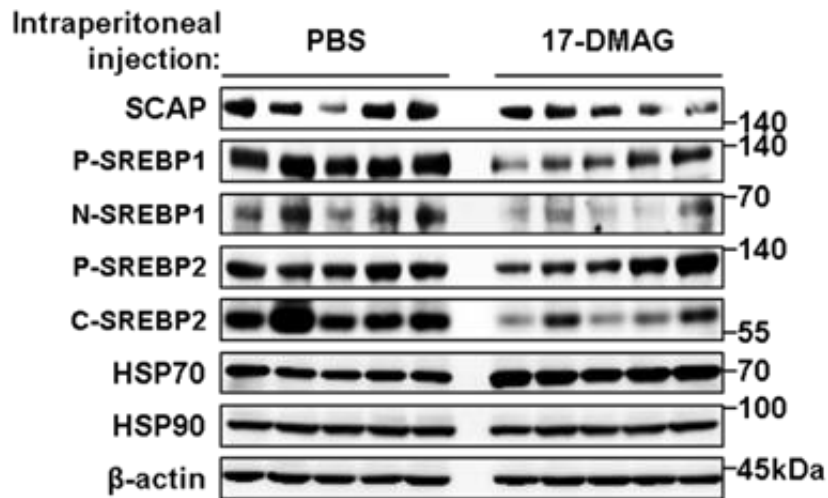
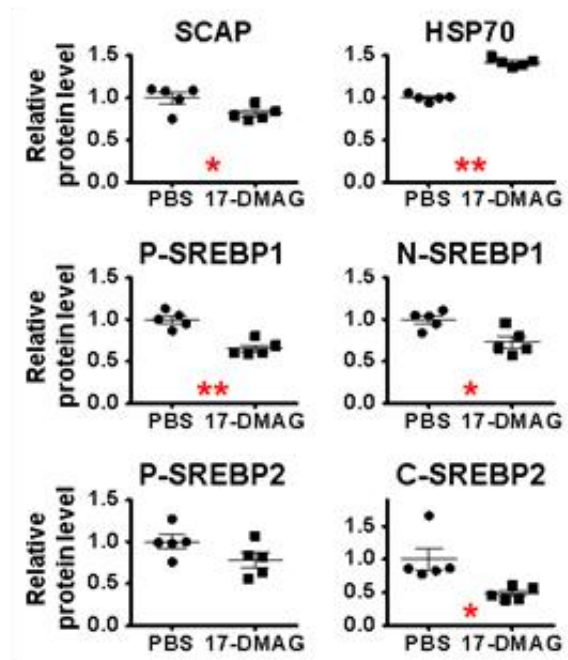
A**B**

Fig. 24. 17-DMAG decreases SCAP/SREBP proteins in mouse livers

(A) Immunoblot analysis of liver proteins from mice i.p. injected with 5 mg/kg body weight of 17-DMAG or equivalent volume of PBS for three times at 12-h intervals. anti-SCAP (C-20), anti-SREBP1 (2A4), anti-SREBP2 (1C6), anti-Hsp70 (3A3), anti-Hsp90 (F-8) and anti- β -actin (AC-15) antibodies. (B) Relative protein level was normalized to β -actin. Data for each mouse are presented with mean \pm SD indicated by horizontal lines and error bars. Asterisks indicate data is significantly different from PBS control (*, $p < 0.05$; **, $p < 0.01$).

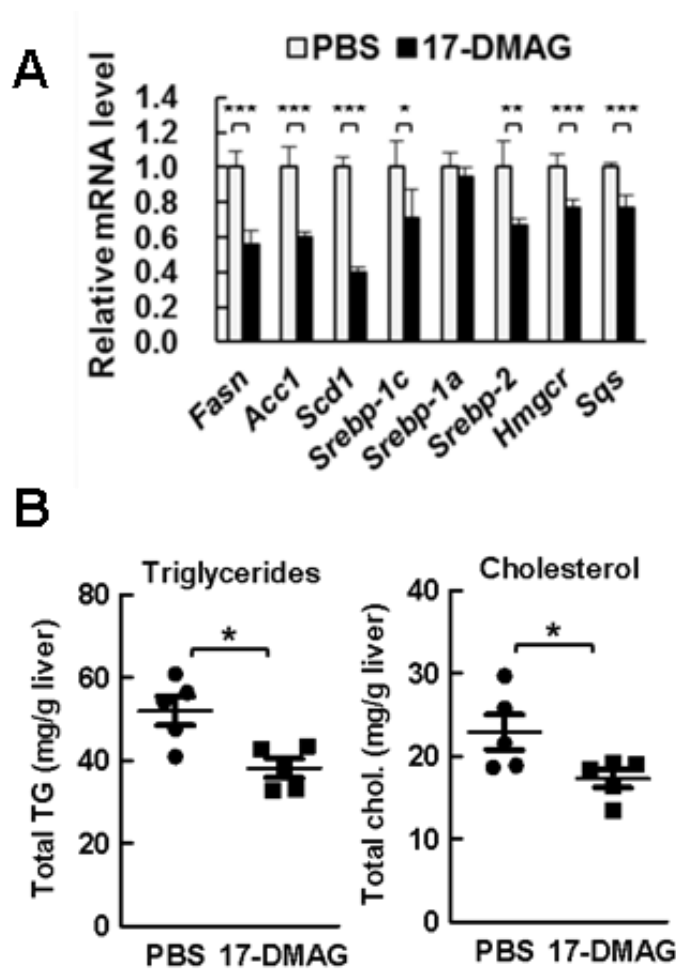


Fig. 25. 17-DMAG inhibits SREBP activity and reduces lipid levels

(A) Real-time qPCR analysis of SREBP-target mRNA expression in liver samples from mice treated with 17-DMAG or PBS. Data are represented as mean \pm SD ($n = 3$). Asterisks indicate values were significantly different from DMSO control (*, $p < 0.05$; **, $p < 0.01$; ***, $p < 0.005$). (B) Triglyceride and cholesterol levels in liver samples from mice treated with 17-DMAG or PBS. Data for each mouse are presented with mean \pm SD indicated by horizontal lines and error bars. Asterisks indicate data is significantly different from PBS control (*, $p < 0.05$).

3-4. Discussion

SREBP is the master transcription regulator of the genes involved in lipid metabolism. SCAP is a membrane-bound sterol sensor that chaperones SREBP function. SCAP binds to cholesterol via its ER luminal loop 1, which interacts with loop 7 and causes a change in the conformation of COPII binding domain on the cytosolic loop 6. The conformational change results in the inhibition of the ER-to-Golgi transport of the SCAP/SREBP complex (23, 24). Although the transmembrane domains of SCAP have been studied in molecular detail, less attention has been paid to the cytosolic C terminus of SCAP. In the present study, we showed that Hsp90 binds to the C-termini of SCAP and SREBP to form a stable complex, thereby exerting a regulatory effect on the stability of SCAP/SREBP and the activation of SREBP. The direct causal relation between elevated Hsp90 and increased SREBP protein level and activity provide important evidence for the development of potential therapeutic target to treat both metabolic diseases and cancers in which both SREBP and Hsp90 highly expressed.

Taipale and colleagues has previously uncovered the possibility that WD40 domain might comprise a novel Hsp90 client protein fold (53). We demonstrate here the interaction between SCAP C-terminus and Hsp90. Although Hsp90 is a cytoplasmic chaperone, it is capable of interacting with ER- and Golgi-membrane-bound SCAP and SREBP (**Fig. 2, 3, and 20**). The ability of cytoplasmic chaperone Hsp90 to modulate an ER membrane-bound protein has been demonstrated previously. The Hsp90 chaperone system was reported to control the ER-associated degradation and maturation of the thiazide-sensitive cotransporter (NCC), which is the primary mediator of salt reabsorption in animal. Inhibition of Hsp90 activity accelerated NCC degradation via ubiquitin-proteasome pathway, while Hsp70/Hsp90 organizer proteins stabilized NCC proteins (54). These findings support the idea that Hsp90 machinery mediates the quality control of ER proteins. Correspondingly, we found that Hsp90 inhibition destabilized SCAP and SREBP proteins and accelerated their degradation (**Fig. 11**).

Two distinct pathways have been reported for SCAP degradation. As detailed in the Introduction, SREBP is cleaved by site-1 protease (S1P) and site-2 protease in the Golgi apparatus. It was reported that S1P cleavage is critical for Golgi-to-ER recycling of SCAP, with reduction in SREBP cleavage by S1P leading to SCAP degradation in the lysosome (63). On the other hand, it was also demonstrated in glioblastoma cells that N-glycosylation of SCAP is crucial for its stability, in which glucose depletion accelerating the proteasomal degradation of SCAP (25). Therefore, putting together the data from this study and the data from other groups, it is likely that both the proteasomal and the lysosomal pathways take part in regulating the degradation of SCAP under different circumstances.

We found that Hsp90 inhibition also led to SREBP degradation; however, in the absence of SCAP, 17-AAG had little effect on SREBP-1 precursor, whereas overexpression of SCAP restored the effect of 17-AAG on SREBP (**Fig. 15 and 16**). This indicates that SREBP degradation induced by 17-AA is at least in part caused by SCAP decay, given that SREBP degrades rapidly in the absence of SCAP (6).

While it is known that binding of cholesterol to SCAP and binding of 25-HC to Insig can both change the conformation of SCAP into which favors Insig binding and inhibits SCAP/Sec23/24 interaction (21–24), manipulation of sterols in the culture medium had no obvious effect on Hsp90-SCAP/SREBP binding (**Fig. 17**). These results are comprehensible considering the fact that the conformational changes induced by sterols are made on the transmembrane domain of SCAP (22–24), while Hsp90 interacts to the cytosolic WD40 domain of SCAP independently of the sterol-mediated conformational changes. In addition, the status of SREBP processing had little effect on 17-AAG-induced SCAP degradation (**Fig. 18**). These findings support the notion that Hsp90 regulates the functional stability of SCAP/SREBP complex rather than the response to sterol changes.

In addition to the maintenance of SCAP and SREBP protein complex stability, two studies also demonstrate the ability of Hsp90 to facilitate protein transportation around ER and the Golgi apparatus. In mammalian cells, Hsp90 was shown to modulate ER-to-Golgi transport of Rab GTPase by forming a complex with guanine nucleotide dissociation inhibitor, which directs the recycling of Rab1 (64). In plants, Hsp90 and its co-chaperones Hop/Sti1 interact with the ER-bound rice chitin receptor OsCERK1 and facilitate the ER-to-plasma membrane trafficking of OsCERK1 via a Sar1-dependent pathway (65). These studies show that Hsp90 is indeed involved in the trafficking of certain membrane-bound proteins by forming a complex with the target. Herein, we presented clear evidence that Hsp90 interacts with and stabilizes SCAP/SREBP proteins during their localization and transport around ER and the Golgi apparatus and even after the proteolytic processing of SREBP (**Fig. 19–21**). More studies are required to elucidate the details of Hsp90-mediated SCAP/SREBP trafficking.

Finally, Hsp90 is highly expressed in various types of tumors and has long been a potential target for cancer therapy, owing to its crucial role in the progression and survival of cancer cells (41). Given that the SREBP/SCAP system plays a fundamental role in life-sustaining lipid metabolism, our findings suggest Hsp90 may be the link between tumorigenesis and lipid metabolism. This is supported by our finding that increased Hsp90 expression caused a significant increase in intracellular lipids (**Fig. 9**).

Recent studies have revealed more links between SCAP/SREBP and tumorigenesis. In glioblastoma cells, SCAP acted as a key glucose-response protein and knockdown or dominant negative of SCAP reduced tumor growth and prolonged survival of tumor-bearing mice (25, 48). Inhibition of SCAP and SREBP has been shown to suppress glioblastoma tumor growth and increase the sensitivity of non-small cell lung cancer cells to chemical treatment (49). These results are in agreement with a scenario in which increased Hsp90 expression is associated with more stabilized SCAP/SREBP, consequently a more robust lipid biosynthesis, and ultimately a more favorable environment for tumorigenesis.

In conclusion, we identified Hsp90 as a new SREBP regulator that interacts with the SCAP/SREBP complex. Hsp90 inhibition decreased SCAP/SREBP proteins, downregulated SREBP-target gene, and reduced lipid levels *in vitro* and *in vivo*. We demonstrated a clear connection between Hsp90 and lipid metabolism, one that may shed light on the mechanism linking Hsp90 with tumorigenesis.

CHAPTER 4

SREBP-binding sites in SCAP WD40 domain

4-1. Preface

It was reported in 1997 that SCAP and SREBP2 interact via the cytosolic C-termini of both sides (26). Although the report used hamster SCAP to study its interaction to human SREBP2, since the amino acid sequence of SCAP is highly conserved in mammals (>90% identical; Supplementary figure S1), the finding can generally be applied to human and other mammals. The crystal structure of Scp1 and Sre1 protein complex, the fission yeast homologs of SCAP and SREBP1, was solved in 2015 and refined in 2016 (27, 28). The structure of Scp1/Sre1 complex not only provided solid evidence showing that SCAP C-terminus is indeed consisted of a WD40 domain but also revealed a arginine/lysine-rich patch that was crucial to SREBP-binding. However, the amino sequence of Scp1 shares only 12% of identity with mammalian SCAP proteins. Hence, advance in the knowledge of the interaction between human SCAP and SREBP has been limited since 1997. In this study, we made efforts to elucidate the details in SCAP/SREBP binding. SCAP mutant plasmids were constructed, transfected into HEK293 cells, and the ectopically expressed SCAPs were immunoprecipitated to study SREBP-binding activity.

4-2. Materials and methods

Reagents

Protease inhibitor cocktail and calpain inhibitor were purchased from Nacalai Tesque (Kyoto, Japan). PMSF was purchased from Sigma-Aldrich (Saint Louis, MO). HyClone FBS was purchased from GE Healthcare Life Sciences (Chicago, IL). DMEM was purchased from Wako (Osaka, Japan). Other chemicals were purchased either from Wako or Nacalai Tesque.

Antibodies

Anti-FLAG M2 affinity gel, mouse IgG-agarose, monoclonal mouse anti-FLAG (M2), and anti- β -actin (AC-15) antibodies were purchased from Sigma-Aldrich. Monoclonal mouse anti-SREBP1 (2A4) and anti-SREBP2 (1C6) antibodies were purchased from Santa Cruz Biotechnology (Santa Cruz, CA). Peroxidase-conjugated affinity-purified donkey anti-mouse IgG was purchased from Jackson ImmunoResearch (West Grove, PA).

Plasmid constructs

The FLAG-tagged full length (residues aa2–1279), N-terminal domain (aa2–731), and C-terminal domain of human SCAP (aa732–1279) plasmids were constructed as described in **Section 2-2, page 17**. To construct truncated FLAG-C-SCAP plasmids, the desired fragments of SCAP were cloned into p3 \times FLAG-CMV-7.1 vector (Sigma-Aldrich) using NotI and XbaI restriction enzyme sites. The

domains in each truncated C-SCAP are illustrated in **Fig. 26**. To construct point-mutated FLAG-SCAP plasmids, primer sets carrying the desired mutation are used to clone point-mutated C-SCAP flanked by NotI and XbaI restriction sites. The C-SCAP mutants are then either cloned into p3×FLAG-CMV-7.1 vector or FLAG-N-SCAP plasmid using NotI/XbaI restriction sites to construct mutated FLAG-C-SCAP or FLAG-fl-SCAP plasmids, respectively. The sequences of all the primers used in cloning PCR fragments for plasmid construction are listed in Supplementary Table S1.

Cell cultures

HEK293 cells were maintained in complete DMEM supplemented with 10% (v/v) FBS, 100 units per ml penicillin, and 100 µg per ml streptomycin. One day before transfection, the cells were seeded in 6-well plates at a density of 2.5×10^5 per well, respectively. At a confluency of 50%–70%, the cells were transfected with indicated plasmids (2 µg per well) by the calcium phosphate method as described in **Section 2-2, page 11**. One day after transfection, the culture medium was replaced by fresh complete medium supplemented with 2.5 µM of MG132 to keep the protein level of ectopically expressed SCAP. The cells were harvested for anti-FLAG immunoprecipitation 36–48 h after transfection. All cell cultures were maintained in a humidified incubator at 37°C under an atmosphere of 5% CO₂.

Immunoprecipitation

The lysis buffer for immunoprecipitation experiments is consisted of 25 mM Tris-HCl (pH 7.4), 150 mM NaCl, 1 mM EDTA, 5% glycerol, and 0.5% Nonidet P-40. Immediately before applying to the cells, protease inhibitor cocktail, PMSF, and Calpain inhibitors were added to the lysis buffer to a final concentration of 1% (v/v), 1 mM, and 0.5 mM, respectively. For anti-FLAG immunoprecipitation, HEK293 cells transfected with indicated plasmids were washed with 0.5 ml per well of ice-cold PBS and then harvested in 0.5 ml of ice-cold PBS by a cell scraper. The following procedures were carried out either on ice or at 4°C using ice-cold buffers. The cells were centrifuged at 1,500×g for 5 min and the cell pellet was resuspended in 0.5 ml of lysis buffer by vortexing for 10 sec. The cells were then homogenized by passing through a 25-gauge needle 20 times followed by centrifugation at 13,000×g for 10 min to remove debris and insoluble. The supernatant cell lysates were collected, in which 50 µl was saved as the sample for input control, and the rest of the cell lysates were precleared by incubating with either mouse IgG agarose (20 µl per sample) for at least 1 h with gentle rotation to remove non-specific binding proteins. Anti-FLAG immunoprecipitation was performed using the cell lysates precleared by mouse IgG agarose. Immunoprecipitation was carried out using anti-FLAG M2 affinity gel following the manufacturer's protocol. The immunoprecipitated gels were washed with 25 volumes of PBS for three times and then resuspended in 1× Laemmli dye. The 50 µl input cell lysates were mixed with 10 µl of 6× Laemmli dye. The suspended gels and the input lysates were incubated in a 95°C heat block for 5 min, cooled on ice for 10 min, and then centrifuged at 13,000×g for 10 min. The supernatant was collected for immunoblotting. The 6× Laemmli dye is consisted of 1 M Tris-HCl pH 6.8, 30% glycerol, 10% SDS, and 0.03% bromophenol blue.

4-3. Results

4-3-1. Truncation of WD repeats reduces SREBP-binding ability of SCAP

Based on sequence homology, 7 WD40 repeats are annotated in human SCAP in the UniProt protein database [Q12770 (SCAP_HUMAN)]. In the beginning of this study, we constructed 10 SCAP mutants with truncation from N-terminal, C-terminal, or both ends to study if one or more of the WD40 repeats are more critical to SREBP-binding. The domain structures of wild type and mutant human C-SCAP constructs are listed in **Fig. 26**. SREBP-binding was evaluated by immunoprecipitation of ectopic C-SCAP and immunoblotting the precipitates using anti-SREBP1 and anti-SREBP2 antibodies.

The protein level of ectopically expressed C-SCAP mutants were kept at a comparable level by applying a sub-lethal 2.5 μ M of MG132 to the cells 24 h before harvest. As shown in the bottom panel of **Fig. 27**, we were able to detect a consistent signal level among wild type and C-SCAP mutants in the input samples. In addition, the protein level of precursor SREBP was unaffected by the ectopic C-SCAP. The samples from cells transfected with empty vector and wild type C-SCAP serves as positive and negative control respectively. As we have shown in **Fig. 1B** in **Chapter 2**, both SREBP precursors were co-precipitated with C-SCAP (**Fig. 27**, top panel lane 2). Truncation from the N-terminal to WD2 or WD3 reduced SREBP-binding ability of C-SCAP (**Fig. 27**, top panel lanes 4–5). Truncation from the C-terminal to WD7, WD6, or WD5 reduced SREBP-binding ability of C-SCAP (**Fig. 27**, top panel lanes 6–8). Nevertheless, while truncation from both ends also led to a decrease in the SREBP-binding ability (**Fig. 27**, top panel lanes 9–12), the level of decrease was comparable to those observed in N- or C-terminal truncations. Although the binding pattern of different versions of C-SCAP to SREBP1 and SREBP2 is generally the same, we noticed a discrepancy. When truncated from the N-terminal to the first WD repeat, the binding between C-SCAP and SREBP2 alone was reduced, while the C-SCAP mutant had a comparable SREBP1-binding ability as the wild type C-SCAP (**Fig. 27**, top panel lane 3).

These results suggest that all of the WD40 repeats contribute partially to SREBP-binding. In fact, as reviewed by Stirnimann and colleagues (29), the majority of WD40 domain-binding proteins interact with the top surface of the WD40 β -propeller structure (Supplementary Fig. S4). In such condition, most or all of the WD40 repeats would have contribute to the binding, forming a tight and cooperative interaction. However, if this is the case for SCAP/SREBP interaction, it would be difficult to identify a specific WD40 repeat or domain that is responsible for the interaction. Therefore, another approach was employed for further study.

4-3-2. L1178A and R1248A point mutations reduce SREBP-binding ability of SCAP

Based on the observation that the majority of WD40 domain-interacting proteins bind to the top of WD40 domain, Wang and colleagues developed a database to estimate the potential protein-protein

interacting sites in WD40 domain (66). Taking advantage of this database, we obtained the predicted 3D structure of human SCAP (Supplementary Fig. S5) including 7 potential protein-protein interacting residues (**Table 2**). We note here that the WD40 repeats predicted in the UniProt database and the WD40 protein database are different (**Fig. 27** vs. **Table 2**). To evaluate the involvement of these residues in SREBP-binding, we constructed C-SCAP plasmids that had point mutation at each potential protein-protein interacting residue for immunoprecipitation experiments.

The protein level of ectopically expressed C-SCAP was kept to a comparable level among different versions of C-SCAP using sub-lethal 2.5 μM of MG132, and the protein level of SREBP precursors was unaffected by ectopically expressed C-SCAP (**Fig. 28**, lanes 10–18). While point mutation at 5 of the potential residues had negligible effect on SREBP binding, alanine mutation at leucine 1178 and arginine 1248 dramatically reduced the SREBP-binding ability of C-SCAP (**Fig. 28**, lanes 8 and 9). This result indicates the potential involvement of L1178 and R1248 in SREBP-binding. To further investigate these residues, we constructed full-length (fl) wild type, L1178A, and R1248A SCAP for immunoprecipitation experiment. As a result, while L1178A fl-SCAP dramatically lost its SREBP1-binding ability and partially lost its SREBP2-binding activity, R1248A fl-SCAP almost completely lost its ability to bind to both SREBPs (**Fig. 29**, lanes 3 and 4). In summary, using the WD40 protein database (66), we identified L1178 and R1248 as two potential SREBP-binding amino acid residues.

4-3-3. Identification of potential SREBP-binding arginine/lysine-rich regions

We have found two potential SREBP-binding residues, L1178 and R1248, this corresponds to the observation that deletion of aa1196–1279 ($\Delta\text{WD7-c}$) reduced C-SCAP/SREBP binding (**Fig. 27**, top panel, lane 6). Nonetheless, we were convinced that most if not all of the WD40 repeats take part in SREBP-binding. Thus, we continued to search for more potential residues. The crystal structure of Scp1/Sre1 (yeast SCAP/SREBP) complex revealed an arginine/lysine (R/K)-rich region in Scp1 that contributed greatly to Sre1-binding. However, all the potential Sre1-binding residues in Scp1 were not conserved in human SCAP (Supplementary Fig. S6).

Although the amino acid residues were not conserved, it is still plausible that human SCAP also possesses similar R/K regions that interact with SREBP. Thus, we began to search for the R/K or charged region in human SCAP. To that end, we constructed 16 full-length (fl) SCAP plasmids carrying either an arginine (R) to glutamic acid (E) or a lysine (K) to glutamic acid (E) mutation for immunoprecipitation experiments. Despite the effort to keep the ectopically expressed fl-SCAP protein to a comparable level by applying sub-lethal 2.5 μM of MG132, the protein level of some fl-SCAP mutants still varied (**Fig. 28**, input). Nonetheless, while wild type fl-SCAP co-precipitates both SREBP precursors (**Fig. 28**, lane 2), 8 of the fl-SCAP mutant had reduced SREBP-binding ability. R984E, K1019E, R1102E, R1187E, and R124E fl-SCAP dramatically lost their ability to bind to both SREBP precursors (**Fig. 28**, lanes 3, 6, 12, 16, and 18), whereas K1018E, R1051E, and K1086E fl-SCAP lost

their ability to bind to SREBP2 (**Fig. 28**, lanes 5, 9, and 10). However, one more round of screening was necessary since the protein level of ectopically expressed fl-SCAP was inconsistent among others.

In the next round of screening, in addition to the 8 fl-SCAP mutants described above, we constructed 5 more plasmids encoding fl-SCAP mutants carrying a histidine (H) to glutamic acid (E) mutation, and a fl-SCAP mutant plasmid carrying aspartic acid 1162 to lysine (D1162K) point mutation. This time we were able to keep ectopically expressed fl-SCAP to a comparable level (**Fig. 31**, input). As shown by the immunoprecipitation experiment, R984E, K1018E, R1019E, R1187E, and R1248E mutations that were identified in the first round of screening, and H1118E, D1162K, and L1178A mutations reduced SREBP-binding ability of fl-SCAP dramatically (**Fig. 31**, IP: FLAG). To conclude the screening, we tested these 8 mutants once more by repeating the immunoprecipitation experiment. As a result, all of the 8 fl-SCAP mutants R984E, K1018E, R1019E, H1118E, D1162K, L1178A, R1187E, and R1248E had dramatically lost their SREBP-binding ability (**Fig. 32**). This result concludes the findings in our point mutated SCAP studies (4-3-2 and 3).

Table 2. Prediction of protein-protein interaction sites using WD40 protein database

WD	Start	End	Amino acid sequence	potential *PPI sites
1	955	994	KGSPSLAWAPSAEGSIWSLELQGNLIVVGRSSGRLEV WDAIEGV	W971
2	999	1034	LCCSSEEVSSGITALVFLDKRIVAARLNGSLDFFSLETH TALSPLQFRGTPGRGSSPASPVSSTTVAC	L1025
3	1069	1106	HLTHTVPCA H QKPITALKARLVTGS Q DHTLRVFRLED S	Q1097
4	1110	1147	CCLFTLQ G HSGAITTVYIDQTMVLASGG Q DGAICLWD VLTGS	Q1138
5	1152	1187	RVSHVFA H RGD V TSLTCTTS CVISSGL D DLISIWDRSTGI	D1162 L1178
6	1192	1227	KFYSIQQDLGCGASLGVISDNLLVTGGQGCVSFWDLN YGDLL	-
7	1234	1272	QTVYLGKNSEA Q PAR Q ILVLDNAAIVCNFGSELSLVY V	R1248

The 7 WD40 repeats annotated in the WD40 protein database (66) Predictions of residues involved in the DHSW tetrad hydrogen structure motif are highlighted in blue. Predictions of residues involved in protein-protein interaction (*PPI) are highlighted in red.

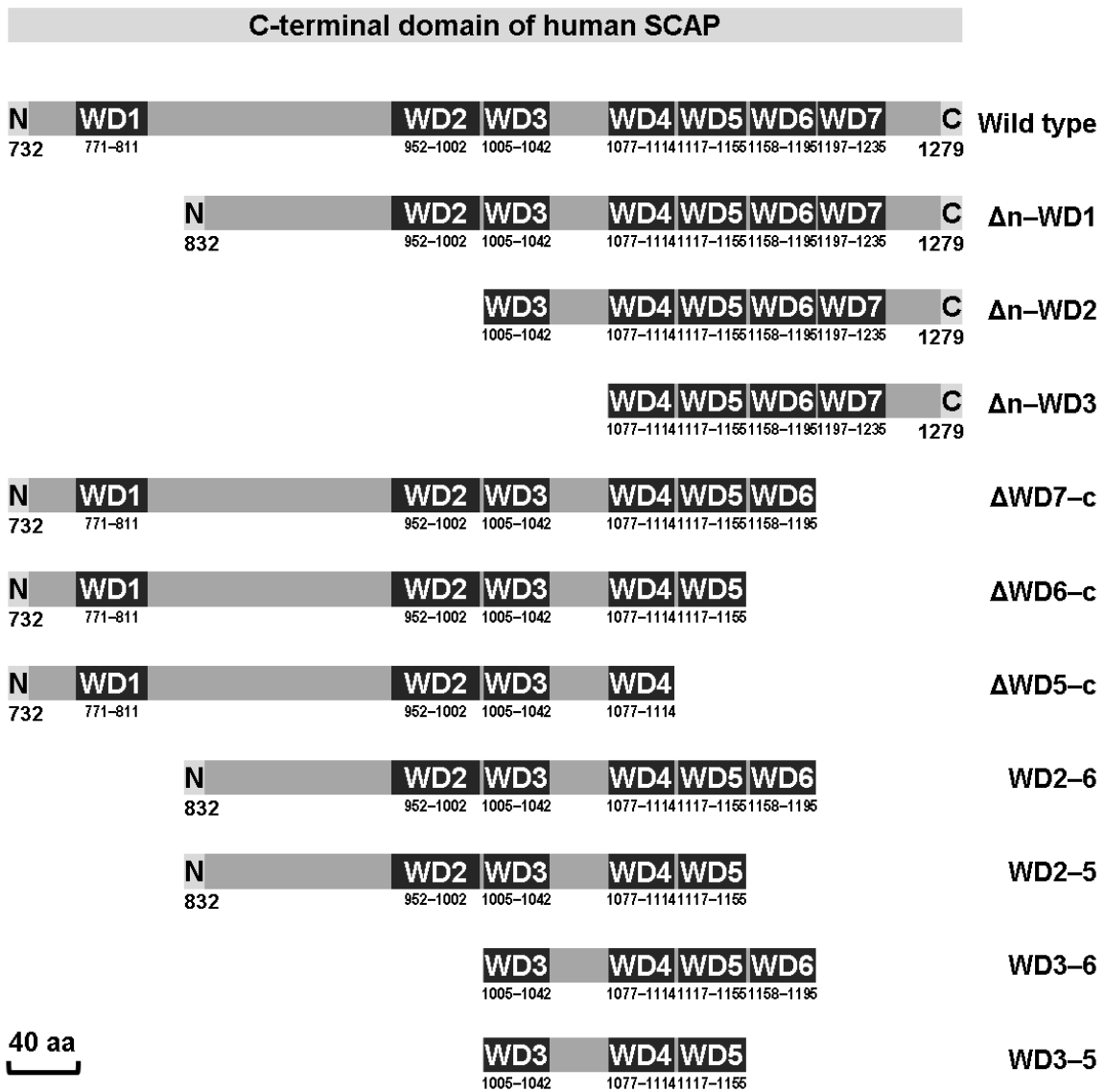


Fig. 26. Schematic diagrams of human SCAP C-terminus constructs

The domain structure of human SCAP C-terminus including 7 potential WD40 repeats annotated in the UniProt Data base [Q12770 (SCAP_HUMAN)] is shown on top. The domain structures of the truncated SCAP constructs are aligned below.

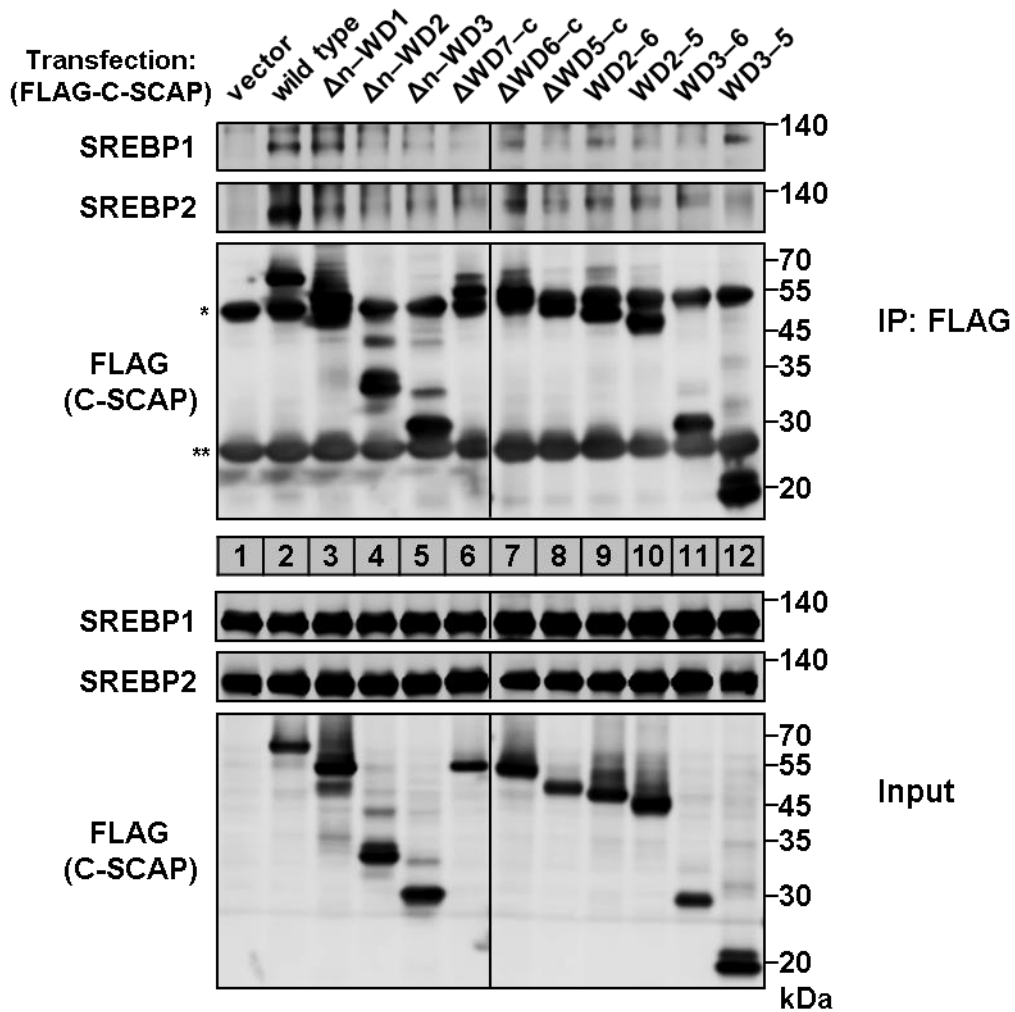


Fig. 27. Truncation from N- or C-terminal end reduces SCAP(C)/SREBP binding

Immunoblots of the anti-FLAG immunoprecipitated and input samples from HEK293 cells transfected with vectors (lane 1) or FLAG-tagged wild type (lane 2), N-terminal truncated (lanes 3–5), C-terminal truncated (lanes 6–8), or both ends truncated (lanes 9–12) C-terminal SCAP. Lanes 1–6 and lanes 7–12 are from two membranes with the background adjusted to comparable level. The vertical lines indicate the margins of each membrane. The asterisks indicate the heavy chain (*) and the light chain (**) of IgG from the anti-FLAG affinity gel.

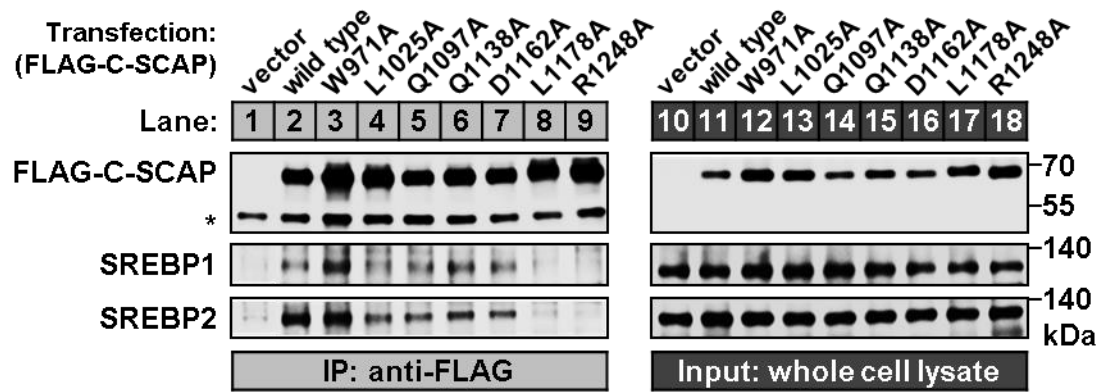


Fig. 28. L1178A and R1248A point mutations reduces SCAP(C)/SREBP binding

Immunoblots of the anti-FLAG immunoprecipitated and input samples from HEK293 cells transfected with vectors (lanes 1 and 10) or FLAG-tagged wild type (lanes 2 and 11), or point mutated (lanes 3–9 and 12–18) C-terminal SCAP. The asterisk indicates IgG heavy chain.

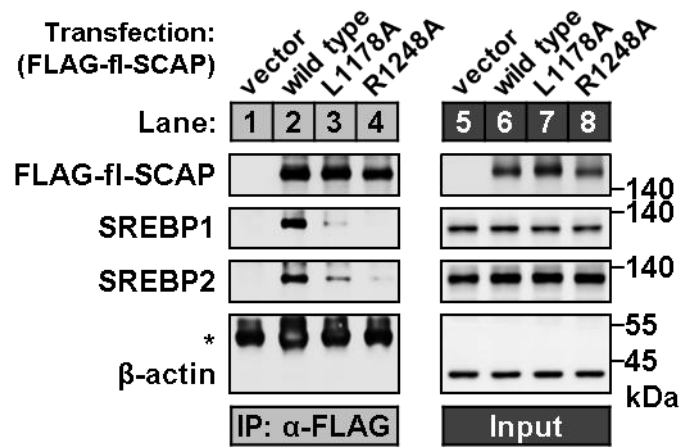


Fig. 29. L1178A and R1248A point mutations reduces SCAP(f)/SREBP binding

Immunoblots of the anti-FLAG immunoprecipitated and input samples from HEK293 cells transfected with vectors (lanes 1 and 5) or FLAG-tagged wild type (lanes 2 and 6), or point mutated (lanes 3–4 and 7–8) full-length SCAP. The asterisk indicates IgG heavy chain.

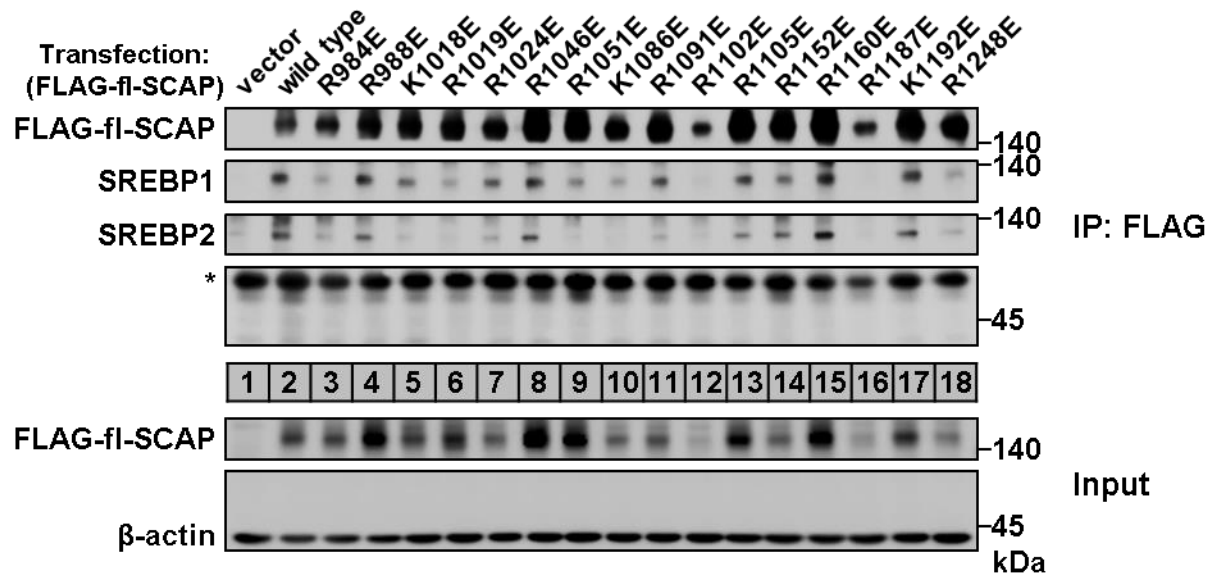


Fig. 30. Screening for arginine/lysine mutation that reduces SCAP(fl)/SREBP binding

Immunoblots of the anti-FLAG immunoprecipitated and input samples from HEK293 cells transfected with vectors (lane 1) or FLAG-tagged wild type (lanes 2), or point mutated (lanes 3–18) full-length SCAP. The asterisk indicates IgG heavy chain.

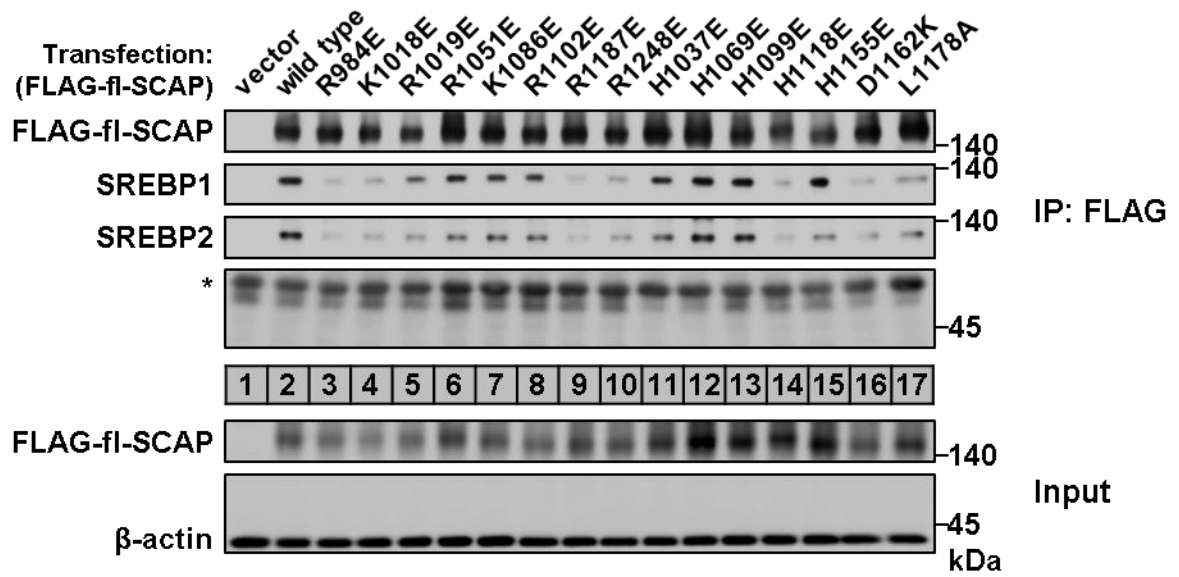


Fig. 31. Screening for point mutation that reduces SCAP(fl)/SREBP binding

Immunoblots of the anti-FLAG immunoprecipitated and input samples from HEK293 cells transfected with vectors (lane 1) or FLAG-tagged wild type (lanes 2), or point mutated (lanes 3–17) full-length SCAP. The asterisk indicates IgG heavy chain.

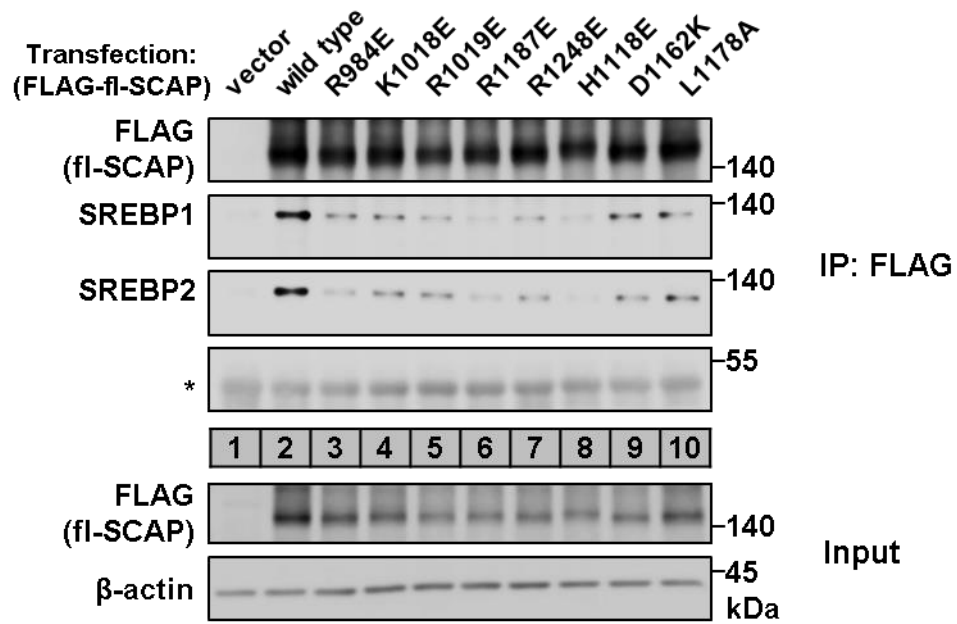


Fig. 32. Identification of 8 point mutations that reduce SCAP(fI)/SREBP binding

Immunoblots of the anti-FLAG immunoprecipitated and input samples from HEK293 cells transfected with vectors (lane 1) or FLAG-tagged wild type (lanes 2), or point mutated (lanes 3–10) full-length SCAP. The asterisk indicates IgG heavy chain.

4-4. Discussion

The binding between SCAP and SREBP is critical not only to the stability of SREBP precursors but also crucial for the transport of SREBP from the ER to the Golgi apparatus for proteolytic activation. The ability of SCAP to sense membrane cholesterol also makes it a key regulator of SREBP activation (22). However, up to present the only molecular level research of SCAP/SREBP interaction was carried out in 1997, which showed that the C-terminal domain of each side is responsible for the interaction (26). One of the most challenging obstacles of the study is perhaps the complex nature of WD40 domain that made the crystallization of SCAP futile despite several attempts (27). Nonetheless, Wang and colleagues succeeded in obtaining the crystal structure of Scp1 (yeast SCAP) by removing the fragments that caused aggregation and destabilization of the protein from wild type Scp1. The structure revealed a positively charged arginine/lysine region that is crucial to Sre1 (yeast SREBP)-binding. The region was given a name 'R/K-patch' (27, 28). However, the amino acid sequences of mammalian and yeast SCAP share only 12% identity and we failed to identify any conserved residue of the yeast R/K-patch in the sequences of human or mammalian SCAP (Supplementary Fig. S6).

In our first attempt to investigate SCAP/SREBP binding, we discovered that although the SREBP-binding ability was substantially reduced by truncation of SCAP from either or both N- and C-terminal ends, there remained certain degree of SREBP-binding ability even in severely truncated SCAP that consisted of only 3 WD40 repeats. This suggests that perhaps all of the WD40 repeats contribute partially to SREBP-binding. It has been reviewed that the majority of WD40 domain-binding protein interact with the top surface of WD40 domain (33). Take the first resolved WD40 protein structure for example: the β -subunit of transducin is consisted of a WD40 domain, which interact with the α -subunit using its top surface. The α/β subunit interaction involves 5 of the 7 WD40 repeats of β -subunit (67, 68). The second crystal structure of WD40 protein is the β -TrCP1, which is an F-box protein subunit in the Skp, Cullin, F-box-containing (SCF) E3 ligase complex. As a subunit of E3 ligase, β -TrCP1 interacts with one of its clients, β -catenin using its top surface. The interaction involves all of the 7 WD40 repeats in the domain (69, 70).

Considering the likelihood of SCAP interacts with SREBP using its top surface, we employed another approach and identified 8 potential SREBP-interacting residues residing within aa984–1248, encompassing 6 of the 7 predicted WD40 repeats predicted by the WD40 protein database (66). This fit with our consideration that SREBP binds to most if not all of the repeats. Moreover, in the truncated SCAP experiment, which was based on the WD40 repeats predicted by the UniProt database, deletion of N-terminal to the first WD40 repeat (Δ N-WD1) resulted in a relatively mild reduction of SREBP-binding activity. This can be explained by the fact that SCAP/ Δ N-WD1 (aa832–1279) includes all of the 8 potential SREBP-interacting residues. We also noticed that even with only 3 WD40 repeats, SCAP/WD3–5 was still able to interact with SREBP to a readily detectable level. This can also be explained by the fact that SCAP/WD3–5 (aa1005–1195) includes 6 of the 8 potential SREBP-binding residues R984, K1018, R1019, H1118, D1162, L1178, and R1187.

In summary, we conclude that SREBP interacts to a surface of SCAP WD40 domain that involves at least 8 amino acids within aa984–1248. However, based on the nature of WD40 domain-mediated protein-protein interaction, especially those involving the top surface of WD40 domain, it is likely that more residues might contribute to SREBP-binding. To exemplify the complexity, it was discovered that the β -TrCP1/ β -catenin interaction actually involves over 13 residues on the top surface of β -TrCP1 (70).

CHAPTER 5

Comprehensive Discussion

Lipids are fundamental elements of life that serve as major sources of stored energy, comprise vital components of cellular membrane, and form steroid hormones (71, 72). Therefore, the biosynthesis of fatty acids and cholesterol is tightly regulated, primarily by the SREBP family of transcription factors. SREBP activation is associated to and regulated by SCAP, the SREBP chaperone. Although the SREBP-SCAP regulatory circuits of lipid metabolism has been studied extensively, some questions still remain. In this study we attempted to address 2 questions focusing of the SCAP C-terminus. The first question is whether other factors interact with SCAP and regulate SCAP/SREBP-mediated lipid homeostasis; and the second question is to elucidate the SREBP-binding motif in the C-terminus of SCAP.

It has been demonstrated in 1997 that SCAP and SREBP interact through the C-termini of both sides (26). One interesting fact of the C-terminal of SCAP is that it is consisted of a WD40 domain (27, 28). The WD40 domain is characterized by repeated sequences that usually include a conserved tryptophan-aspartic acid (WD) near the C-terminal end of each sequence (73). The typical β -propeller structure of WD40 domain is usually comprised of 7 WD40 repeats. However, some WD40 domain has 8 or more WD40 repeats, such as the WD40 domain of Scp1, the SCAP homolog in fission yeast, is comprised of 8 WD40 repeats (27). WD40 domain containing proteins are often referred to as WD40 proteins (29). WD40 proteins comprise approximately 1% of the human proteome and are involved in a broad range of biological activities, including signal transduction, ubiquitination, cell cycle regulation (29). One of the main features of WD40 domain is the ability to interact with a wide array of protein partners and serve as a protein hub to mediate formation of diverse protein complexes. One representative example is the DNA damage-binding protein 1 (DDB1), a WD40 protein that acts as the substrate-recognition subunit of the cullin-RING E3 ligase complex. DDB1 can interact with over 30 different substrates (74).

It is interesting that SCAP possesses a WD40 domain, which suggests the possibility that in addition to SREBP, SCAP can interact with multiple protein partners and these protein partners may probably regulate or be regulated by SCAP or the SCA/SREBP complex. In **Chapter 2**, we identified a list of proteins that potentially interact with the WD40 domain of SCAP. Among which we performed further studies on Hsp90. The reason that we chose Hsp90 was that it has been reported to be involved in lipid regulation (42, 43, 50–52). We showed in **Chapter 2** that Hsp90 interacts with the C-termini of SCAP and SREBP rather than the N-termini (**Fig. 4–6**). This finding suggests that Hsp90 might interact with the SCAP/SREBP complex. *In vitro* binding assay might be required to examine whether Hsp90 binds individually to SCAP and SREBP or to the SREBP/SCAP complex. However, since the WD40 domain is just a portion of SCAP C-terminus, it is also possible that Hsp90 interacts with other portion of the SCAP C-terminus. In addition, since Hsp90 is a cytoplasmic chaperone and that the matured N-terminal SREBP is localized in the nucleus, the difference in localization might also explain the lack of Hsp90/N-SREBP interaction. Nonetheless, we also identified Hsp70 as a SCAP WD40 domain-binding protein. Hsp70 is core co-chaperone of Hsp90. In the Hsp90 chaperoning cycle of cytoplasmic proteins, the Hsp90 clients first bind to Hsp70, and the client-Hsp70 complex binds to the N-terminal domain of

Hsp90. Thus, the transfer of client protein to Hsp90 by Hsp70 is required for Hsp90 chaperoning cycle. Whether it is also the case for Hsp90/SCAP/SREBP complex formation requires more investigations.

Nonetheless, it should also be noted here that Hsp90 regulates its clients by more than one way. For example, Hsp90 facilitate the correct folding of newly synthesized proteins and ensure their maturation (32). Hsp90 can also protect the stability of matured proteins, or even inactivate its clients by preventing their release from the Hsp90 chaperone complex (33). Hsp90 can also regulate its client by promoting their transport from the ER to their designated organelles. For instance, as mentioned in **Section 3-4**, Hsp90 regulates the ER-to-Golgi transport of Rab GTPase and ER-to-plasma membrane trafficking of OsCERK1 (64, 65). In **Chapter 3** we show that Hsp90 inhibition destabilize SCAP/SREBP proteins, indicating that Hsp90 might be involved in the maturation of SREBP precursor and SCAP; however, at this point it is difficult to rule out the possibility that other ER-bound chaperones can also facilitate the maturation of SCAP and SREBP, and Hsp90-binding only protects the stability of the correctly folded SCAP and SREBP proteins. In addition, Hsp90 can also regulate the transport of SCAP/SREBP from the ER to the Golgi apparatus by helping the formation of a larger protein complex. Nevertheless, since SCAP is essential to the ER-to-Golgi transport of SCAP/SREBP complex, it is rather difficult to use the current method, Hsp90 inhibition, to study the contribution of Hsp90 to SCAP/SREBP transport. Since Hsp90 inhibition leads to rapid degradation of SCAP and SREBP, which would ultimately cause the decrease SCAP/SREBP in the Golgi, causing a confusing result as whether the decrease is due to SCAP/SREBP degradation or inhibited ER-to Golgi-transport.

Despite all kinds of mechanisms described above, we did find out that Hsp90-SCAP/SREBP binding occurs in both the ER and the Golgi apparatus (**Fig. 20**). This suggests that Hsp90 might contribute by protecting the protein stability of correctly folded SCAP and SREBP rather by facilitating their correct folding because if the latter is the case, based on current understanding of Hsp90 chaperone machinery, SCAP and SREBP would have been released from the Hsp90 chaperone system after maturation (33). The question remained is that whether Hsp90 is required for the transportation of SCAP and SREBP. If Hsp90 helps ER-to-Golgi transport of SCAP/SREBP complex, it is still unclear why Hsp90 continued to bind to SCAP and the cleaved C-terminus of SREBP after the processing of SREBP. Hence, at the current stage, perhaps it is only safe to conclude that Hsp90 functions to protect the stability of SCAP during its cycling around the ER and the Golgi apparatus, and to protect SREBP precursor during their transport to the Golgi apparatus and its processing by site-1 and site-2 proteases.

One key finding in **Chapter 3** is that Hsp90 inhibition caused proteasome-dependent degradation of SCAP and SREBP precursors, causing the downregulation of SREBP-target genes and the reduction of intracellular or liver lipid levels. Although it has been reported previously that SCAP is degraded by the proteasome-dependent mechanism when SCAP N-glycosylation is inhibited (25), it is the first report of proteasome-dependent SREBP precursor degradation. As a supporting evidence we present data that

proteasome inhibition restored the protein level of precursor SREBP1 in *SCAP*-deficient SRD-13A cells (Supplementary Fig. S7). It has been reported that F-box/WD40 protein 7 (Fbw7) is involved in the ubiquitination and the proteasomal degradation of matured SREBP1 and SREBP2 (75–77). In that report, the authors identified a CTD motif that is regulated by the glycogen synthase kinase 3 (GSK-3) in SREBP1a. GSK-3 phosphorylates T426 and S430 of SREBP1a, and the phosphorylated SREBP1a is recognized by Fbw7 (75). However, a subsequent *in vivo* study found that inhibition of Fbw7 did not alter the expression of SREBP1c or its target genes in the livers, suggesting that other E3 ligase might be involved (78). A more recent report also showed that the ring finger protein 20 (RNF20) is involved in the ubiquitination and proteasomal degradation of matured SREBP1c (79). In that study, the authors showed that RNF20 physically interacted with nuclear SREBP1c and promotes poly-ubiquitination and proteasomal degradation of SREBP1c. In addition, they also demonstrated that RNF20 expression was induced by fasting through a PKA-dependent pathway, whereas Fbw7 mRNA level was unchanged by fasting or refeeding or PKA activation in mice (79).

In contrast to the studies on nuclear SREBP degradation, little has been done on the mechanism of the degradation of SREBP precursors. It was demonstrated that in SRD-13A cells that lacked functional *SCAP*, that precursor SREBP is rapidly degraded (6). It also has been demonstrated that overexpression of Trc8, an ER-bound ring finger domain-containing E3 ligase, destabilized SREBP precursors in a ring finger domain- and proteasome-dependent manner (80). In addition, a previous study conducted by our laboratory showed that Trc8 regulated the ER-to-Golgi transport of SREBP by competing with Sec24 for the *SCAP*-binding site. However, this regulation is independent to the E3 ligase activity of Trc8 (81). Here we add to that the degradation of SREBP precursors observed in *SCAP*-deficient cells is also through proteasome-dependent mechanism (Supplementary Fig. S7). On the other hand, although we and others (25) have observed proteasome-dependent degradation of *SCAP*, the E3 ligase responsible for the ubiquitination of *SCAP* is not yet identified. Identification of the E3 ligase of *SCAP* and SREBP precursor will provide insight to the regulatory mechanism of their degradation.

Notwithstanding the limited knowledge of *SCAP*/SREBP proteasome degradation, the sterol-induced proteasome degradation of HMG-CoA reductase, an ER-bound sterol sensing enzyme, has been studied in detail. In essence, the interplay among Insig-1, Insig-2, and ER-bound E3 ligases gp78/AMFR and Trc8 collaboratively mediates the HMG-CoA degradation. Insig-1 binds to gp78, whereas both Insig-1 and Insig-2 bind to Trc8. When intracellular sterol level rises, Insig-1 serves as a bridge between gp78 and HMG-CoA reductase, whereas Insig-1/-2 bridges Trc8 to HMG-CoA reductase. Then, both gp78- and Trc8-mediate ubiquitination lead to the extraction of HMG-CoA reductase from the ER membrane and bound for proteasome degradation (82). It would be interesting to investigate the involvement of gp78 and Trc8 in the ER-associated degradation of *SCAP* and SREBP precursors. In addition to gp78 and Trc8, another ring finger domain containing E3 ligase, ring finger protein 5 (RNF5), might also be involved in the proteasome degradation of *SCAP*. RNF5 mediate the ubiquitination of STING/MITA. The aa111 to aa150 sequence in the membrane-bound portion of STING is critical for STING/RNF5 interaction, and the K150 is important to RNF5-mediated STING ubiquitination (83). Interestingly, a

recent report revealed the interaction between the transmembrane domains of SCAP and STING (30). To evaluate the possibility that RNF5 might also interact with the transmembrane domain of SCAP, we analyzed the alignment of the aa111–150 sequence of STING with the 8 transmembrane domains of SCAP. Intriguingly, we found that the third transmembrane helix of SCAP shares 43% (9/21) identity and 62% (13/21) similarity with the aa111–150 RNF5-binding domain of STING. Hence, it would also be interesting to investigate the involvement of RNF5 in SCAP proteasome degradation.

Furthermore, it was discovered that N-glycosylation on the asparagine residues in luminal loop 1 and loop 7 protected SCAP from proteasome degradation. When N-glycosylation was inhibited by culturing the cells in glucose-deprived medium or by mutations at the glycosylation sites, SCAP was destabilized and degraded through a proteasome-dependent mechanism (25). Therefore, it would also be intriguing to investigate the effect of N-glycosylation on the accessibility of SCAP to E3-ligase-binding.

Another major finding in **Chapter 3** is that knockdown of Hsp90 led to the reduction of intracellular lipid levels, whereas overexpression of Hsp90 increased SCAP and SREBP protein levels, and raised intracellular lipid levels. There have been reports indicating the positive relation between Hsp90 and lipid biosynthesis; however, here we demonstrate the first direct evidence showing the causal relation between Hsp90 and SCAP/SREBP-mediated lipid biogenesis. Of note, a number of reports have shown the interaction between peroxisome proliferator-activated receptor gamma (PPAR γ), a key regulator of adipocyte differentiation, and Hsp90 (42, 50–52). It was first discovered in adipose tissues that Hsp90 interacted with and chaperoned PPAR γ and regulates the survival and differentiation of adipocytes (50). The PPAR γ -Hsp90 interaction was demonstrated in 3T3-L1 cells by anti-PPAR γ immunoprecipitation. It was also showed that the interaction was hindered by Hsp90 inhibitor geldanamycin (GA), which led to the decrease in PPAR γ protein. Other groups that used different Hsp90 N-terminal inhibitors such as radicicol or GA analogs 17-AAG and 17-DMAG also report similar findings that Hsp90 inhibition led to the decrease in PPAR γ proteins and the reduction of adipogenesis (51, 52).

In addition to adipose tissues, It was also reported that Hsp90 played a role in regulating PPAR γ and lipid homeostasis in mouse fatty livers (42). In a *Sec61a1* mutant murine model of nonalcoholic fatty liver disease (NAFLD), *Sec61a1* mutant mice showed a 3-fold higher content of liver triglycerides and spontaneously developed hepatic steatosis. The authors reported that gene expressions of both *Ppar γ 1* and *Ppar γ 2* were significantly upregulated, while expressions of lipogenic genes *Srebfl1*, *Dgat2*, *Acacb*, and *Scd1* were downregulated in *Sec61a1* mutant mice. It was discovered that Hsp90 protein level was elevated in *Sec61a1* mutant mice presumably due to ER stress response caused by *Sec61a1* mutation. It was showed by anti-PPAR γ immunoprecipitation that PPAR γ interacted to Hsp90 in livers from wild type mice and showed that 17-DMAG decreased the protein level of PPAR γ in livers from *Sec61a1* mutant mice (42) The authors suggested the relations between elevated Hsp90, PPAR γ , and fatty liver.

However, it is confusing that while hepatic lipogenic genes were downregulated and both fatty acids and cholesterol synthesis were reduced, *Sec61a1* mutant mice still exhibit higher liver triglycerides and develop hepatic steatosis. In addition, it was showed that both the gene expression and protein level of PPAR γ are induced in *Sec61a1* mutant mice, but whether the increase of PPAR γ protein was a result of upregulation of *Ppar γ* genes or because of the stabilization by Hsp90 was not addressed. In fact, in our anti-Hsp90 immunoprecipitation, we were only able to detect PPAR γ 2 but not PPAR γ 1 (Supplementary Fig. 8) in the precipitated samples, suggesting that Hsp90 might interact specifically to PPAR γ 2. This was not addressed in previous reports because all of which performed anti-PPAR γ immunoprecipitation that would have co-precipitated Hsp90 bound to either PPAR γ 1 or PPAR γ 2. Since *Ppar γ* transcription may also be affected by Hsp90, it is confusing whether Hsp90 regulate PPAR γ at transcriptional level or at protein level. Add to that, the cycloheximide-chase experiment conducted in 3T3-L1 cells actually showed a negligible difference between DMSO and GA treated group in the presence of cycloheximide (50). The experiment conducted on overexpressed FLAG-PPAR γ and FLAG-Hsp90 in HEK293 cells did show the protective effect of Hsp90 on PPAR γ in the presence of cycloheximide (42); however, the experiment had GAPDH, which is an endogenously expressed protein as the only control, leaving room for discussion whether the difference among groups were from differential expression of overexpressed proteins or from the authors' claims. That said, it is clear PPAR γ plays critical roles in lipid biogenesis, especially in adipose tissues. There is also substantial evidence indicating that Hsp90 play a crucial role in adipocyte differentiation and the pathogenesis of fatty liver diseases. However, based on current data, the connection between Hsp90 and PPAR γ is rather vague.

In addition to PPAR γ , another report has demonstrated the link between Hsp90 and lipid metabolism in the liver. In human patients suffering alcoholic cirrhosis and in mice treated with chronic or acute alcohol, Hsp90 expression and triglycerides level were significantly elevated in the livers (43). It was demonstrated that in alcohol-fed mice, Hsp90 inhibition by 17-DMAG prevented the downregulation of PPAR α and restored expressions of fatty acid oxidative genes. Moreover, 17-DMAG also prevented the induction of nuclear SREBP1 and restored the expression of lipogenic genes in alcohol-fed mice (43). These results demonstrate the positive relation between Hsp90 and SREBP-mediated lipogenesis.

Since we also showed that Hsp90 inhibition resulted in a downregulation of SREBP1c and SREBP2 genes, it is also necessary to clarify whether Hsp90 affect the protein level of SREBP alone or also the transcription of SREBP genes. To that end, we demonstrate here the data showing that SREBP1c and SREBP2 gene expressions were not altered after 12 or 24 h of 17-AAG treatment (Supplementary Fig. 9). This suggests that the gene expression of SREBP were downregulated after the reduction of SREBP proteins. In addition, previous studies have pointed out the possibility that Hsp90 may also regulate the activity of nuclear SREBP through the mTORC1/lipin 1 pathway. The translocation of nuclear SREBP (nSREBP) is regulated by lipin 1, which inhibit nuclear localization of nSREBP, thereby inhibiting its activity. The activity of lipin 1 is negatively regulated by mTORC1 pathway (76). On the other hand, it has been reported that Hsp90 inhibition led to the disruption of mTORC1 complex by dissociating Raptor/mTOR interaction (84). Therefore, inhibition of Hsp90 may lead to the blockage of mTORC1

pathway, which would result in the increase of lipin 1 activity to interfere the translocation of nSREBP. To investigate this pathway, we treated HEK293 cells with mTOR inhibitors rapamycin and Torin1, and compared the effects with 17-AAG. As a result, we did find that the phosphorylation of mTOR Ser2448 and p70 S6 kinase Thr389 were decreased by mTOR inhibitors and 17-AAG (Supplementary Fig. S10). In addition, while matured nuclear SREBP1 (nSREBP1) was decreased by Torin 1, both nSREBP1 and nSREBP2 were decreased by 17-AAG treatment (Supplementary Fig. S11, nuclear extracts, lanes 5–8). Nonetheless, unlike 17-AAG that decreased both SCAP and SREBP protein levels, mTOR inhibitors increased the protein level of SREBP precursors, presumably through inhibition of SREBP processing (Supplementary Fig. S11, cytoplasmic fractions, lanes 1–4; References 13–16).

Hsp90 has been a target for the development of anti-cancer therapy due to its activity to regulate key cellular processes including cell cycle and proliferation (33, 55, 56). Although a number of reports have been published (42, 43, 50–52), the role of Hsp90 in regulating lipid homeostasis is still elusive. Based on the data present here, we propose that Hsp90 mediates lipid metabolism by directly maintaining the protein level of SCAP/SREBP. Hsp90 protects SCAP and SREBP from proteasomal degradation that would happen rapidly in the absence of Hsp90. The chaperoning cycle of Hsp90 might occur from the ER throughout the ER-Golgi-ER cycling of SCAP and the proteolytic processing of SREBP precursors. Interestingly, recent studies on SCAP and SREBP revealed the interconnection between SCAP/SREBP and tumor growth. For example, it was demonstrated in glioblastoma cells, SCAP act as glucose sensor that linked the elevated glucose uptake induced by EGFR-signaling to increased lipogenesis and tumor growth (25). The study elucidated the pathway by which glucose-mediated N-glycosylation stabilized SCAP and facilitated subsequent activation of SREBP. In the absence of glucose, sterol depletion failed to induce SREBP processing due to the degradation of SCAP. In mice xenografts, inhibition of SCAP or N-glycosylation of SCAP significantly reduced lipid biosynthesis and tumor growth, extending the survival time of tumor-bearing mice (25). The same group also discovered a regulatory mechanism in glioblastoma cells in which microRNA (miR)-29 expression was induced by SREBP, and the induced miR-29 feedback inhibited both SCAP and SREBP by binding to their 3' untranslated regions. It was demonstrated that expression of miR-29 mimics inhibited SCAP/SREBP activation and tumor growth, prolonging the survival of tumor-bearing mice (48). In addition, it was also reported in lung cancer that inhibition of SREBP enhanced the sensitivity of anti-cancer drug gefitinib (49). These studies present recent discoveries of the links between SCAP/SREBP-mediated lipid homeostasis and tumorigenesis.

In conclusion, with the attempt to find novel SCAP-binding proteins, we discovered Hsp90 as a new SREBP regulator that forms complex with SCAP and SREBP. We demonstrated that Hsp90 positively regulates the protein stability of SCAP/SREBP and lipid homeostasis. This finding explains at least in part the concurrent increase of Hsp90 and SREBP expressions and lipogenesis in cancer cells and fatty livers. The direct causal relation between Hsp90 and SREBP in maintenance of lipid homeostasis open new avenue as to the development of strategies against both cancer and metabolic diseases. In addition, we discovered a core surface consisted of at least 8 amino acids that is potentially the SREBP-binding region, providing further knowledge of the molecular interaction between human SCAP and SREBP.

References

- (1) Brown, M. S. and Goldstein J. L. (1997) The SREBP pathway: regulation of cholesterol metabolism by proteolysis of a membrane-bound transcription factor. *Cell* **89**, 331–340
- (2) Espenshade, P. J. (2006) SREBPs: sterol-regulated transcription factors. *J. Cell Sci.* **15**, 973–976
- (3) Goldstein, J. L., DeBose-Boyd, R. A., and Brown, M. S. (2006) Protein sensors for membrane sterols. *Cell* **124**, 35–46
- (4) Ye, J. and DeBose-Boyd, R. A. (2011) Regulation of cholesterol and fatty acid synthesis. *Cold Spring Harb. Perspect. Biol.* **3**, a004754
- (5) Inoue, J. and Sato, R. (2013) New insights into the activation of sterol regulatory element-binding proteins by proteolytic processing. *Biomol. Concepts* **4**, 417–423
- (6) Rawson, R. B., DeBose-Boyd, R., Goldstein, J. L., and Brown, M. S. (1999) Failure to cleave sterol regulatory element-binding proteins (SREBPs) causes cholesterol auxotrophy in Chinese hamster ovary cells with genetic absence of SREBP cleavage-activating protein. *J. Biol. Chem.* **274**, 28549–28556
- (7) Sakai, J., Nohturfft, A., Goldstein, J. L., and Brown, M.S. (1998) Cleavage of sterol regulatory element-binding proteins (SREBPs) at site-1 requires interaction with SREBP cleavage-activating protein. Evidence from *in vivo* competition studies. *J. Biol. Chem.* **273**, 5785–5793
- (8) Sakai, J., Rawson, R. B., Espenshade, P. J., Cheng, D., Seegmiller, A. C., Goldstein, J. L., and Brown, M. S. (1998) Molecular identification of the sterol-regulated luminal protease that cleaves SREBPs and controls lipid composition of animal cells. *Mol. Cell* **2**, 505–514
- (9) Brown, M. S., and Goldstein, J. L. (2009) Cholesterol feedback: from Schoenheimer’s bottle to Scap’s MELADL. *J. Lipid Res.* **50**, S15-S27
- (10) Horton, J. D., Goldstein, J. L., and Brown, M. S. (2002) SREBPs: activators of the complete program of cholesterol and fatty acid synthesis in the liver. *J. Clin. Invest.* **109**, 1125–1131
- (11) Radhakrishnan, A., Goldstein, J. L., McDonald, J. G., and Brown, M. S. (2008) Switch-like control of SREBP-2 transport triggered by small changes in ER cholesterol: a delicate balance. *Cell Metab.* **8**, 512–521
- (12) Sun, L.-P., Li, L., Goldstein, J. L., and Brown, M. S. (2005) Insig required for sterol-mediated inhibition of Scap/SREBP binding to COPII proteins *in vitro*. *J. Biol. Chem.* **280**, 26483–26490
- (13) Porstmann, T., Santos, C. R., Griffiths, B., Cully, M., Wu, M., Leever, S., Griffiths, J. R., Chung, Y. L., and Schulze, A. (2008) SREBP activity is regulated by mTORC1 and contributes to Akt-dependent cell growth. *Cell Metab.* **8**, 224–236
- (14) Li, S., Brown, M. S., and Goldstein, J. L. (2010) Bifurcation of insulin signaling pathway in rat liver: mTORC1 required for stimulation of lipogenesis, but not inhibition of gluconeogenesis. *Proc. Natl. Acad. Sci. U. S. A.* **107**, 3441–3446
- (15) Duvel, K., Yecies, J. L., Menon, S., Raman, P., Lipovsky, A. I., Souza, A. L., Triantafellow, E., Ma, Q., Gorski, R., Cleaver, S., Vander Heiden, M. G., MacKeigan, J. P., Finan, P. M., Clish, C. B., Murphy, L. O., and Manning, B. D. (2010) Activation of a metabolic gene regulatory network downstream of mTOR complex 1. *Mol. Cell* **39**, 171–183

- (16) Yecies, J. L., Zhang, H. H., Menon, S., Liu, S., Yecies, D., Lipovsky, A. I., Gorgun, C., Kwiatkowski, D. J., Hotamisligil, G. S., Lee, C. H., and Manning, B. D. (2011) Akt stimulates hepatic SREBP1c and lipogenesis through parallel mTORC1-dependent and independent pathways. *Cell Metab* **14**, 21–32
- (17) Li, Y., Xu, S., Mihaylova, M. M., Zheng, B., Hou, X., Jiang, B., Park, O., Luo, Z., Lefai, E., Shyy, J. Y., Gao, B., Wierzbicki, M., Verbeuren, T. J., Shaw, R. J., Cohen, R. A., and Zang, M. (2011) AMPK phosphorylates and inhibits SREBP activity to attenuate hepatic steatosis and atherosclerosis in diet-induced insulin-resistant mice. *Cell Metab.* **13**, 376–88
- (18) Shackelford, D. B. and Shaw, R. J. (2009) The LKB1-AMPK pathway: metabolism and growth control in tumour suppression. *Nat. Rev. Cancer* **9**, 563–575
- (19) Han, J., Li, E., Chen, L., Zhang, Y., Wei, F., Liu, J., Deng, H., and Wang, Y. (2015) The CREB coactivator CRTC2 controls hepatic lipid metabolism by regulating SREBP1. *Nature* **524**, 243–246
- (20) Xu, D., Wang, Z., Zhang, Y., Jiang, W., Pan, Y., Song, B. L., and Chen, Y. (2015) PAQR3 modulates cholesterol homeostasis by anchoring Scap/SREBP complex to the Golgi apparatus. *Nat. Commun.* **6**, 8100
- (21) Nohturfft, A., Brown, M. S., and Goldstein, J. L. (1998) Topology of SREBP cleavage-activating protein, a polytopic membrane protein with a sterol sensing domain. *J. Biol. Chem.* **273**, 17243–17250
- (22) Motamed, M., Zhang, Y., Wang, M. L., Seemann, J., Kwon, H. J., Goldstein, J. L., and Brown, M. S. (2011) Identification of luminal Loop 1 of Scap protein as the sterol sensor that maintains cholesterol homeostasis. *J. Biol. Chem.* **286**, 18002–18012
- (23) Zhang, Y., Motamed, M., Seemann, J., Brown, M. S., and Goldstein, J. L. (2013) Point mutation in luminal loop 7 of Scap protein blocks interaction with loop 1 and abolishes movement to Golgi. *J. Biol. Chem.* **288**, 14059–14067
- (24) Zhang, Y., Lee, K. M., Kinch, L. N., Clark, L., Grishin, N. V., Rosenbaum, D. M., Brown, M. S., Goldstein, J. L., and Radhakrishnan, A. (2016) Direct demonstration that loop1 of Scap binds to loop7: a crucial event in cholesterol homeostasis. *J. Biol. Chem.* **291**, 12888–12896
- (25) Cheng, C., Ru, P., Geng, F., Liu, J., Yoo, J. Y., Wu, X., Cheng, X., Euthine, V., Hu, P., Guo, J. Y., Lefai, E., Kaur, B., Nohturfft, A., Ma, J., Chakravarti, A., and Guo, D. (2015) Glucose-mediated N-glycosylation of SCAP is essential for SREBP-1 activation and tumor growth. *Cancer Cell* **28**, 569–581
- (26) Sakai, J., Nohturfft, A., Cheng, D., Ho, Y. K., Brown, M. S., and Goldstein, J. L. (1997) Identification of complexes between the COOH-terminal domains of sterol regulatory element-binding proteins (SREBPs) and SREBP cleavage-activating protein. *J. Biol. Chem.* **272**, 20213–20221
- (27) Gong, X., Li, J., Shao, W., Wu, J., Qian, H., Ren, R., Espenshade, P., and Yan, N. (2015) Structure of the WD40 domain of SCAP from fission yeast reveals the molecular basis for SREBP recognition. *Cell Res.* **25**, 401–411

- (28) Gong, X., Qian, H., Shao, W., Li, J., Wu, J., Liu, J.-J., Li, W., Wang, H.-W., Espenshade, P., and Yan, N. (2016) Complex structure of the fission yeast SREBP-SCAP binding domains reveals an oligomeric organization. *Cell Res.* **26**, 1197–1211
- (29) Stirnimann, C. U., Petsalaki, E., Russell, R. B., and Müller, C. W. (2010) WD40 proteins propel cellular networks. *Trends Biochem. Sci.* **35**, 565–574
- (30) Chen, W., Li, S., Yu, H., Liu, X., Huang, L., Wang, Q., Liu, H., Cui, Y., Tang, Y., Zhang, P., and Wang, (2016) ER Adaptor SCAP Translocates and Recruits IRF3 to Perinuclear Microsome Induced by Cytosolic Microbial DNAs. *PLoS Pathog.* **12**, e1005462
- (31) Csermely, P., Schnaider, T. Soti, C., Prohászka, Z., and Nardai, G. (1998) The 90-kDa molecular chaperone family: structure, function, and clinical applications. A comprehensive review. *Pharmacol. Ther.* **79**, 129–168
- (32) Chen, B., Piel, W. H., Gui, L., Bruford, E., and Monteiro, A. (2005) The HSP90 family of genes in the human genome: insights into their divergence and evolution. *Genomics* **86**, 627–637
- (33) Taipale, M., Jarosz, D. F., and Lindquist, S. (2010) HSP90 at the hub of protein homeostasis: emerging mechanistic insights. *Nat. Rev. Mol. Cell Biol.* **11**, 515–528
- (34) Whitesell, L. and Lindquist, S. (2009) Inhibiting the transcription factor HSF1 as an anticancer strategy. *Expert Opin. Ther. Targets* **13**, 469–478
- (35) Sorger, P. K. and Pelham, H. R. (1987) Purification and characterization of a heat-shock element binding protein from yeast. *EMBO J.* **6**, 3035–3041
- (36) Nadeau, K., Das, A., and Walsh, C. T. (1993) Hsp90 chaperonins possess ATPase activity and bind heat shock transcription factors and peptidyl prolyl isomerases. *J. Biol. Chem.* **268**, 1479–1487
- (37) Shiau, A. K., Harris, S. F., Southworth, D. R., and Agard, D. A. (2006) Structural analysis of *E. coli* hsp90 reveals dramatic nucleotide-dependent conformational rearrangements. *Cell* **127**, 329–340
- (38) Ali, M. M., Roe, S. M., Vaughan, C. K., Meyer, P., Panaretou, B., Piper, P. W., Prodromou, C., and Pearl, L. H. (2006) Crystal structure of an Hsp90-nucleotide-p23/Sba1 closed chaperone complex. *Nature* **440**, 1013–1017
- (39) Dollins, D. E., Warren, J. J., Immormino, R. M., and Gewirth, D. T. (2007) Structures of GRP94-nucleotide complexes reveal mechanistic differences between the Hsp90 chaperones. *Mol. Cell* **28**, 41–56
- (40) Chehab, M., Caza, T., Skotnicki, K., Landas, S., Bratslavsky, G., Mollapour, M., and Bourboulia, D. (2015) Targeting Hsp90 in urothelial carcinoma. *Oncotarget* **6**, 8454–8473
- (41) Whitesell, L. and Lindquist, S. L. (2005) HSP90 and the chaperoning of cancer. *Nat. Rev. Cancer* **5**, 761–772
- (42) Wheeler, M. C. and Gekakis, N. (2014) Hsp90 modulates PPAR γ activity in a mouse model of nonalcoholic fatty liver disease. *J. Lipid Res.* **55**, 1702–1710

- (43) Ambade, A., Catalano, D., Lim, A., Kopoyan, A., Shaffer, S. A., and Mandrekar, P. (2014) Inhibition of heat shock protein 90 alleviates steatosis and macrophage activation in murine alcoholic liver injury. *J. Hepatol.* **61**, 903–911
- (44) Brown, M. S. and Goldstein, J. L. (2008) Selective versus total insulin resistance: a pathogenic paradox. *Cell Metab.* **7**, 95–96
- (45) Kammoun, H. L., Chabanon, H., Hainault, I., Luquet, S., Magnan, C., Koike, T., Ferré, P., and Foufelle, F. J. (2009) GRP78 expression inhibits insulin and ER stress-induced SREBP-1c activation and reduces hepatic steatosis in mice. *J. Clin. Invest.* **119**, 1201–1215
- (46) Perry, R. J., Samuel, V. T., Petersen, K. F., Shulman, G. I. (2014) The role of hepatic lipids in hepatic insulin resistance and type 2 diabetes. *Nature* **510**, 84–91
- (47) Eason, K. and Sadanandam, A. (2016) Molecular or metabolic reprogramming: what triggers tumor subtypes? *Cancer Res.* **76**, 5195–5200
- (48) Ru, P., Hu, P., Geng, F., Mo, X., Cheng, C., Yoo, J. Y., Cheng, X., Wu, X., Guo, J. Y., Nakano, I., Lefai, E., Kaur, B., Chakravarti, A., and Guo, D. (2016) Feedback loop regulation of SCAP/SREBP-1 by miR-29 modulates EGFR signaling-driven glioblastoma growth. *Cell Rep.* **16**, 1527–1535
- (49) Li, J., Yan, H., Zhao, L., Jia, W., Yang, H., Liu, L., Zhou, X., Miao, P., Sun, X., Song, S., Zhao, X., Liu, J., and Huang, G. (2016) Inhibition of SREBP increases gefitinib sensitivity in non-small cell lung cancer cells. *Oncotarget* **7**, 52392–52403
- (50) Nguyen, M. T., Csermely, P. and Söti, C. (2013) Hsp90 chaperones PPAR γ and regulates differentiation and survival of 3T3-L1 adipocytes. *Cell Death Differ.* **20**, 1654–1663
- (51) He, Y., Li, Y., Zhang, S., Perry, B., Zhao, T., Wang, Y., and Sun, C. (2013) Radicol, a heat shock protein 90 inhibitor, inhibits differentiation and adipogenesis in 3T3-L1 preadipocytes. *Biochem. Biophys. Res. Commun.* **436**, 169–174
- (52) Desarzens, S., Liao, W. H., Mammi, C., Caprio, M., and Faresse, N. (2014) Hsp90 blockers inhibit adipocyte differentiation and fat mass accumulation. *PLoS ONE* **9**, e94127
- (53) Taipale, M., Krykbaeva, I., Koeva, M., Kayatekin, C., Westover, K. D., Karras, G. I., and Lindquist, S. (2012) Quantitative analysis of HSP90-client interactions reveals principles of substrate recognition. *Cell* **150**, 987–1001
- (54) Donnelly, B. F., Needham, P. G., Snyder, A. C., Roy, A., Khadem, S., Brodsky, J. L., and Subramanya, A. R. (2013) Hsp70 and Hsp90 multichaperone complexes sequentially regulate thiazide-sensitive cotransporter endoplasmic reticulum-associated degradation and biogenesis. *J. Biol. Chem.* **288**, 13124–3135
- (55) Johnson, J. L. (2012) Evolution and function of diverse Hsp90 homologs and cochaperone proteins. *Biochim. Biophys. Acta.* **1823**, 607–613
- (56) Stankiewicz, M. and Mayer, M. P. (2012) The universe of Hsp90. *Biomol. Concepts* **3**, 79–97
- (57) Bhat, R., Tummalapalli, S. R., and Rotella, D. P. (2014) Progress in the discovery and development of heat shock protein 90 (Hsp90) inhibitors. *J. Med. Chem.* **57**, 8718–8728

- (58) Zhang, L., Fok, J. H., and Davies, F. E. (2014) Heat shock proteins in multiple myeloma. *Oncotarget* **5**, 1132–1148
- (59) Proia, D. A. and Kaufmann, G. F. (2015) Targeting heat-shock protein 90 (HSP90) as a complementary strategy to immune checkpoint blockade for cancer therapy. *Cancer Immunol. Res.* **3**, 583–589
- (60) Sato, R., Miyamoto, W., Inoue, J., Terada, T., Imanaka, T., and Maeda, M. (1999) Sterol regulatory element-binding protein negatively regulates microsomal triglyceride transfer protein gene transcription. *J. Biol. Chem.* **274**, 24714–14720
- (61) Borkovich, K. A., Farrelly, F. W., Finkelstein, D. B., Taulien, J., and Lindquist, S. (1989) hsp82 is an essential protein that is required in higher concentrations for growth of cells at higher temperatures. *Mol. Cell Biol.* **9**, 3919–3930
- (62) Kim, H. R., Kang, H. S., and Kim, H. D. (1999) Geldanamycin induces heat shock protein expression through activation of HSF1 in K562 erythroleukemic cells. *IUBMB Life* **48**, 429–433
- (63) Shao, W. and Espenshade, P. J. (2014) Sterol regulatory element-binding protein (SREBP) cleavage regulates Golgi-to-endoplasmic reticulum recycling of SREBP cleavage-activating protein (SCAP). *J. Biol. Chem.* **289**, 7547–7557
- (64) Chen, C. Y. and Balch, W. E. (2006) The Hsp90 chaperone complex regulates GDI-dependent Rab recycling. *Mol. Biol. Cell* **17**, 3494–3507
- (65) Chen, L., Hamada, S., Fujiwara, M., Zhu, T., Thao, N. P., Wong, H. L., Krishna, P., Ueda, T., Kaku, H., Shibuya, N., Kawasaki, T., Shimamoto, K. (2010) The Hop/Sti1-Hsp90 chaperone complex facilitates the maturation and transport of a PAMP receptor in rice innate immunity. *Cell Host Microbe* **7**, 185–196
- (66) Wang, Y., Hu, X. J., Zou, X. D., Wu, X. H., Ye, Z. Q., and Wu, Y. D. (2015) WDSPdb: a database for WD40-repeat proteins. *Nucleic Acids Res.* **43**(Database issue), D339–D344
- (67) Lambright, D. G., Sondek, J., Bohm, A., Skiba, N. P., Hamm, H. E., and Sigler, P. B. (1996) The 2.0 Å crystal structure of a heterotrimeric G protein. *Nature* **379**, 311–319
- (68) Gaudet, R., Bohm, A., and Sigler, P. B. (1996) Crystal structure at 2.4 angstroms resolution of the complex of transducin betagamma and its regulator, phosducin. *Cell* **87**, 577–588
- (69) Wu, G., Xu, G., Schulman, B. A., Jeffrey, P. D., Harper, J. W., and Pavletich, N. P. (2003) Structure of a beta-TrCP1-Skp1-beta-catenin complex: destruction motif binding and lysine specificity of the SCF(beta-TrCP1) ubiquitin ligase. *Mol. Cell* **11**, 1445–1456
- (70) Hao, B., Oehlmann, S., Sowa, M. E., Harper, J. W., and Pavletich, N. P. (2007) Structure of a Fbw7-Skp1-cyclin E complex: multisite-phosphorylated substrate recognition by SCF ubiquitin ligases. *Mol. Cell* **26**, 131–143
- (71) Van Meer, G., Voelker, D. R., and Feigenson, G. W. (2008) Membrane lipids: where they are and how they behave. *Nat. Rev. Mol. Cell Biol.* **9**, 112–124
- (72) Nohturfft, A. and Zhang, S. C. (2009) Coordination of lipid metabolism in membrane biogenesis. *Annu. Rev. Cell Dev. Biol.* **25**, 539–566

- (73) Fong, H. K., Hurley, J. B., Hopkins, R. S., Miake-Lye, R., Johnson, M. S., Doolittle, R. F., and Simon, M. I. (1986) Repetitive segmental structure of the transducin beta subunit: homology with the CDC4 gene and identification of related mRNAs. *Proc. Natl. Acad. Sci. U. S. A.* **83**, 2162–2166
- (74) Angers, S., Li, T., Yi, X., MacCoss, M.J., Moon, R.T., Zheng, N. (2006) Molecular architecture and assembly of the DDB1-CUL4A ubiquitin ligase machinery. *Nature* **443**, 590–593
- (75) Sundqvist, A., Bengoechea-Alonso, M.T., Ye, X., Lukiyanchuk, V., Jin, J., Harper, J. W., Ericsson, J. (2005) Control of lipid metabolism by phosphorylation-dependent degradation of the SREBP family of transcription factors by SCF(Fbw7). *Cell Metab.* **1**, 379–391
- (76) Peterson, T. R., Sengupta, S. S., Harris, T. E., Carmack, A. E., Kang, S. A., Balderas, E., Guertin, D. A., Madden, K. L., Carpenter, A. E., Finck, B.N., and Sabatini, D.M. (2011) mTOR complex 1 regulates lipin 1 localization to control the SREBP pathway. *Cell* **146**, 408–420
- (77) Dong, Q., Giorgianni, F., Beranova-Giorgianni, S., Deng, X., O'Meally, R. N., Bridges, D., Park, E. A., Cole, R. N., Elam, M. B., Raghov, R. (2015) Glycogen synthase kinase-3-mediated phosphorylation of serine 73 targets sterol response element binding protein-1c (SREBP-1c) for proteasomal degradation. *Biosci Rep.* **36**, e00284
- (78) Kumadaki, S., Karasawa, T., Matsuzaka, T., Ema, M., Nakagawa, Y., Nakakuki, M., Saito, R., Yahagi, N., Iwasaki, H., Sone, H., Takekoshi, K., Yatoh, S., Kobayashi, K., Takahashi, A., Suzuki, H., Takahashi, S., Yamada, N., and Shimano, H. (2011) Inhibition of ubiquitin ligase F-box and WD repeat domain-containing 7a (Fbw7a) causes hepatosteatosis through Krüppel-like factor 5 (KLF5)/peroxisome proliferator-activated receptor γ 2 (PPAR γ 2) pathway but not SREBP-1c protein in mice. *J. Biol. Chem.* **286**, 40835–40846
- (79) Lee, J. H., Lee, G. Y., Jang, H., Choe, S. S., Koo, S. H., and Kim, J. B. Ring finger protein 20 regulates hepatic lipid metabolism through protein kinase A-dependent sterol regulatory element binding protein1c degradation. *Hepatology* **60**, 844–857
- (80) Lee, J. P., Brauweiler, A., Rudolph, M., Hooper, J. E., Drabkin, H. A., and Gemmill, R. M. (2010) The TRC8 ubiquitin ligase is sterol regulated and interacts with lipid and protein biosynthetic pathways. *Mol. Cancer Res.* **8**, 93–106
- (81) Irisawa, M., Inoue, J., Ozawa, N., Mori, K., and Sato, R. (2009) The sterol-sensing endoplasmic reticulum (ER) membrane protein TRC8 hampers ER to Golgi transport of sterol regulatory element-binding protein-2 (SREBP-2)/SREBP cleavage-activated protein and reduces SREBP-2 cleavage. *J. Biol Chem.* **284**, 28995–29004
- (82) Jo, Y., Lee, P. C., Sguigna, P. V., DeBose-Boyd, R. A. (2011) Sterol-induced degradation of HMG CoA reductase depends on interplay of two Insigs and two ubiquitin ligases, gp78 and Trc8. *Proc. Natl. Acad. Sci. U. S. A.* **108**, 20503–20508
- (83) Zhong, B., Zhang, L., Lei, C., Li, Y., Mao, A. P., Yang, Y., Wang, Y. Y., Zhang, X. L., Shu, H. B. (2009) The ubiquitin ligase RNF5 regulates antiviral responses by mediating degradation of the adaptor protein MITA. *Immunity* **30**, 397–407

- (84) Ohji, G., Hidayat, S., Nakashima, A., Tokunaga, C., Oshiro, N., Yoshino, K., Yokono, K., Kikkawa, U., and Yonezawa, K. (2006) Suppression of the mTOR-raptor signaling pathway by the inhibitor of heat shock protein 90 geldanamycin. *J. Biochem.* **139**, 129–135

Publication

Kuan, Y.-C., Hashidume, T., Shibata, T., Uchida, K., Shimizu, M., Inoue, J. and, Sato, R. (2017) Heat shock protein 90 modulates lipid homeostasis by regulating the stability and function of sterol regulatory element-binding protein (SREBP) and SREBP cleavage-activating protein. *J. Biol. Chem.* (Accepted)

論文の内容の要旨

応用生命化学 専攻
平成 26 年博士課程 入学
氏名 官 彦州
指導教員名 佐藤 隆一郎

論文題目

Study on heat shock protein 90 complex formation with SCAP/SREBP and regulation of SREBP function
(熱ショックタンパク質 90 による SCAP/SREBP 複合体形成と SREBP 活性調節に関する研究)

Chapter 1: *Introduction*

Sterol regulatory element-binding proteins (SREBPs) are the master transcription factors that control the expression of genes involved in fatty acids and cholesterol biosynthesis. SREBPs are synthesized on the endoplasmic reticulum (ER) membrane as inactive precursors. Upon synthesis, SREBP binds to its membrane-bound chaperone, SREBP cleavage-activating protein (SCAP). SCAP-binding protects SREBP from rapid degradation and promotes the transport of SREBP to the Golgi apparatus, in which SREBP is cleaved by site-1 and site-2 proteases. The N-terminal transactivation domain of SREBP is released by the proteolytic cleavage and translocates to the nucleus. Hence, SCAP/SREBP-binding is critical to SREBP function and lipid metabolism. It was demonstrated in 1997 that the C-terminal of SREBP interacted with SCAP C-terminus, which contains at least four WD40 repeats. However, up to present there is limited advance in the knowledge regarding the molecular detail of SCAP/SREBP-interaction. In addition, SREBP also plays essential roles in tumorigenesis. Dysregulations of SREBP and lipogenesis is a common strategy of cancer cells to manipulate energy metabolism. Intriguingly, heat shock protein 90 (Hsp90), a conserved chaperone that regulates most of the important cellular processes, is also highly expressed in most cancer cells, chaperoning essential proteins for cancer survival and progression. Recent studies also revealed the involvement of Hsp90 in adipogenesis and fatty liver diseases. Nonetheless, how Hsp90 manipulates lipid metabolism and interplays with SREBP are largely unknown. In this study, we aimed to uncover the molecular detail in the interaction between SCAP and SREBP. In addition, with the attempt to discover new SCAP-binding proteins that regulate SCAP/SREBP, we identified Hsp90 as a novel SREBP regulator. We performed a series of experiments to investigate the interaction between Hsp90 and SCAP/SREBP protein complex and to elucidate the regulatory effect of Hsp90 on SREBP and lipid biogenesis. We demonstrate here that Hsp90 regulates lipid homeostasis through directly controlling the protein level of SCAP and SREBP.

Chapter 2: *Hsp90 physically interacts with the C-termini of SCAP and SREBP*

The C-terminal of SCAP contains a WD40 domain, which is featured by the ability to interact with a wide array of proteins. In this part of the study, we aimed to find new SCAP-binding proteins by a mass spectrum-based proteomic approach. We overexpressed the C-terminus of human SCAP (C-SCAP) in human embryonic kidney 293 cells. C-SCAP-binding proteins were immunoprecipitated and subjected to electrospray ionization quadrupole time-of-flight mass spectrum analysis. More than 40 potential C-SCAP-binding proteins were identified, in which Hsp90 had relatively high sequence coverage (>30%). Since Hsp90 played critical roles in both cancer and lipid metabolism, we were particularly interested in the link between Hsp90 and SCAP. We performed immunoprecipitation experiments using FLAG-SCAP, FLAG-SREBP, and Myc-Hsp90 overexpressed proteins. We showed that Hsp90 interacted with the C-termini of SCAP and SREBP, possibly forming an Hsp90/SCAP/SREBP complex. In agreement with the overexpressed protein experimental result, we were able to co-immunoprecipitate endogenous SCAP and SREBP with Hsp90. Taken together, we demonstrated that Hsp90 formed a protein complex with SCAP and SREBP by interacting with their C-termini. This finding also suggests the possibility that Hsp90 might mediate lipid metabolism by direct regulation of SCAP and SREBP proteins.

Chapter 3: *Hsp90 modulates lipid homeostasis by regulating the stability of SCAP and SREBP*

Hsp90 and SREBP play indispensable roles in sustaining cancer cells survival and coordinating lipid homeostasis. However, the link between Hsp90 and SREBP is elusive. To study the effect of Hsp90 on SCAP/SREBP, we treated human hepatoma HepG2 cells with an Hsp90 inhibitor 17-(Allylamino)-17-demethoxygeldanamycin (17-AAG). 17-AAG decreased SCAP/SREBP protein level, downregulated SREBP-target gene expression, and reduced intracellular triglycerides and total cholesterol levels. This result implies that Hsp90 positively regulates SREBP via controlling SCAP/SREBP protein level. To test this inference, we knockdowned or overexpressed Hsp90 in HepG2 cells by small interfering RNA (siRNA) or lentivirus infection, respectively. Knockdown of Hsp90 substantially reduced the protein level of SCAP/SREBP, causing decreases in triglycerides and total cholesterol levels, whereas Hsp90 overexpression had the opposite effect. These results clearly demonstrate that Hsp90 regulates lipids biogenesis by controlling SCAP/SREBP proteins. We further investigated Hsp90-induced decrease of SCAP/SREBP using protein translation inhibitor cycloheximide (CHX). CHX-chase assay showed that 17-AAG accelerated the degradation of SCAP/SREBP proteins. Moreover, co-treatment of proteasome inhibitor MG132 cancelled the effect of 17-AAG on SCAP/SREBP degradation. These results indicate that Hsp90 stabilizes SCAP/SREBP proteins by protecting them from proteasomal degradation.

Since Hsp90 is a cytoplasmic chaperone and SCAP and SREBP are membrane-bound, we investigated if Hsp90 is indeed associated with SCAP/SREBP on the ER and Golgi membrane. By cell fractionation experiments, we showed that Hsp90 co-existed with SCAP/SREBP and co-immunoprecipitated with

SCAP in both the ER and Golgi fractions. Moreover, we also found that the interaction between Hsp90 and SCAP/SREBP was independent to intracellular sterol levels. Application of cholesterol and 25-hydroxycholesterol (25-HC) had negligible effect on Hsp90-SCAP/SREBP interaction. In contrast, 17-AAG dramatically inhibited Hsp90-SCAP/SREBP binding. Furthermore, reduction of SCAP/SREBP induced by 17-AAG was unaffected by 25-HC treatment. Altogether, these data suggests that binding to Hsp90 is crucial for the stabilization of SCAP/SREBP complex; however, the binding and stabilizing effect of Hsp90 on SCAP/SREBP is independent to intracellular sterol levels.

Finally, to test our findings *in vivo*, we treated C57/BL6Ncr1 mice with a more potent 17-AAG analog, 17-dimethylaminoethylamino-17-demethoxygeldanamycin (17-DMAG) by intraperitoneal injections. In agreement with the *in vitro* data, 17-DMAG treatment substantially decreased the protein level of SCAP/SREBP in mouse livers. Moreover, 17-DMAG downregulated hepatic expressions of SREBP-target genes and reduced triglycerides and total cholesterol levels in mouse livers. Taken together, we demonstrated that Hsp90 interacted with SCAP/SREBP on both the ER and Golgi membrane, keeping SCAP and SREBP proteins at steady levels through preventing their proteasomal degradation, thereby maintaining SREBP-target gene expressions and lipid homeostasis in hepatocytes and in mouse livers.

Chapter 4: *SREBP-binding sites in SCAP WD40 domain*

The binding between SCAP and SREBP C-termini has been revealed for nearly 2 decades, however, little is known about the detail of human SCAP/SREBP interaction. To elucidate SREBP-binding motif in SCAP, we developed two strategies based on current knowledge of the WD40 domain structure of SCAP C-terminus. First, using the 7 WD40 annotations of the UniProt database, we constructed SCAP truncated mutants lacking WD40 repeat(s) on its N-terminal, C-terminal, or both ends. Second, taking advantage of a WD40 protein database (WDSPdb) and the crystal structure of yeast SCAP, we deduced more than 30 potential SREBP-binding residues and constructed SCAP mutants carrying corresponding point mutations. SREBP-binding ability of the truncated and point mutated SCAP mutants were tested by co-immunoprecipitation assays. Truncation from N-terminus to WD2–WD3 or from C-terminus to WD7–WD5 dramatically reduced SREBP-binding ability of SCAP. However, simultaneous truncation from both termini showed no incremental effect, in which SCAP mutant having only WD3–WD5 still possessed SREBP-binding ability. This data implies that all WD40 repeats in SCAP contribute partially to SREBP-binding and prompt us to search for the amino acids residues crucial for SREBP-binding.

Based on the information retrieved from the WDSPdb, we constructed 7 SCAP mutant plasmids each carried a point mutation at a potential protein-protein interaction site. Immunoprecipitation experiments revealed that point mutations at leucine 1178 (L1178) and arginine 1248 (R1248) substantially reduced SREBP-binding ability. In addition, structure of yeast SCAP/SREBP1 complex unveiled a positively charged, arginine and lysine-rich region (R/K-patch) in the WD40 domain of SCAP that is essential to

SREBP-binding. Hence, we constructed over 20 plasmids each carried a point mutation at a charged residue, arginine (R), lysine (L), histidine (H), or aspartic acid (D), and tested the effect on SREBP-binding. Immunoprecipitation assays showed that mutations at R984, K1018, R1019, H1118, D1162, and R1187 substantially decreased SREBP-binding ability of SCAP.

In summary, we identified R984, K1018, R1019, H1118, D1162, L1178, R1187, and R1248 as the potential SREBP-binding residues. Interestingly, all these residues reside within WD2–WD7 (aa984–1248) of SCAP, explaining that SREBP-binding ability was uncompromised in WD1-deleted SCAP (aa832–1279) and that SCAP mutant with only WD3–WD5 (aa1005–1195) was still bound to SREBP.

Chapter 5: *Comprehensive discussion*

SREBP plays crucial roles in lipid metabolism and is hijacked by cancer cells to manipulate energy metabolism to favor survival and progression of tumors. Of equal importance, Hsp90 is one of the most abundant and perhaps the most important chaperone in cells. It regulates most of the cellular processes such as signal transduction and cell proliferation and is highly expressed in cancer cells to maintain key proteins required for the malignancies of tumors. However, although extensive studies have advanced greatly the fields of both SREBP and Hsp90 researches, the connection between Hsp90 and SREBP is largely unknown. In this study, with the attempt to identify new SCAP-binding proteins, we identified Hsp90 as a new SREBP regulator that forms complex with SCAP and SREBP. We demonstrated a clear positive regulatory effect of Hsp90 on the protein stability of SCAP/SREBP and on lipid homeostasis. This finding explains at least partially the concurrent increase of Hsp90 and SREBP expressions and lipogenesis in cancer cells and fatty livers. The direct and causal relation between Hsp90 and SREBP in maintenance of lipid homeostasis open new avenue as to the development of strategies against both cancer and metabolic diseases. In addition, we discovered a core surface consisted of at least 8 amino acid residues that is potentially the SREBP-interacting region of SCAP. This finding provides a more in-depth knowledge as to the molecular detail in the interaction between human SCAP and SREBP.

Publication:

Kuan, Y.-C., Hashidume, T., Shibata, T., Uchida, K., Shimizu, M., Inoue, J. and, Sato, R. (2017)
Heat shock protein 90 modulates lipid homeostasis by regulating the stability and function of sterol regulatory element-binding protein (SREBP) and SREBP cleavage-activating protein. *J. Biol. Chem.*
(Accepted)

Acknowledgement

First and foremost, I would like to express my sincere gratitude to Professor Ryuichiro Sato, the advisor of this study, my mentor, for his invaluable guidance and discussion inputs that led to every breakthrough made in this study and for his generous and timely support throughout my life in Japan.

I would like to express my appreciation to Dr. Jun Inoue for his patience and keen advices during each and every one of the discussion that greatly strengthened the quality of this study. I especially thank Dr. Makoto Shimizu for his expert teaching on experimental techniques and giving valuable suggestions. I also thank Dr. Yoshio Yamauchi for his informative comments that added new values to this study.

I would like to pay my gratitude to Professor Koji Uchida and Dr. Takahiro Shibata for their expertise in mass spectrum analysis, which led to the grand finding of this study, Hsp90. I thank them dearly and sincerely for providing excellent technical and academic recommendations that enhanced this study.

I thank Dr. Hashidume for his expert technical supports in all of the animal experiments conducted in this study and for his precious advices on experimentations. I thank Dr. Yuichi Watanabe for his kind suggestions on experimentations and for the small bench chat that brightened up my day. I also thank Dr. Takashi Sasaki and Dr. Miho Chikazawa for their daily hard work that motivates me to keep up.

I'd like to pay thanks to former members of this laboratory. To Dr. Shingo Miyata for teaching me the art of immunoblotting that has benefited my research tremendously; To Dr. Juan Li and Ms. Jiao Guo for their kind accompany and assistance during my first year in Japan; To Dr. Ryuto Maruyama for his kindness and teaching on RNA handling; and finally to Ms. Asuka Kato for being a friendly tutor.

I thank Ms. Tzu-Wen Hong for her friendship and help to me and my wife in and outside the laboratory. I thank all members of the laboratory for without anyone of you the laboratory won't function properly. I thank you all for doing your part, which made possible for my daily work and therefore this study.

With full gratitude, I thank wholeheartedly to my parents, aunt Chóu, and big brother for their strong and reliable supports that walked me through all hardships, letting me to concentrate solely on my work.

Finally, with love in my heart, I thank my dear wife.

Thank you for keeping me company in this foreign country. Thank you for all the delicious food that keeps my spirit high every day. Thank you for creating me a home to work hard for. Thank you for all the contributions and endeavor that helped me pulled through the PhD course and completed this study.

Financial Supports

I pay my sincere gratitude to thank

The Japan-Taiwan Interchange Association of Government of Japan,

The Foundation for Dietary Scientific Research of Nisshin Seifun Group,

The Tojuro Iijima Foundation for Food Science & Technology of Yamazaki Baking Co., Ltd,

and The University of Tokyo for financial supports to me or to this research.

APPENDIX

Tables S1–S3

Figures S1–S11

Supplementary Table S1

Primer sequences for PCR cloning

Plasmid	forward primer (5' to 3')	reverse primer (5' to 3')
FLAG-fl-SCAP	tgacaagcttacctgactgaaaggctgcgtg	gctctagatcagtcagcttctccagcaca
FLAG-N-SCAP	tgacaagcttacctgactgaaaggctgcgtg	attcgcggccgcgcgtagaggcagagcagcag
FLAG-C-SCAP	ataagaatgcggccgcggtgctatgccgcgcaactacg	gatctctagatcagtcagcttctccagcaca
FLAG-fl-SREBP1	ataagaatgcggccgcgacgagccaccttcagc	gctctagactagctggaagtgcagctggtc
FLAG-N-SREBP1	ataagaatgcggccgcgcatggacgagccaccttcagc	gctctagactagcagggcagctggcagcggg
FLAG-C-SREBP1	ataagaatgcggccgcgcttcttctgtctacggtgagcc	gctctagactagctggaagtgcagctggtc
FLAG-fl-SREBP2	ataagaatgcggccgcgacgacagcggcgagctg	gctctagatcaggagcggcaatggcagctg
FLAG-N-SREBP2	ataagaatgcggccgcgacgacagcggcgagctg	gctctagacggattcttctgtgtgcctc
FLAG-C-SREBP2	gcttgcggccgcggaagctgctggttcatggggagc	gctctagatcaggagcggcaatggcagctg
FLAG-C-SCAP/ Δ N-WD1	cgcgaaattcacaggagagctgggaacgacttt	gatctctagatcagtcagcttctccagcaca
FLAG-C-SCAP/ Δ N-WD2	cgcgaaattcacaggagctctcagcagcattaccg	gatctctagatcagtcagcttctccagcaca
FLAG-C-SCAP/ Δ N-WD1	cgcgaaattcatgtcacacaaaaacccatcaca	gatctctagatcagtcagcttctccagcaca
FLAG-C-SCAP/ Δ WD7-C	ataagaatgcggccgcggtgctatgccgcgcaactacg	tagagtcgacttaggagtagaacttgatgcctgtgc
FLAG-C-SCAP/ Δ WD6-C	ataagaatgcggccgcggtgctatgccgcgcaactacg	tagagtcgacttaatggctgacccggctgccagt
FLAG-C-SCAP/ Δ WD5-C	ataagaatgcggccgcggtgctatgccgcgcaactacg	tagagtcgacttaagggtgaagaggcagcagcag
FLAG-C-SCAP/WD2-6	cgcgaaattcacaggagagctgggaacgacttt	tagagtcgacttaggagtagaacttgatgcctgtgc
FLAG-C-SCAP/WD2-5	cgcgaaattcacaggagagctgggaacgacttt	tagagtcgacttaatggctgacccggctgccagt
FLAG-C-SCAP/WD3-6	cgcgaaattcacaggagctctcagcagcattaccg	tagagtcgacttaggagtagaacttgatgcctgtgc
FLAG-C-SCAP/WD3-5	cgcgaaattcacaggagctctcagcagcattaccg	tagagtcgacttaatggctgacccggctgccagt
FLAG-C-SCAP/W971A	gttccatcgctagcttggagct	agctcaagctagcagtggaac
FLAG-C-SCAP/L1025A	tgccagggcctaaccgttccct	agggaaccgttagcccgctgca
FLAG-C-SCAP/Q1097A	tgggagcgtgaccacacact	agtgtgtggtcagcgtcccca
FLAG-C-SCAP/Q1138A	tggaggagcagatggggccat	atggccccatctgctctcca
FLAG-C-SCAP/D1162A	accgtgggctgtcacctcc	ggaggtgacagccccaggt
FLAG-C-SCAP/L1178A	gcagtgccgctgatgacctat	atgaggtcatcagcgcactg
FLAG-C-SCAP/R1248A	agcctgccgcccagatcctg	caggatctggcgagcaggt
FLAG-fl-SCAP/R984E	gtggtggggaaagcagcgg	ccgctgcttccccaccac
FLAG-fl-SCAP/988E	agcagcggcgaactggagtg	cacctcagttgccgctgct
FLAG-fl-SCAP/K1018E	cttggacgaagattgtggctg	cagccacaatcttctgccaag
FLAG-fl-SCAP/R1019E	cttggacaagaattgtggctg	gcagccacaatttcttctgccaag
FLAG-fl-SCAP/R1024E	gtggctgcagagctcaacggt	accgttgagctctgcagccac
FLAG-fl-SCAP/R1046E	cctgcagttgaaggaccacca	tgggtccctcaaacgcagg
FLAG-fl-SCAP/R1051E	accccagggaaggcagcttc	ggaactgcctcccctggggt
FLAG-fl-SCAP/K1086E	acagccctggaagccgctgct	agcagcggcttccaggcgtgt
FLAG-fl-SCAP/R1091E	cgctgctgggaattgtgact	agtaccaaattcccagcagcg
FLAG-fl-SCAP/R1102E	cacacactggaggtgttccgctc	gacggaacacctcagctgtgtg
FLAG-fl-SCAP/R1105E	gagagtgttcaactggaggact	agtccctcagttcgaacctctc
FLAG-fl-SCAP/R1152E	actggcagcgaagtgcagcctg	catggctgacttgcctgccagt
FLAG-fl-SCAP/R1160E	gtttgctcacgaggggatgct	gacatccccctgtagcaaac
FLAG-fl-SCAP/R1187E	catctgggacgaaagcacagc	gcctgtgcttctgcccagatg
FLAG-fl-SCAP/K1192E	cacaggcatcagttctactcc	ggagtagaactcagctgctgtg
FLAG-fl-SCAP/R1248E	cagcctgccgaacagatcctg	caggatctgttcggcagcgtg
FLAG-fl-SCAP/H1037E	cttggagaccgaaactgcctc	gagggcagttcggctccaag
FLAG-fl-SCAP/H1069E	gtggcctgtgaactgaccaca	tgtggctcagttcacaggccac
FLAG-fl-SCAP/H1099E	agccaagacgagacactgagag	ctctcagtgctgcttggct
FLAG-fl-SCAP/H1118E	cttcagggcgagtcaggggc	gcccctgactcgcctgaag
FLAG-fl-SCAP/H1155E	ccgggtcagcgaagtgttctg	agcaaaccttgcctgaccgg
FLAG-fl-SCAP/D1162K	tcaccgtgggaaggtcacctc	gaggtgaccttcccagctga
Myc-HSP90	gctggctagcatggacctgaggaagtgaccatggag	tcgagcggccgcatcacttctccatgcgagacg
Synthetic oligos		
NotI-Myc-Myc-XbaI_fwd	ggccgctagcagcagaagctgatctcagaggaggacctgagcagaagctgatctcagaggaggacct	
NotI-Myc-Myc-XbaI_rev	ctagaggtcctcctctgagatcagcttctgctcaggtcctcctctgagatcagcttctgctcgtgctg	

Supplementary Table S2

Proteins specifically identified in the SCAP sample and have >100 of MS scores

#	UniProt ID	Protein Description	Score	*PSM
1	SCAP_HUMAN	SREBP cleavage-activating protein	1676	49
2	HSP76_HUMAN	Heat shock 70 kDa protein 6	782	16
3	K2C6C_HUMAN	Keratin, type II cytoskeletal 6C	686	43
4	TBB3_HUMAN	Tubulin beta-3	677	33
5	HS90B_HUMAN	Heat shock protein HSP 90-beta	619	32
6	TBB2A_HUMAN	Tubulin beta-2A chain	581	35
7	TBA1B_HUMAN	Tubulin alpha-1B chain	553	34
8	K1C15_HUMAN	Keratin, type I cytoskeletal 15	390	21
9	HS90A_HUMAN	Heat shock protein HSP 90-alpha	362	21
10	K2C1B_HUMAN	Keratin, type II cytoskeletal 1b	360	15
11	K1H1_HUMAN	Keratin, type I cuticular Ha1	294	24
12	K1C19_HUMAN	Keratin, type I cytoskeletal 19	284	17
13	ACTC_HUMAN	Actin, alpha cardiac muscle 1	277	20
14	TBB6_HUMAN	Tubulin beta-6 chain	268	13
15	KT33B_HUMAN	Keratin, type I cuticular Ha3-II	261	23
16	NUCL_HUMAN	Nucleolin	252	19
17	KRT83_HUMAN	Keratin, type II cuticular Hb3	227	25
18	TCPG_HUMAN	T-complex protein 1 subunit gamma	221	21
19	CH60_HUMAN	60 kDa heat shock protein, mitochondrial	218	16
20	KRT86_HUMAN	Keratin, type II cuticular Hb6	217	24
21	KR87P_HUMAN	Putative keratin-87 protein	200	23
22	EFTU_HUMAN	Elongation factor Tu, mitochondrial	190	16
23	POTEF_HUMAN	POTE ankyrin domain family member F	183	17
24	PHB_HUMAN	Prohibitin	172	8
25	KRT85_HUMAN	Keratin, type II cuticular Hb5	171	21
26	ADT3_HUMAN	ADP/ATP translocase 3	167	22
27	RL5_HUMAN	60S ribosomal protein L5	166	16
28	ACTBL_HUMAN	Beta-actin-like protein 2	164	8
29	PHB2_HUMAN	Prohibitin-2	164	8
30	K22O_HUMAN	Keratin, type II cytoskeletal 2 oral	157	15
31	TCPA_HUMAN	T-complex protein 1 subunit alpha	150	18
32	KRT35_HUMAN	Keratin, type I cuticular Ha5	150	12
33	GRP78_HUMAN	78 kDa glucose-regulated protein	145	13
34	K2C72_HUMAN	Keratin, type II cytoskeletal 72	133	13
35	TRAP1_HUMAN	Heat shock protein 75 kDa	130	4
36	ATPB_HUMAN	ATP synthase subunit beta, mitochondrial	123	15
37	KRT82_HUMAN	Keratin, type II cuticular Hb2	119	4
38	RS28_HUMAN	40S ribosomal protein S28	119	7
39	KRT36_HUMAN	Keratin, type I cuticular Ha6	118	16
40	TBA8_HUMAN	Tubulin alpha-8 chain	108	13
41	GBLP_HUMAN	Guanine nucleotide-binding protein subunit	103	12
42	MPCP_HUMAN	Phosphate carrier protein, mitochondrial	102	7

*Total number of identified peptide sequences (peptide spectrum matches) for the protein.

Supplementary Table S3

Primer sequences for real-time quantitative PCR

<i>Human</i>	Forward primer (5' to 3')	Reverse primer (5' to 3')
<i>18S</i>	ACCGCAGCTAGGAATAATGGA	GCCTCAGTTCCGAAAACCA
<i>SREBP-1c</i>	GGAGGGGTAGGGCCAACGGCCT	CATGTCTTCGAAAGTGCAATCC
<i>FAS</i>	GCAAATTCGACCTTTCTCCAGAA	GTAGGACCCCGTGGAAATGTC
<i>ACC1</i>	TGGGCCTCAAGAGGATTTGT	TCCACTGTTGGCTGATACATAGATG
<i>SQS</i>	ATGACCATCAGTGTGGAAAAGAAG	CCGCCAGTCTGGTTGGTAA
<i>HMGCR</i>	TACCATGTCAGGGGTACGTC	CAAGCCTAGAGACATAATCATC
<i>HMGCS</i>	GACTTGTGCATTCAAACATAGCAA	GCTGTAGCAGGGAGTCTTGGTACT
* <i>SCD1</i>	Hs00748952_s1	
* <i>SREBP-2</i>	Hs00190237_m1	
<i>Mouse</i>	Forward primer (5' to 3')	Reverse primer (5' to 3')
<i>36B4</i>	TGCATCAGTACCCCATCTATCA	AAGGTGTAATCCGTCTCCACAGA
<i>Scd1</i>	CCGGAGACCCCTTAGATCGA	TAGCCTGTAAAAGATTTCTGCAAACC
<i>Srebp-1c</i>	GAGCCATGGATTGCACATTT	CGGGAAGTCACTGTCTTGGT
<i>Srebp-1a</i>	GAACAGACAGTGGCCGAGAT	GGGAGTCACTGTCTTGGTTG
<i>Hmgcr</i>	CCGGCAACAACAAGATCTGTG	ATGTACAGGATGGCGATGCA
<i>Sqs</i>	CACACTGGCTGCCTGTTACAA	CCCCTTCCGAATCTTCACTACTC
* <i>Fasn</i>	MM00662319_M1	
* <i>Acc1</i>	MM01304286_M1	
* <i>Srebp-2</i>	MM01306283_M1	

* TaqMan probe identification numbers.

CLUSTAL 2.1 Multiple Sequence Alignments

Sequence type explicitly set to Protein
Sequence format is Pearson
Sequence 1: SCAP_human 1279 aa
Sequence 2: SCAP_mouse 1276 aa
Sequence 3: SCAP_rat 1276 aa
Sequence 4: SCAP_bovin 1278 aa
Sequence 5: SCAP_monkey 1278 aa
Sequence 6: SCAP_hamster 1276 aa
Start of Pairwise alignments
Aligning...

Sequences (1:2) Aligned. Score: 91.4577
Sequences (1:3) Aligned. Score: 92.0063
Sequences (1:4) Aligned. Score: 91.9405
Sequences (1:5) Aligned. Score: 97.9656
Sequences (1:6) Aligned. Score: 91.5361
Sequences (2:3) Aligned. Score: 98.1191
Sequences (2:4) Aligned. Score: 89.8903
Sequences (2:5) Aligned. Score: 91.8495
Sequences (2:6) Aligned. Score: 96.3166
Sequences (3:4) Aligned. Score: 90.4389
Sequences (3:5) Aligned. Score: 92.4765
Sequences (3:6) Aligned. Score: 96.9436
Sequences (4:5) Aligned. Score: 92.5665
Sequences (4:6) Aligned. Score: 90.3605
Sequences (5:6) Aligned. Score: 92.0063

Fig. S1. Amino acid sequence alignment score of mammalian SCAP

Alignment score of mammalian SCAP using 'Multiple Sequence Alignment by CLUSTALW.'

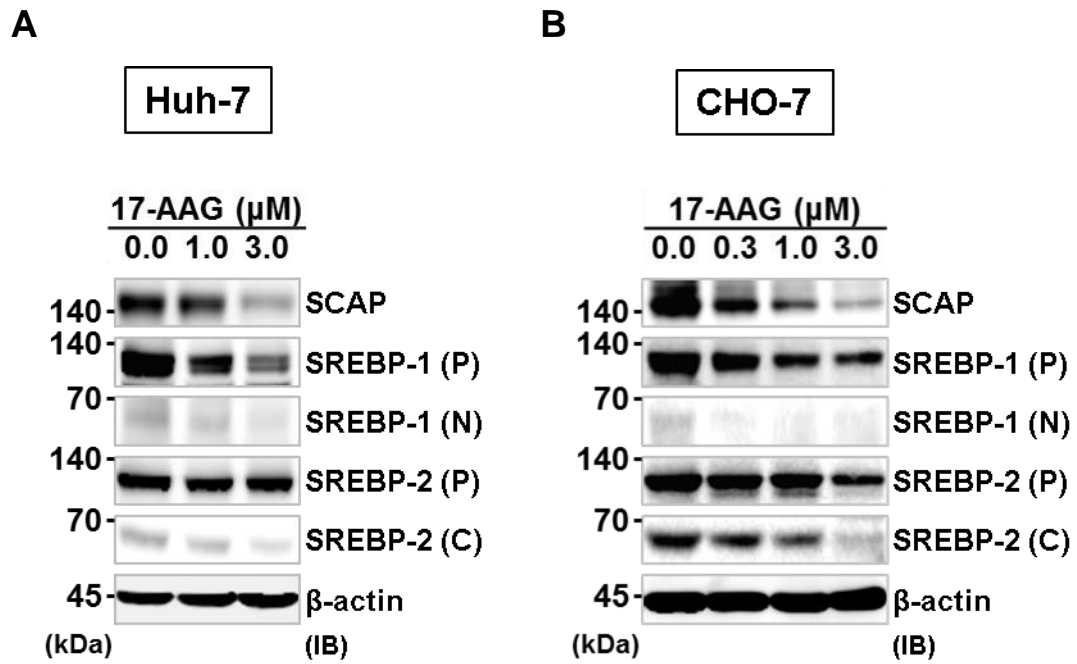


Fig. S2. 17-AAG decreased SCAP and SREBP protein levels in Huh-7 and CHO-7 cells

(A) Huh-7 cells and (B) CHO-7 cells were treated with 17-AAG (0–3 μM) for 24 h and then harvested for immunoblotting using anti-SREBP1 (2A4) and anti-SREBP2 (1C6) antibodies. Anti-SCAP clones C-20 and 9D5 were used to detect human (Huh-7) and hamster (CHO-7) SCAP, respectively.

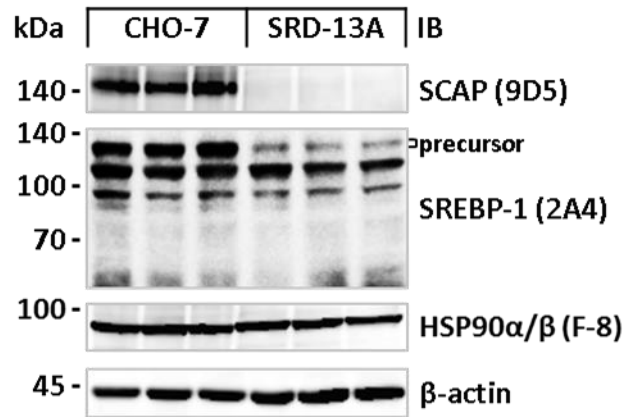


Fig. S3. Protein profile comparison between CHO-7 and SRD-13A

Expression profiles of SCAP, SREBP, and Hsp90 in CHO-7 cells and SRD13A cells were analyzed by immunoblotting using anti-SCAP (9D5), anti-SREBP1 (2A4), and anti-HSP90 (F-8) antibodies.

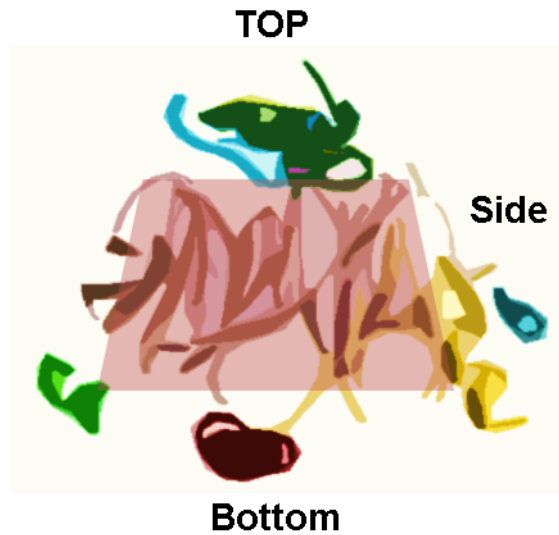


Fig. S4. WD40 domain–peptide interactions

This is an imitation of a figure shown page 569, Box I, Figure I of reference 29[Stirnemann, C. U., Petsalaki, E., Russell, R. B., and Müller, C. W. (2010) WD40 proteins propel cellular networks. *Trends Biochem. Sci.* 35, 565–574]. This image shows the interaction between WD40 domain (center) and its binding proteins (other color). The majority of proteins bind to the top surface of the WD40 protein.

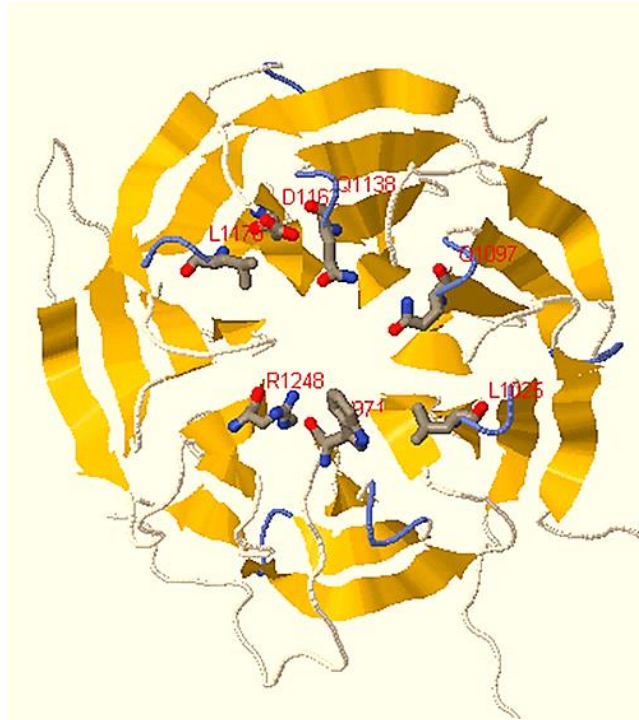


Fig. S5. Structure prediction of human SCAP WD40 domain

This image was obtained from the WD40 protein data base [Reference 66: Wang, Y., Hu, X. J., Zou, X. D., Wu, X. H., Ye, Z. Q., and Wu, Y. D. (2015) WDSPdb: a database for WD40-repeat proteins. *Nucleic Acids Res.* 43(Database issue), D339–D344] by entering the Uniprot ID of human SCAP (SCAP_HUMAN) in search box of the database. The 7 potential protein-protein interaction sites are indicated by red letters.

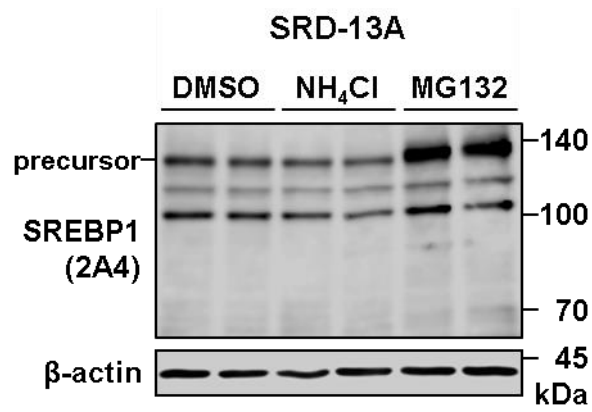


Fig. S7. Proteasome inhibition rescued SREBP protein in SCAP deficient cells

SCAP-deficient SRD-13A cells were treated with 0.1% DMSO, 10 mM ammonium chloride, or 10 μM MG132 for 24 h and then harvested for immunoblotting using anti-SREBP1 (2A4) antibody.

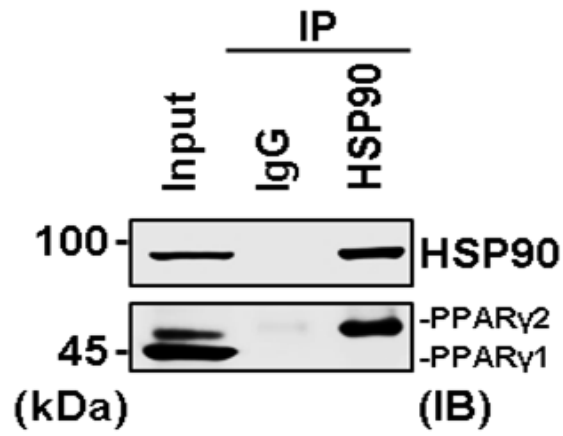


Fig. S8. Hsp90 interacts with PPAR γ 2 but not PPAR γ 1

HepG2 cell lysates were analyzed by anti-Hsp90 immunoprecipitation. The 10% cell lysate input, control IgG precipitates, and anti-Hsp90 precipitates were analyzed by immunoblots using anti-HSP90 (F-8) and anti-PPAR γ (H-100) antibodies.

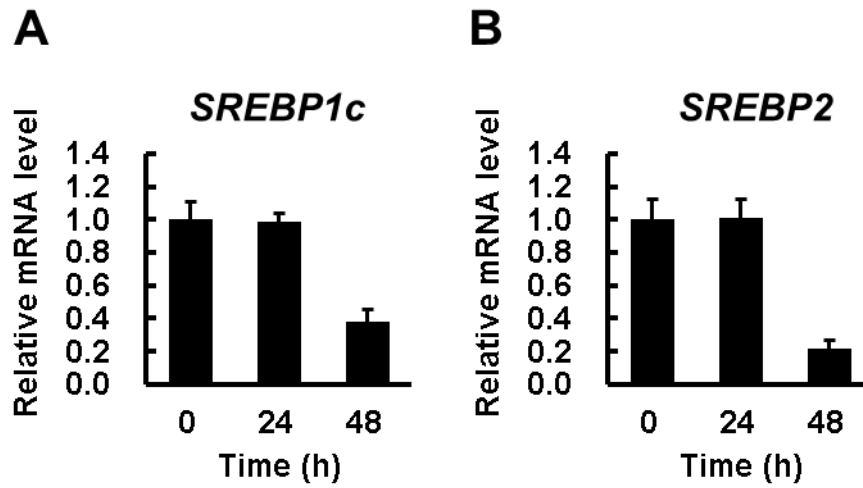


Fig. S9. *SREBP* transcription was downregulated after 24 h of 17-AAG treatment

HepG2 cells were treated with 3 μ M of 17-AAG for 0–48 h and then harvested for total RNA extraction. The total RNA was reverse transcribed to complementary cDNA and used for real-time quantitative PCR analysis to measure the mRNA level of (A) *SREBP1c* and (B) *SREBP2*.

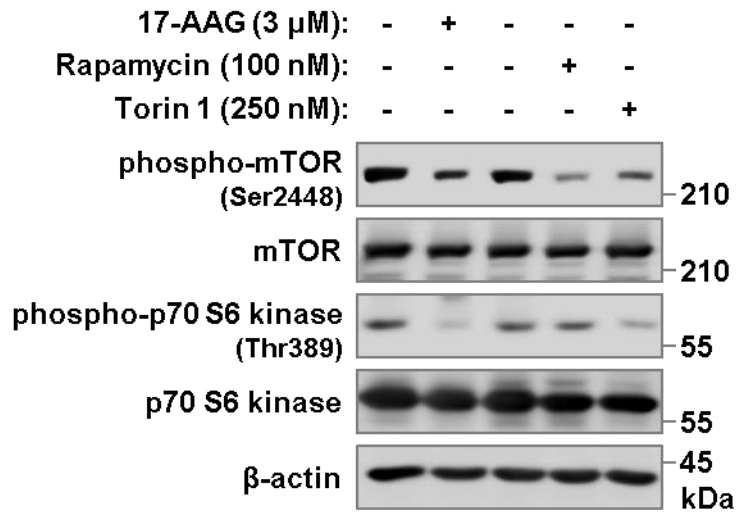


Fig. S10. 17-AAG inhibited mTOR and p70 S6 kinase phosphorylation

HEK293 cells were treated with Hsp90 inhibitor and mTOR inhibitors for 24 h and then harvested for immunoblotting using anti-mTOR (7C10), anti-phospho-mTOR (Ser2448), anti-p70 S6 Kinase, and anti-phospho-p70 S6 Kinase (Thr389) antibodies.

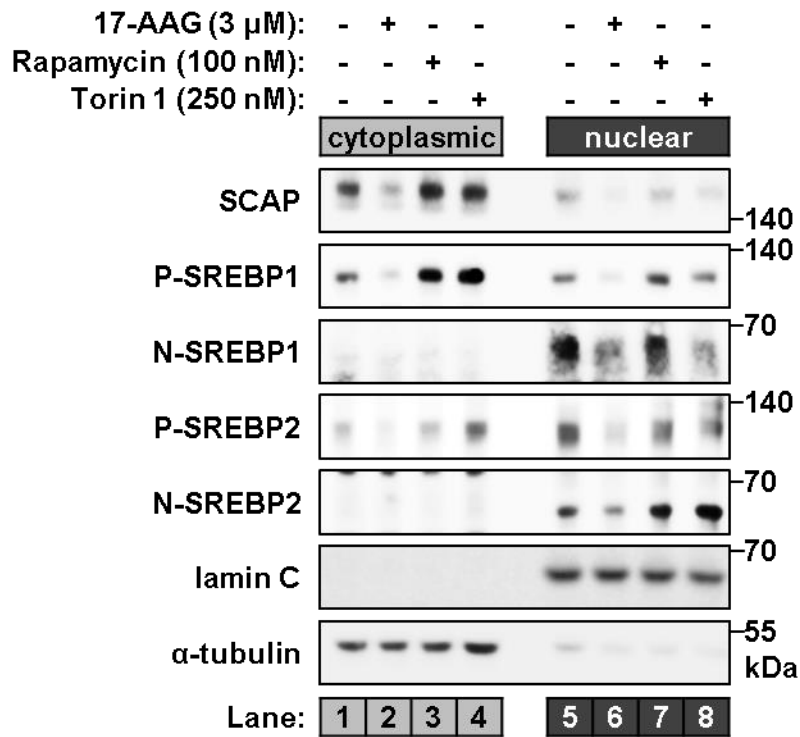


Fig. S11. 17-AAG decreased nuclear matured SREBP1 and SREBP2

HEK293 cells were treated with Hsp90 inhibitor and mTOR inhibitors for 24 h and then harvested for nucleus and cytoplasm separation. The cytoplasmic and the nuclear fractions were analyzed by immunoblots using anti SCAP (C-20), anti-SREBP1 (2A4), and anti-SREBP2 (RS004) antibodies. Lamin C and α -tubulin were immunoblotted as markers of nucleus and cytoplasm, respectively.

